Dissertation

Deciphering the structure and plasticity of glutamatergic synapses in the hippocampus

with the aim of achieving a doctoral degree (Dr. rer. nat.)

at the Faculty of Mathematics, Informatics and Natural Sciences

Department of Biology

University of Hamburg

Submitted by

Tomas Fanutza

Hamburg, 2023

Practical work was conducted between February 2019 and June 2023 in the research group “Neuronal Protein Transport” at the Center for Molecular Neurobiology Hamburg (ZMNH), University Medical Center Hamburg-Eppendorf.

Evaluators

Prof. Dr. Thomas G. Oertner
Institute for Synaptic Physiology, Center for Molecular Neurobiology Hamburg, University Medical center Hamburg-Eppendorf, Hamburg, Germany

Prof. Dr. Marina Mikhaylova
RG Neuronal Protein Transport, Center for Molecular Neurobiology Hamburg, University Medical Center Hamburg-Eppendorf, Hamburg, Germany
RG Optobiology, Institute of Biology, Humboldt-University Berlin, Germany

Members of the examination board

Prof. Dr. Marina Mikhaylova
RG Neuronal Protein Transport, Center for Molecular Neurobiology Hamburg, University Medical Center Hamburg-Eppendorf, Hamburg, Germany
RG Optobiology, Institute of Biology, Humboldt-University Berlin, Germany

Prof. Dr. Dietmar Kuhl
Institute of Molecular and Cellular Cognition, Center for Molecular Neurobiology Hamburg, University Medical center Hamburg-Eppendorf, Hamburg, Germany

Prof. Dr. Markus Glatzel
Institute of Neuropathology, University Medical center Hamburg-Eppendorf, Hamburg, Germany

Date of disputation 29.09.2023

Supervisor

Prof. Dr. Marina Mikhaylova
RG Neuronal Protein Transport, Center for Molecular Neurobiology Hamburg,
University Medical Center Hamburg-Eppendorf, Hamburg, Germany
RG Optobiology, Institute of Biology, Humboldt-University Berlin, Germany

Co-supervisors

Prof. Dr. Thomas Oertner
Institute for Synaptic Physiology, Center for Molecular Neurobiology Hamburg,
University Medical center Hamburg-Eppendorf, Hamburg, Germany

Prof. Dr. Simon Wiegert
RG Synaptic Information Processing, Center for Molecular Neurobiology Hamburg,
University Medical center Hamburg-Eppendorf, Hamburg, Germany
Medical Faculty Mannheim, University of Heidelberg, Germany

Publications

The following publications result from theoretical work conducted during my doctoral program.

1. Bär J, **Fanutza T**, Reimann C, Seipold L, Grohe M, Bolter JR, Delfs F, Schweizer M, Saftig P, Mikhaylova M.
   Presynaptic plasticity at hippocampal mossy-fiber:CA3 synapses relies on non-enzymatic functions of disintegrin/metalloproteinase ADAM10
   In preparation for submission.

2. Bucher M*, **Fanutza T***, Mikhaylova M.
   Cytoskeletal makeup of the synapse: Shaft versus spine.
   *Cytoskeleton (Hoboken). 2020 Mar;77(3-4):55-64. doi: 10.1002/cm.21583. Epub **2019 Dec 4**. PMID: 31762205. Review. * shared first authorship*

The following publications did not result from practical work conducted in the frame of this dissertation but relate to previous work published during the PhD.

3. Fulton S, Wenderski W, Lepack A, Eagle A, **Fanutza T**, Bastle R, Ramakrishnan A, Hays E, Neal A, Bendl J, Farrelly L, Al-Kachak A, Lyu Y, Cetin B, Chan J, Tran T, Neve R, Roper R, Brennand K, Roussos P, Schimenti J, Friedman A, Shen L, Blitzer RD, Robison A, Crabtree G, Maze I.
   Rescue of Down syndrome related deficits by Brwd1 copy number restoration in trisomic mice. *Nat Commun. **2022 Oct 26**;13(1):6384. doi: 10.1038/s41467-022-34200-0.PMID: 36289231*

4. Beckmann ND, Lin WJ, Wang M, Cohain AT, Charney AW, Wang P, Ma W, Wang YC, Jiang C, Audrain M, Comella PH, Fakira AK, Hariharan SP, Belbin GM, Girdhar K, Levey AI, Seyfried NT, Dammer EB, Duong D, Lah JJ, Haure-Mirande JV, Shackleton B, **Fanutza T**, Blitzer RD, Kenny E, Zhu J, Haroutunian V, Katsel P, Gandy S, Tu Z, Ehrlich ME, Zhang B, Salton SR, Schadt EE.
   Multiscale causal networks identify VGF as a key regulator of Alzheimer's disease.
   *Nat Commun. **2020 Aug 7**;11(1):3942. doi: 10.1038/s41467-020-17405-z.*
   PMID: 32770063

5. Readhead B, Haure-Mirande JV, Mastroeni D, Audrain M, **Fanutza T**, Kim SH, Blitzer RD, Gandy S, Dudley JT, Ehrlich ME.
   miR155 regulation of behavior, neuropathology, and cortical transcriptomics in Alzheimer's disease. *Acta Neuropathol. 2020 Sep;140(3):295-315. doi: 10.1007/s00401-020-02185z. Epub **2020 Jul 14**. PMID: 32666270*

6. Cirnaru MD, Melis C, **Fanutza T**, Naphade S, Tshilenge KT, Muntean BS, Martemyanov KA, Plotkin JL, Ellerby LM, Ehrlich ME.
Nuclear Receptor Nr4a1 Regulates Striatal Striosome Development and Dopamine D 1 Receptor Signaling. **eNeuro.** ***2019 Oct 10****;6(5): eNeuro.0305-19.2019. doi: 10.1523/ENEURO.0305-19.2019. Print 2019 Sep/Oct.*

7. Haure-Mirande JV, Wang M, Audrain M, **Fanutza T**, Kim S, Heja S, Readhead B, Dudley J, Blitzer RD, Schadt E, Zhang B, Ehrlich ME, Gandy S. Correction: Integrative approach to sporadic Alzheimer's disease: deficiency of TYROBP in cerebral Aβ amyloidosis mouse normalizes clinical phenotype and complement subnetwork molecular pathology without reducing Aβ burden.
Mol Psychiatry. ***2019 Mar 24****;(3):472. doi: 10.1038/s41380-018-0301-4.PMID: 30464330*

8. Haure-Mirande JV, Wang M, Audrain M, **Fanutza T**, Kim S, Heja S, Readhead B, Dudley J, Blitzer RD, Schadt E, Zhang B, Ehrlich ME, Gandy S. Integrative approach to sporadic Alzheimer's disease: deficiency of TYROBP in cerebral Aβ amyloidosis mouse normalizes clinical phenotype and complement subnetwork molecular pathology without reducing Aβ burden.
Mol Psychiatry. 2019 Mar;24(3):431-446. doi: 10.1038/s41380-018-0255-6. Epub ***2018 Oct*** *3. PMID: 30283032*

9. Audrain M, Haure-Mirande JV, Wang M, Kim SH, **Fanutza T**, Chakraborty P, Golde TE, Blitzer RD, Schadt EE, Zhang B, Ehrlich ME, Gandy S. Integrative approach to sporadic Alzheimer's disease: deficiency of TYROBP in a tauopathy mouse model reduces C1q and normalizes clinical phenotype while increasing spread and state of phosphorylation of tau.
Mol Psychiatry. 2019 Sep;24(9):1383-1397. doi: 10.1038/s41380-018-0258-3. Epub ***2018 Oct*** *3. PMID: 30283031*

Abstract

The ability of neurons to communicate and store information depends on specialized contact sites called synapses. The glutamatergic synapses show high degree of heterogeneity in terms of morphology, molecular composition and function among excitatory neurons of different brain regions. The molecular composition of excitatory synapses relies on various processes, including protein transport from the soma, facilitated by cytoskeletal structures and motor proteins, local protein synthesis, mobilization into the cellular membrane, and removal through endocytosis. Additionally, change of the synaptic protein landscape via proteolytic cleavage as well as surface diffusion of membrane proteins are essential factors in maintaining the integrity and functionality of synapses. The activity of multiple postsynaptic membrane proteins involved in these processes at hippocampal glutamatergic synapses is regulated by A Disintegrin And Metalloproteinase 10 (ADAM10), a protein highly expressed in the central nervous system and whose proteolytic function is critical for several protein mechanisms occurring in dendritic spine synapses. The first aim of this thesis is to explore the subcellular synaptic localization of ADAM10 as well as its impact on the short-term plasticity and synaptic transmission of hippocampal glutamatergic synapses. Importantly, we found that ADAM10 is present in presynaptic neurons where it is highly enriched in the membrane of presynaptic vesicles located at glutamatergic mossy fiber terminals connecting to the CA3 region, the area involved in encoding short-term memory, suggesting that ADAM10 could contribute to mechanisms of plasticity. Therefore, I investigated the impact of this metalloproteinase on the short-term plasticity of mossy fibers-CA3 (MF-CA3) synapses by employing electrophysiology techniques in order to measure field excitatory postsynaptic potentials (fEPSP) by using acute brain slices from conditional ADAM10 knockout mice (ADAM10 cKO). The findings demonstrate that although MF-CA3 synapses have no drastic morphological defects, they show impairments in vesicle release and short-term facilitation plasticity. I found that this phenotype depends on the cytosolic domain of ADAM10 rather than its proteolytic activity, suggesting a new role of this metalloproteinase never investigated before.

Hippocampal glutamatergic synapses can be also formed between Schaffer collaterals fibers and CA1 pyramidal cells (SC-CA1). In mature hippocampal CA1 neurons, the majority of excitatory synapses are located on dendritic spines. Nonetheless, a subpopulation of glutamatergic terminals makes synaptic contacts directly on dendritic shafts. As synapses signify the site of signal transmission and propagation, their distribution, density and individual strength are of great importance to understand the connectivity of the neural network. Yet, the morphological and functional properties of the excitatory shaft synapse remain largely unknown. Thus, a second aim of this thesis is to get new insights into the structure and function of glutamatergic shaft synapses by looking at the density distribution in dendrites and their molecular composition in analogy to spine synapses as well as by investigating their plasticity. Using brain slices from rat, I found that mature glutamatergic CA1 pyramidal cells receive inputs predominantly in dendritic spines compared to shaft synapses. I observed that proteins which are typically found in spine synapses are also present in excitatory shaft synapses suggesting they have a similar composition. Furthermore, I demonstrated that excitatory shaft synapses can be an active site for synaptic transmission and show plasticity upon glycine stimulation to induce chemical long-term potentiation (cLTP). These findings suggest that excitatory shaft synapses could be functional components of the hippocampal glutamatergic system, as they are structurally modulated upon long-term potentiation. Thus, they may represent an independent type of excitatory synapses where information is computed and translated into memory.

Zusammenfassung

Die Fähigkeit von Neuronen zur Kommunikation und zur Speicherung von Informationen hängt von spezialisierten Kontaktstellen namens Synapsen ab. Glutamaterge Synapsen exzitatorischer Neuronen verschiedener Gehirnregionen zeigen eine hohe Heterogenität in Bezug auf Morphologie, molekulare Zusammensetzung und Funktion. Die Zusammensetzung von glutamatergen Synapsen hängt entscheidend von mehreren Prozessen ab, einschließlich dem Transport von Proteinen aus dem Zellkörpermittels

Zytoskelett und Motorproteinen, sowie lokaler Synthese von synaptischen Proteinen und ihrer Entfernung über Endozytose. Weitere wesentliche Faktoren in der Integrität und Funktionalität von Synapsen sind proteolytische Spaltung sowie die Oberflächendiffusion von Membranproteinen. Die Aktivität mehrerer postsynaptischer Membranproteine, die an diesen Prozessen beteiligt sind, wird durch „A Disintegrin And Metalloproteinase 10“ (ADAM10) reguliert, ein Protein, das im Zentralnervensystem stark exprimiert wird und dessen proteolytische Funktion in dendritischen Synapsen von entscheidender Bedeutung ist. Das erste Ziel dieser Arbeit ist es, die subzelluläre synaptische Lokalisation von ADAM10 sowie dessen Auswirkungen auf die Kurzzeitplastizität und synaptische Transmission von glutamatergen Synapsen im Hippocampus zu erforschen. Wir haben dabei herausgefunden, dass ADAM10 in präsynaptischen Neuronen lokalisiert ist, wo es in der Membran präsynaptischer Vesikel angereichert ist, die mit den glutamatergen Moosfaser-Terminals im CA3-Gebiet verbunden sind, welches an der Kodierung des Kurzzeitgedächtnisses beteiligt ist. Dies legt nahe, dass ADAM10 ebenfalls an Mechanismen der Kurzzeitplastizität beteiligt sein könnte. Daher untersuchte ich mittels Elektrophysiologie-Techniken zur Messung von feldexzitatorischen postsynaptischen Potentialen (fEPSP) den Einfluss dieser Metalloprotease auf die Kurzzeitplastizität der Moosfaser-CA3 (MF-CA3) Synapsen in akuten Hirnschnitten von konditionalen ADAM10-Knockout-Mäusen (ADAM10 cKO), Die Ergebnisse zeigen, dass MF-CA3-Synapsen zwar keine drastischen morphologischen Defekte aufweisen, aber Beeinträchtigungen bei der Vesikelfreisetzung und der Kurzzeit-Plastizität aufweisen. Es wurde festgestellt, dass dieser Phänotyp von der zytosolischen Domäne von ADAM10 abhängt, nicht von seiner proteolytischen Aktivität, was auf eine neue Rolle dieser Metalloprotease hinweist, die zuvor noch nicht untersucht wurde.

Glutamaterge Synapsen im Hippocampus können auch zwischen Schaffer-Kollateralen-Fasern und CA1-Pyramidenzellen (SC-CA1) gebildet werden. Bei ausgereiften CA1-Neuronen im Hippocampus befinden sich die meisten erregenden Synapsen auf dendritischen Dornen. Es gibt jedoch eine Untergruppe von glutamatergen Terminals, die synaptische Kontakte direkt auf dem dendritischen Schaft bilden. Da Synapsen den Ort der

Signalübertragung und -ausbreitung darstellen, sind ihre Verteilung, Dichte und individuelle Stärke von großer Bedeutung, um die Konnektivität des neuronalen Netzwerks zu verstehen. Die morphologischen und funktionellen Eigenschaften dieser exzitatorischen Schaftsynapsen sind jedoch weitgehend unbekannt. Daher war ein zweites Ziel dieser Arbeit, neue Einblicke in die Struktur und Funktion der glutamatergen Schaftsynapsen zu gewinnen, indem ihre Verteilung in Dendriten, ihre molekulare Zusammensetzung in Analogie zu Dornsynapsen, und ihre Plastizität beschrieben wurden. Hier wurde festgestellt, dass reife glutamaterge CA1-Pyramidenzellen im Hippocampus von Ratten hauptsächlich Inputs via dendritischer Dornsynapsen anstatt Schaftsynapsen erhalten. Es wurde beobachtet, dass Proteine, die typischerweise in Dornsynapsen zu finden sind, auch in exzitatorischen Schaftsynapsen vorhanden sind, was darauf hinweist, dass sie eine ähnliche Zusammensetzung haben. Darüber hinaus wurde nachgewiesen, dass exzitatorische Schaftsynapsen aktiv Transmissionen weiterleiten und Plastizität zeigen, wenn sie durch Glycin-Stimulation zur Induktion chemischer langfristiger Potenzierung (cLTP) angeregt werden. Diese Ergebnisse legen nahe, dass erregende Schaftsynapsen funktionale Komponenten des glutamatergen Systems im Hippocampus sein könnten, da sie strukturell moduliert werden können, um eine langfristige Potenzierung zu ermöglichen. Somit könnten sie einen unabhängigen Typ erregender Synapsen darstellen, die an der Informationsverarbeitung und -speicherung beteiligt sind.

Contents

Abbreviations

ADAM10 A Disintegrin And Metalloproteinase 10

AIS Axon initial segment

AMPAR 2-amino- 3-(3-hydroxy-5-methyl-isoxazol-4-yl) propanoic acid receptor

ANOVA Analysis of Variance

AP Action potential

APP Amyloid precursor protein

AZ Active Zone

CaM Calmodulin

cAMP Cyclic adenosine monophosphate

CaMKII Calcium/calmodulin-dependent protein kinase II

cLTP Chemical long-term potentiation

cKO Conditional knock out

CRSPR Clustered Regularly Interspaced Short Palindromic Repeats

DCG-IV 2',3'-Dicarboxycyclopropyl glycine

DGCs Dentate gyrus granule cells

DIV Day(s) in vitro

DMEM Dulbecco's Modified Eagle's Medium

E/I Excitation/Inhibition

eGFP Enhanced green fluorescent protein

EM Electron microscopy

F-actin Filamentous actin

fEPSP field excitatory post-synaptic potential

GABA Gamma-aminobutyric acid

GKAP Guanylate kinase-associated proteins

iGluR Ionotropic glutamate receptor

INs Inhibitory neurons

LTD Long-term depression

LTP Long-term potentiation MAGUK Membrane-associated guanylate kinase

MAGUK Membrane-associated guanylate kinase

MF Mossy fibers

MFB Mossy fibers bouton

NCAM1 Neural cell adhesion molecule 1

NMDAR N-methyl-D-aspartate receptor

PBS Phosphate-buffered saline

PCs Pyramidal cells

PKA protein kinase A

PLL Poly-L-lysine

Pr Probability of release

PSD Post-synaptic density

SCs Schaffer Collaterals

SD Standard deviation

SEM Standard error of the mean

SHANK3 SH3 and multiple ankyrin repeat domains protein 3

SynGAP Synaptic Ras GTPase-activating protein

Syt-1 Synaptotagmin-1

Syt-7 Synaptotagmin-7

STED Stimulated emission depletion

SVs Synaptic vesicles

VGCC Voltage gated calcium channel

WT Wild type

1 Introduction

1.1 Neuronal structure and function

1.1.1 Neuronal morphology

The mammalian brain is an incredibly complex and fascinating structure that is continuously under intense scientific investigation. As a highly plastic organ, the brain regulates most of the body's functions, including movements and sensations, organizes perceptions, generates cognitive states and relative behavior. All these operational roles are accomplished by an enormous number of heterogeneous neuronal circuits differing in their functions and structures. The brain consists of a huge number of excitable nerve cells called neurons, and the number can vary among different species. The human brain consists of 86 billion neurons, in rats 200 million, in mice 71 million (Herculano-Houzel, 2009). Despite unequal brain volume between species, neurons share a common trait of being organized in distinct regions, each responsible for specific functions. They have the remarkable ability to transmit information through a combination of electrical and chemical signals, which is made possible by their capacity to maintain a stable membrane potential to finely regulate the release of chemical messengers like the neurotransmitters. The general structure of a neuron in the brain is represented by a cell body (soma), which sprouts out a prolonged singular axon as well as multifunctional branched extensions called dendrites (Spruston, 2008). While specialized dendritic compartments receive input from the axon, the latter provide sites for forwarding signals through the release of neuromodulators (Richards and Van Hooser, 2018). Despite the fundamental similarities in the basic structure of neurons, there exists a significant amount of variation in the morphology of cell bodies, dendritic arborizations, and axon localization and length. These variations can be observed among different species, brain regions, and even among different types of neurons within the same organism (Benavides-Piccione *et al.*, 2020). Neurons are supported by a complementary class of cells called glia cells. Together, they form a complex and extensive network consisting of hundreds of distinct cell types (Zeng and Sanes, 2017). Within this network,

the mechanisms of neurotransmission are tightly regulated by counterbalanced excitatory and inhibitory signals. Collectively, the cells in the brain build an intricate map of neural connections, encompassing the elaborate web of synapses formed by the axons and dendrites of individual neurons. This map not only includes the spatial arrangement of neuronal circuits but also the functional properties of individual connections, such as the strength and plasticity of synaptic transmission.

1.1.2 Hippocampal excitatory and inhibitory neurons

A common class of neurons found in multiple brain areas is represented by excitatory pyramidal cells (PCs), which use glutamate as major neurotransmitter for interneural communication, and are mainly present in the cerebral cortex and subcortical structures such as the hippocampus and amygdala (Spruston, 2008; Bekkers, 2011). PCs share a common morphology, which typically includes a dominant apical dendrite emerging from the upper pole of the cell body. This apical dendrite gives rise to numerous oblique dendritic branches and terminates with a dense cluster of fine dendritic processes called apical tuft. In addition to apical dendrites, pyramidal neurons show a dendritic arbor that extends from the base of the soma, giving rise to basal dendrites. (DeFelipe and Fariñas, 1992; Spruston, 2008). Finally, the axons typically emerge from the base of the soma or sometimes from the dendrites (Thome *et al.*, 2014; Hodapp *et al.*, 2022) and the same axon can project to multiple cells forming several contact sites. Dendrites of pyramidal neurons are covered by spines, small actin-rich protrusions extending from dendritic shaft (Ramón y Cajal S., 1983), that serve as place of contact with other cells where synapses are mainly formed. Another common class of neurons strongly connected to pyramidal cells is represented by the inhibitory neurons or interneurons (INs). Contrary to glutamatergic pyramidal neurons, INs use γ-aminobutyric acid (GABA) as major neurotransmitter, however, they morphologically follow the same pattern observed in excitatory neurons as they possess a cell body, dendrites, and axon. They are typically characterized by a lower number of dendritic spines compared to excitatory neurons, and show high diversity among each other in terms of their morphological characteristics, neurochemical features, physiological and

pharmacological properties (Freund, 1996; Harris *et al.*, 2018). While the role of excitatory neurons is directly related to the multidirectional spreading of network activity, the interneurons regulate the excitability by providing input-specific inhibition (Miles et al., 1996; Contreras, Hines and Hines, 2019) enabling synchronized transmission across large-scale cell populations (Buzsáki and Chrobak, 1995; Cobb S.R et al., 1995). In general, the interplay between the excitation and inhibition system (E/I) is critical for neurons to process information, is highly correlating with the morphology and overall neuronal architecture (Richards and Van Hooser, 2018), and perturbation of these two opposing forces has been linked to different brain states like epilepsy and severe neuropsychiatric disease (Dichter and Ayala, 1987; Yizhar *et al.*, 2011; Taub, Katz and Lampl, 2013)

1.1.3 Hippocampal excitatory and inhibitory synapses

The interaction between neurons takes place at the level of synapses, cell-cell specialized contacts representing the smallest "computational" unit of the brain facilitating the transmission and propagation of electro-chemical signals across brain regions. Synapses exhibit a variety of distinct structures and shapes, which are largely determined by their brain location and the type of cell they are associated with. The differences in morphology and location are reflected in subcellular composition and functional properties of synapses (Yuste, Bonhoeffer and Planck, 2004; Luscher et al., 2011). The two major types of chemical synapses in the brain are the excitatory glutamatergic and inhibitory GABAergic synapses (Figure 1). Although synapses show a high degree of structural and functional heterogeneity, they share common structures that can be described in four modules: the presynaptic active zone (AZ), synaptic vesicles (SVs), synaptic cleft, and postsynaptic density (PSD) (Wichmann and Kuner, 2022).

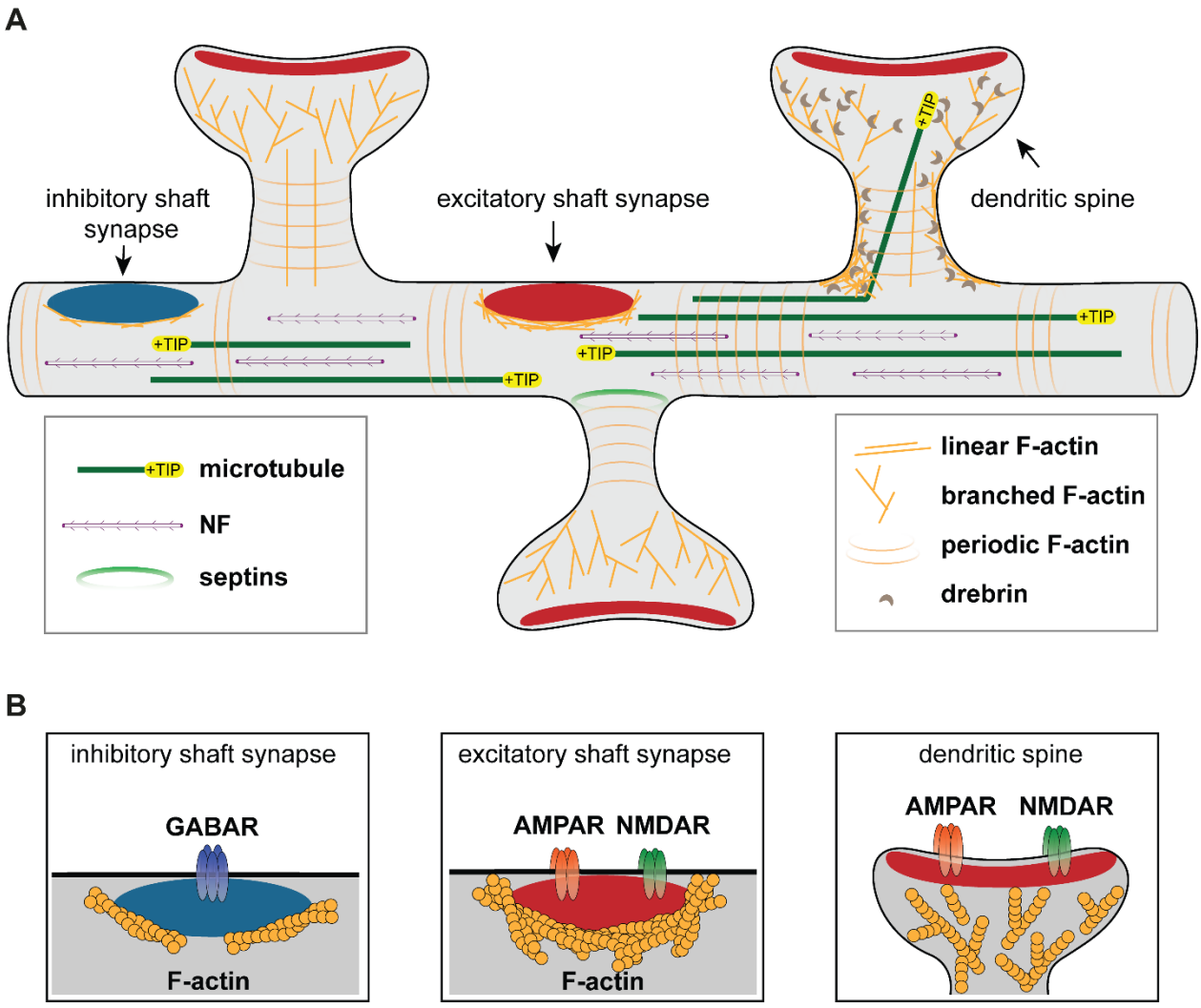

Figure 1: Subcellular organization of dendritic shaft and spine synapses.
(A) Dendritic spine and shaft synapses differ in their cytoskeletal environment and molecular composition between excitatory and inhibitory synapses. In both synapses, neuronal cytoskeleton mediate cargo transport and/or provide mechanical support to the synapse. In glutamatergic synapses, actin filaments (yellow) are found as dense mesh within the spine head while periodic F-actin/spectrin lattice constricts the spine neck and dendrite. Septins (light green) serve as additional constriction and shaping factors at the base of dendritic spines. Microtubules (dark green) serve as "roads" for kinesin- and dynein-driven cargo transport. The fast-growing (+) -end of microtubules (+TIP) is decorated with end-binding proteins such as EB3. In response to synaptic activity, microtubules may enter dendritic spines. This is mediated by the actin-binding protein drebrin (brown). Furthermore, neurofilaments (NF; purple) are found within dendrites and participate in electrical and biochemical signal transduction.
(B) Excitatory and inhibitory synapses: detailed overview.
This figure was taken from the review published by our laboratory (Bucher, Fanutza and Mikhaylova, 2020).

The presynaptic compartment is functionally defined by the AZ, an electron-dense structure localized at the axon terminal membrane containing SVs loaded with neurotransmitters. In addition to SVs, the presynaptic terminal consists of cytoskeletal and scaffolding proteins as well as signaling molecules required to mediate SVs recruitment, docking, priming and fusion, clearance, and endocytosis. These SVs are spatially organized into clusters sometimes docked with the AZ (Schikorski and Stevens, 1997; Imig *et al.*, 2014), which are thought to represent fusion-competent vesicles (Chang, Trimbuch and Rosenmund, 2018) responsible for signal transfer. The neurotransmitters contained inside the vesicles are released from the AZ into the synaptic cleft which provides a defined space for the transmitter diffusion and contains trans-synaptic interacting proteins required for formation and stabilization of synapses. The other critical synaptic element is the PSD, an electron-dense structure that opposes the AZ across the synaptic cleft, and serves as an organizational unit of multiple structural and signaling molecules including cytoplasmic enzymes, ionotropic and metabotropic receptors, cytoskeletal elements, scaffolding proteins and adhesion molecules (Chen *et al.*, 2011; Sheng and Kim, 2011; Wichmann and Kuner, 2022).

Typically, the PSD size is the parameter used to distinguish inhibitory from excitatory synapses, respectively defined as symmetric or asymmetric (Gray EG., 1959; Colonnier, 1968). In the context of an inhibitory system, GABAergic synapses are mainly formed directly on the dendritic shaft or around the soma, while only a few inhibitory synapses in the neocortex are spine synapses (Chiu et al, 2013). The neurotransmitter receptors associated with inhibitory PSDs are the $GABA_A$, and $GABA_B$, which interact directly with gephyrin, a well-known postsynaptic scaffolding protein of inhibitory synapses implicated in regulating the clustering of GABAergic receptors (Prior *et al.*, 1992; Essrich *et al.*, 1998; Lüscher and Keller, 2004; Jacob TC., 2008) and assembling of various inhibitory synapses-specific proteins including the cell-adhesion molecule Neuroligin 2 into the PSD, which is a requirement for intracellular signal transduction (Sheng and Kim, 2011; Crosby *et al.*, 2019).

In contrast to inhibitory synapses, excitatory synapses are much more complex and show a different distribution (Figure 2). During brain development, hippocampal glutamatergic synapses are typically located along the dendritic shaft. It is only after the formation of dendritic spines, through a process known as spinogenesis, that excitatory synapses begin to appear on these protrusions. As neurons mature, glutamatergic synapses are predominantly found on dendritic spines, although direct formation on the dendritic shaft can also infrequently occur (Bourne and Harris, 2011; Reilly, Hanson and Phillips, 2011; Jang *et al.*, 2015; van Bommel *et al.*, 2019; Xu *et al.*, 2020). The dynamics of glutamatergic synapse turnover are a key area of investigation, particularly with regard to whether the dendritic shaft and spine synapses are interconnected or represent independent structures. The glutamatergic PSD exhibit a disc-like shape and consists of two main compartments differing in molecular composition and size: the core and the pallial layer (Dosemeci et al, 2016). Typically, proteins of the membrane-associated guanylate kinases (MAGUK) family like PSD95 and SAP97 as well as guanylate kinase-associated protein (GKAPs) are enriched in the core layer forming a scaffold net binding postsynaptic receptor. These receptors include the ionotropic glutamate receptors (iGluRs) of the N-methyl-$_D$-aspartate (NMDARs), α-amino-3-hydroxy-5-methyl-4-isoxazolepropionic acid receptors (AMPARs) and kainate receptors (Craig *et al.*, 1993; Aoki *et al.*, 1994). These receptors are ligand-gated channels composed of a different set of subunits that can change in composition upon activity, at different synapse types, during development or aging (Dingledine *et al.*, 1999). The subunit combination of GluRs could influence the kinetics of the postsynaptic response determining the function of synapses (Mosbacher *et al.*, 1994; Geiger *et al.*, 1995). Next to ionotropic receptors, the metabotropic glutamatergic receptors (mGluRs) of the family G-protein-coupled receptors are also enriched at this side of the PSD. On the other side, the pallial layer hosts several additional scaffolding proteins of the SHANK/ProSAP family and homer family as well as signaling protein like the Ras-GTPase activating protein SynGAP or Calcium/calmodulin-dependent protein kinase II (CaMKII) (Kim and Sheng, 2004; Dosemeci et al, 2016; Clifton *et al.*, 2019; Falcón-Moya, Losada-Ruiz and Rodríguez-Moreno, 2019; Kursula, 2019). Additionally, L-type calcium channels

and various types of adhesion molecules, such as neuroligin-1, NCAM1, and integrins localized in the proximity of PSD, participate in postsynaptic signaling (Stefen *et al.*, 2016). Although glutamatergic synapses show a highly specialized composition in terms of molecules, they show a peculiar heterogeneity in terms of morphological and functional specialization depending on specific brain regions, cell type and synapse location. Importantly, the formation, plasticity, and stability of synapses are regulated by the neuronal cytoskeleton: actin filaments together with microtubules, neurofilaments, septins, and scaffolding proteins orchestrate the structural organization of synapses, enabling their efficacy in response to synaptic activation (Bucher, Fanutza and Mikhaylova, 2020).

1.2 Synaptic diversity

1.2.1 Heterogeneity of glutamatergic synapses

Excitatory synapses can be subdivided into diverse types, each representing a different category that in turn are thought to ensure neuronal network activity. Synapse heterogeneity is manifested depending on the number of presynaptic contacts in addition to their specific postsynaptic target cell. Functionally, the magnitude of postsynaptic responses are generated by extracellular ionic currents trough postsynaptic receptors and intracellular second messenger signals that are regulated by the PSD, a key aspect for synaptic strength modulation (Cane *et al.*, 2014; Dosemeci et al, 2016). The diversity of PSD is mainly related with neuronal cell type and its molecular and composition, size, as well as number, density, and localization of receptors, which define the kinetics and amplitude of the postsynaptic response. Upon glutamate release from the presynaptic glutamatergic terminals following an action potential (AP), the first and fast response is mediated by the AMPARs which have high affinity to glutamate and are mainly conducting Na^+ ions, leading to a rapid depolarization of the postsynaptic membrane. In contrast, NMDARs have less affinity to glutamate compared to AMPARs, and they can only be activated upon a removal of an internal Mg^+ block, therefore mediating a slower response. Once the

AMPARs are activated, the Na^+ influx depolarizes the postsynaptic membrane and removes the Mg^+ block from the NMDARs, generating influx of Ca^{2+} ions that is followed by the activation of several biochemical downstream cascades and precise molecular reaction pathways (Kennedy, 2016) including surface expression, localization, and removal of receptors (Geiger *et al.*, 2014). From a presynaptic point of view, the number of AZs determines the quantity of SVs docked with the membrane defining the probability of transmitter release (P_r). As consequence, the number of activated postsynaptic receptors can be different from synapse to synapse, which in turn specifies the magnitude of postsynaptic currents and plasticity. Another core feature concerns the spatial organization of molecules. For instance, the arrangement of presynaptic Ca^{2+} channels, responsible for the Ca^{2+} signal magnitude following synaptic activation, controls the P_r and the vesicle refilling mechanisms (Nicoll and Schmitz, 2005) . Finally, the protein content and composition of pre-and postsynaptic cells also contribute to structural differences defining specific responses and functions.

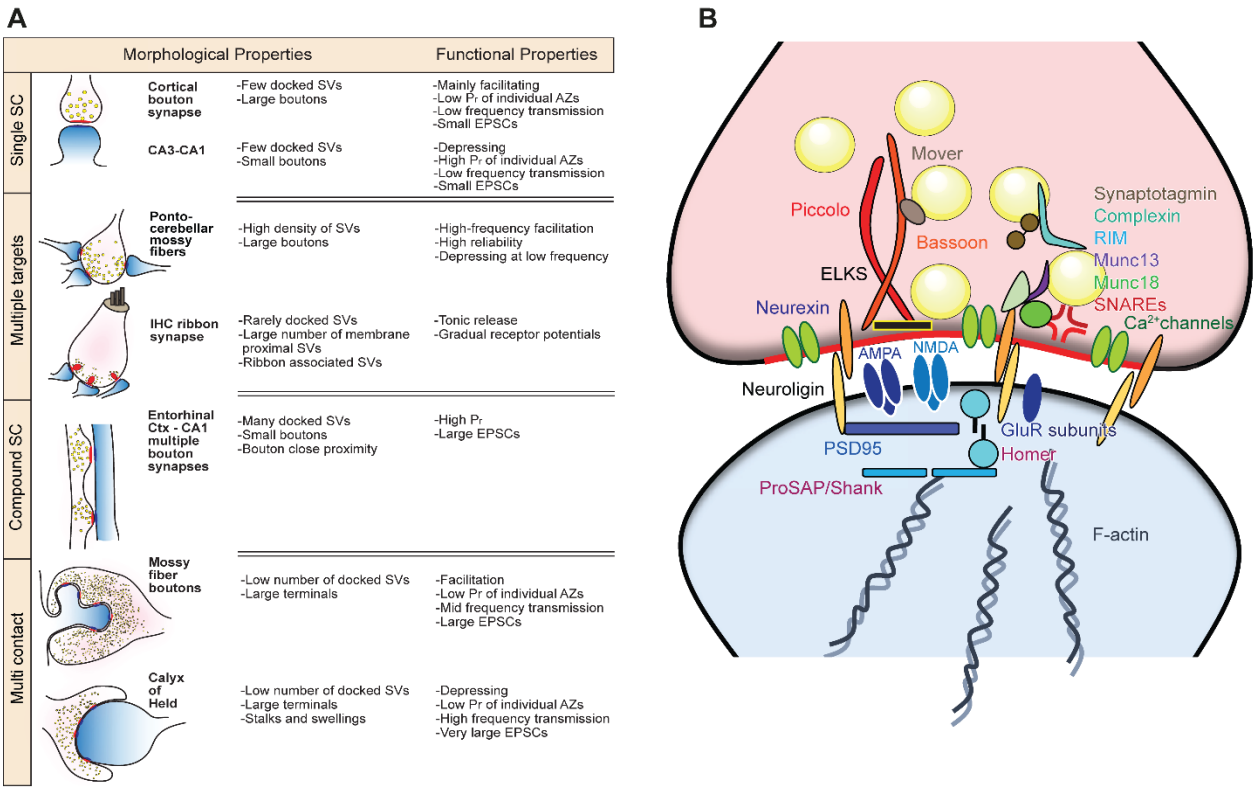

Figure 2: Heterogeneity of glutamatergic synapses.

(A) Example of distinct excitatory synapses. They can vary in the number of individual presynaptic contact sites, as well as their postsynaptic partners. The table is showing some of the most studied glutamatergic synapses characterized by their morphological and functional properties. They have different hallmarks, such as the number of synaptic contact (SC), synaptic vesicle (SV, in yellow), excitatory postsynaptic current (EPSC), release probability (P_r) and active zone (AZ, in red).

(B) Illustrative scheme showing the protein profile typically expressed in the pre and post compartment of a traditional single contact excitatory synapse. This molecular composition of glutamatergic synapses can strikingly diverge in different isoforms and subunits conferring heterogeneity and specifying their synaptic properties. Here are highlighted some of the most relevant synaptic elements such as the postsynaptic density (PSD), the soluble N-ethylmaleimide-sensitive-factor attachment receptor (SNARE), glutamate receptors (GluRs), cell adhesion molecules (CAMs), synaptotagmin and RIM, rab3-interacting molecule. *This figure was taken and adjusted from a review previously published (Wichmann and Kuner, 2022).*

1.2.2 Glutamatergic spine synapses

More than 80% of excitatory synapses terminate on spines, making them the main postsynaptic sites of excitatory neurotransmission. These tiny protrusions arise from the dendrites, sometimes from the soma or even from the axon hillock. Their size ranges from approximately 0.01-1 μm^3, consisting of a spine head (~0.5 μm diameter) and a smaller spine neck (0.1 μm diameter) (Bourne and Harris, 2008). The density of dendritic spines varies in different brain regions and different cell types. Morphologically, spines are categorized either as mushroom spines (large head and narrow neck), thin spines (small head and narrow neck), or filopodia spines. The latter are described as very thin and headless filamentous protrusions of the plasma membrane and are also considered, although with low degree, to be precursors of mature spines (Fiala et al, 1998). Spines can further be morphologically distinguished into stubby spines, structured with no apparent separation between the spine head and neck, and branched spines, which in contrast show two separated heads bifurcating from a single narrow neck (Risher *et al.*, 2014). In neuronal circuits, the morphological state of dendritic spines is constantly changing, however, their

three-dimensional structure can importantly function as biochemical and electrical compartment (Lee et al, 2009a; Cornejo, Ofer and Yuste, 2022). The neck is the most important parameter in enabling biochemical compartmentalization, allowing for the regulation of synaptic strength. For instance, increase of spine neck compartment in response to strong activity has been observed, a mechanism which can amplify the excitatory post synaptic response and possibly trigger induction of plasticity (Grunditz *et al.*, 2008). Moreover, structural changes of the spine neck were proposed to be influenced by synaptic activation, pushing the spine to work in a more balanced equilibrium by changing its membrane voltage potential, independently of neighboring synapses (Araya, Vogels and Yuste, 2014; Tønnesen *et al.*, 2014). The major cytoskeletal component of dendritic spines is F-actin, which can undergo activity-driven remodeling (polymerization, branching, treadmilling) and stabilization, providing high dynamic changes in terms of morphology, including shape and size (Bosch et al, 2014; Bucher, Fanutza and Mikhaylova, 2020). The structural morphology and molecular composition of the spine is thought to be critical for synaptic function, as spine head size correlates with synaptic strength. In the rodent hippocampal region, a correlation between the area of PSD, the spine size, the number of presynaptic docked vesicles and postsynaptic receptors has been observed in multiple studies, which provide the evidence of bigger spines corresponding to stronger synapses (Harris and Stevens, 1989; Knott *et al.*, 2006; Holderith *et al.*, 2012).

1.2.3 CA3 mossy fiber and CA1-Schaffer collateral excitatory spine synapses as examples of synaptic diversity

Probably the two best characterized glutamatergic synaptic contacts of the mammalian central nervous system are the hippocampal mossy fiber synapses, connecting dentate granule cells (DGCs) with CA3 pyramidal cells (CA3 PCs), and the Schaffer collateral synapses, connecting CA3 with CA1 pyramidal cells (CA1 PCs). DGCs send unmyelinated axons (mossy fibers) to the stratum lucidum, where they make synaptic contacts with thorny excrescences, complex postsynaptic elements found on proximal dendrites of CA3 PCs (Figure 2A). The hippocampal mossy fiber bouton-CA3 connections (MF-CA3 PCs)

provide a sparse but powerful synaptic contact via "giant" mossy fiber boutons to CA3 PCs displaying a wide range of short-and long-term plasticity changes (Nicoll and Schmitz, 2005; Nicoll, 2017). MF-CA3 PC synapses are sparsely organized, it is estimated that one CA3 PC is contacted on average by 50 DGCs, and MF boutons, with their special morphology, have an average of 20 release sites, as each bouton harbors many AZ (Chicurel and Harris, 1992; Rollenhagen *et al.*, 2007). The P_r of individual AZs is known to be rather low (Lawrence, Grinspan and McBain, 2004), consequently showing a particular type of plasticity specific to these synapses (Nicoll and Schmitz, 2005). Remarkably, electron microscopy studies of MF-CA3 PC synapses revealed the presence of a small number of docked vesicles responsible for the initial release as well as a second pool located in their vicinity, which instead gives the main contribution to a bigger release. Moreover, a prominent third pool is composed by larger SVs (Vyleta, Borges-Merjane and Jonas, 2016; Maus *et al.*, 2020). The efficacy of these synapses is very high, which might be attributed to multiple synaptic contacts functioning at the same time and to the relative vicinity of AZs to the vesicle pools (Rollenhagen *et al.*, 2007). Collectively, the special pattern of presynaptic activity featured by the MF-CA3 PC synapses determines the magnitude of the excitatory postsynaptic currents (EPSCs). After repetitive presynaptic stimuli, the amplitude of the EPSCs increases exponentially generating very high responses, giving rise to the notion of MF-CA3 as "conditional detonator" synapse (Henze, Wittner and Buzsáki, 2002; Vyleta, Borges-Merjane and Jonas, 2016).

Another well characterized excitatory synapse of the CNS is the Schaffer collateral synapse connecting hippocampal presynaptic CA3 PCs, which project to postsynaptic CA1 PCs. Here, neuronal transmission occurs in a well-defined laminar organization, and in contrast to MF-CA3 synapses, SC-CA1 synapses exhibit one single AZ per bouton (Schikorski and Stevens, 1997) with a relatively high P_r, as the number of docked SVs ready for release is higher, which correspond to a distinct synaptic organizational pattern in comparison to CA3 synapses. Within the hippocampal memory system, CA1 neurons are critically involved in the formation, consolidation, and retrieval of hippocampal-dependent memories.

1.3 Excitatory shaft synapses and their characteristics

The locus of plasticity expression at the glutamatergic synapses of principal neurons varies during developmental stages, reflecting the dynamic nature of the excitatory circuits. Dendritic shafts and dendritic spines are the primary sites where glutamatergic synapses form. In previous studies of shaft synaptogenesis conducted with primary neurons, synapse formation occurs at the contact sites between axon and dendrite after vesicle stabilization (Ziv and Smith, 1996; Ahmari, Buchanan and Smith, 2000; Sabo, Gomes and McAllister, 2006). Interestingly, by the time dendritic spines have emerged, initial axo-dendritic contact has already been made and shaft synapses have already been formed suggesting that synaptogenesis in spines might be somehow dependent on the previously established contact with a shaft as starting point for *de novo* growth of a functional spine (Fiala et al, 1998). However, other findings suggest that spines can grow upon glutamate uncaging stimulation without the need of a dendritic-shaft synapse stage (Kwon and Sabatini, 2011). Further studies described excitatory shaft synapses as an independent category of synaptic contact in the mature brain (Bourne and Harris, 2011; Reilly, Hanson and Phillips, 2011), and distinct excitatory synapses formed on dendritic shafts upon synaptic activation were also described using super-resolution imaging techniques (Xu *et al.*, 2020), suggesting that dendritic shaft synapses could be another computational unit for synaptic transmission. The distribution of excitatory spines synapses versus shaft synapses is not uniform. The density of these synapses differs in ratio depending on the brain region, type of neuron, and developmental stage. In rodents, approximately 7 days after birth, glutamatergic hippocampal neurons contain excitatory synapses predominantly formed on dendritic shafts. However, in the adult hippocampus, the vast majority of glutamatergic synapses form in dendritic spines, and only a small minority of excitatory synapses stay located on dendritic shafts (Boyer, Schikorski and Stevens, 1998; Fiala et al, 1998; Bourne and Harris, 2011; Reilly, Hanson and Phillips, 2011). On the other hand, in midbrain dopamine neurons,

the excitatory synapses are primarily located on dendritic shafts and this pattern does not change during development (Jang *et al.*, 2015). The formation of glutamatergic shaft synapses, but not spine synapses, is promoted by the postsynaptic receptor ephrinB3, as reducing or increasing postsynaptic ephrinB3 expression selectively decreases or increases shaft synapse density, respectively (Aoto *et al.*, 2007). Functionally, shaft and spine synapses show distinct properties as they show different postsynaptic responses most likely due to their diversity in terms of postsynaptic receptor expression (Jang *et al.*, 2015). The cytoskeletal organization of dendritic shaft synapses has been recently observed at the nanoscale level where F-actin filaments share a location with AMPARs and NMDARs and are opposed to active presynaptic terminals (van Bommel *et al.*, 2019). Stimulated emission depletion (STED) microscopy revealed that glutamatergic PSDs on the dendritic shaft are surrounded by F-actin consisting of both branched and longitudinal filaments, similar to the F-actin associated with the PSD inside dendritic spines These F-actin patches can structurally vary in terms of size from 0.1 to 0.2 µm and are not invaded by microtubules. Dynamic polymerization or depolymerization of actin may serve as driving force for the formation or retraction of dendritic spines (Figure 3) as the actin turnover rates at these patches is very similar to that at dendritic spines.

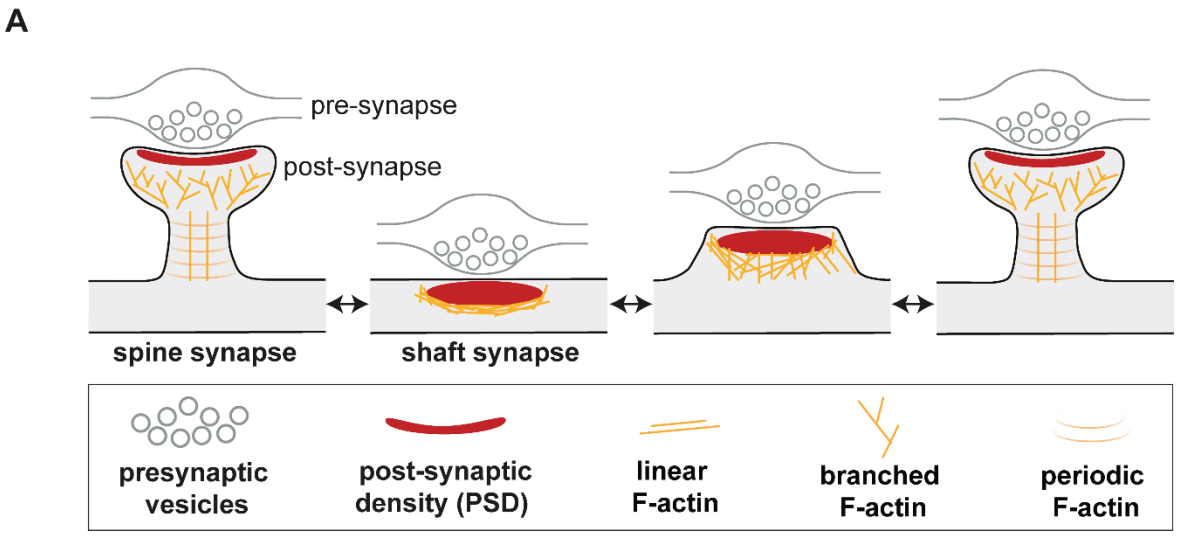

Figure 3: Hypothetical model of glutamatergic synapses turning from spines to shaft and vice versa.

F-actin-dependent spine formation and retraction may be modeled by particular synaptic conditions and through dynamic polymerization and depolymerization of actin. Excitatory spine or shaft synapses are contacted by presynaptic terminals to postsynaptic densities that are highlighted in red. *This figure was taken from the review published by our laboratory (Bucher, Fanutza and Mikhaylova, 2020).*

1.3.1 Role of excitatory shaft synapses in organelle trafficking

The presence of shaft synapses has a strong influence on dendritic organelles transported by motor proteins such as myosins and kinesins. Recent studies have demonstrated that organelles like lysosomes can be trapped deep inside the patches or be localized near the border (Goo *et al.*, 2017; van Bommel *et al.*, 2019) most likely through the interaction between F-actin and actin motor proteins. What could be the functional role of such docking? It has been shown that upon induction of neuronal activity, in addition to the classical role of protein degradation, mature lysosomes can release their content into the extracellular space via Ca^{2+} -dependent exocytosis allowing remodeling of the extracellular matrix in the vicinity of activated spines, which could be a critical step required during synaptic plasticity (Padamsey *et al.*, 2017). Since lysosomes can be docked in close proximity to the shaft synapse, it is possible that shaft synapses can contribute to the control of lysosomal exocytosis. Presumably, dense actin mesh structures surrounding the PSD of shaft synapses or at the base of the spines could stop lysosomes and regulate the trafficking of different other organelles like endosomes.

1.4 Synaptic plasticity

The ability of the brain to process information between neurons at the level of synapses relies on changing their strength in response to specific activity patterns, which is commonly referred to as synaptic plasticity (Hughes, 1958). Synaptic forms of plasticity can be ranging from milliseconds to hours, days, and even longer, playing a central role in the early development of neural circuitry as well as in the capacity of the developed brain to incorporate information from experiences into persistent memory traces. The first proposed idea of synaptic plasticity in strengthening synaptic connections was postulated by Santiago Ramon y Cajal, later reformulated by Donald Hebb (Hebb, 1949), and experimentally proven only in the early 1970s by Bliss and Lomo with the discovery of long-term potentiation (LTP) (Bliss and Lomo, 1973). Following the pioneering discovery of LTP, extensive research efforts have been directed towards elucidating the functional and potential implications of this phenomenon as a cellular and molecular mechanism underlying processes of learning and memory. Its counterpart in terms of function, long-term depression (LTD), was reported for the first time 20 years later by Dudek and Bear as they discovered that weakening synaptic transmission can be activity-dependent (Dudek and Bear, 1992), demonstrating that variation in synaptic strength could be bi-directionally modulated (Mulkey and Malenka, 1992). When both forms of plasticity are taken into consideration, it suggests that memory formation and storage does not merely involve a simple strengthening of synaptic connections. Instead, it is believed to result from a balanced distribution of synaptic weights across neural circuits, with an interplay between LTP and LTD. Not all forms of long-term synaptic plasticity follow the same rules described in the Hebbian theory, which postulates a coordinated response of the postsynaptic site based on the activity of a presynaptic input. For example, when long-term plasticity is induced, activation of the presynaptic neuron will alter the synaptic weight at all its postsynaptic contacts, independent of postsynaptic coordinated activity, indicating that independent mechanisms at pre- and post-synapse coexist in this type of plasticity.

1.4.1 Short-term plasticity: synaptic facilitation

Synapses are regulated by short and long-term changes of synaptic plasticity. Forms of short-term plasticity can last on the order of milliseconds to several minutes (Zucker and Regehr, 2002) playing important roles in temporary neuronal activity adaptations, for instance in response to sensations, behavioral stimuli and short memory consolidation. In a cellular context, short-term plasticity is triggered by repetitive presynaptic action potentials causing a transient accumulation of calcium in nerve terminals, which in turn causes changes in the probability of neurotransmitters release influencing biochemical processes that underlie the exocytosis of synaptic vesicles. Paired pulse stimulation is one of the most commonly used experimental procedures to measure short-term plasticity and study synaptic transmission as it can provide insights into the P_r and the efficacy of the synapse. When two stimuli are delivered within a short time interval ranging from 20 milliseconds to 1 second, the response to the second stimulus can be enhanced (facilitation) or weakened (depression) relative to the response to the first stimulus (Katz and Miledi, 1968). It is generally accepted that use-dependent facilitation is observed at many synapses with a low initial P_r whereas synapses with a high initial P_r usually exhibit use-dependent depression (Zucker and Regehr, 2002), and both are mainly attributed to effects of residual [Ca^{2+}] changes. After an action potential is generated at the axon initial segment (AIS), the depolarization propagates along the axon mainly via ion flux through voltage-sensitive Na+ channels, and reaching the presynaptic terminals induces the opening of voltage gated Ca^{2+} channels (VGCCs) allowing Ca^{2+} influx from the extracellular space. Ca^{2+} signals drop off significantly with distance from opened channels due to diffusion and capture by calcium buffers (Neher, 1998), however, this brief calcium wave known as "Ca_{local}" engages the molecular machinery responsible for vesicle fusion. A smaller amount of residual Ca^{2+} "Ca_{res}" persists for several hundred milliseconds and is mainly responsible for short-term plasticity patterns (Jackman and Regehr, 2017). Not only prolonged elevation of presynaptic calcium is contributing to short term facility, in fact, it can also depend on the number of vesicles released from presynaptic neurons and the number of receptors available

at the postsynaptic site, suggesting that mechanisms of short-term plasticity are not occurring exclusively in one compartment (Jackman and Regehr, 2017).

The molecular machinery mediating vesicle fusion and neurotransmitter release is strongly conserved throughout evolution across species: Ca^{2+} triggers exocytosis of transmitters from SVs in less than a millisecond by binding to Synaptotagmin-1 (syt-1), which together with cytoplasmic proteins like Complexin activates a core fusion machinery composed of SNAREs and SV proteins (Südhof, 2013). These events are confined to active zones, by a network of proteins including RIMs, RIM binding proteins, Munc13s, and many others. One of the ways by which these scaffolding molecules act is that RIMs recruit both calcium channels and Munc13, which makes SVs tethered at the active zone fusion competent (Südhof, 2012; Imig *et al.*, 2014). Several mechanisms for facilitation have been hypothesized and recently confirmed by Jackman and colleagues (Jackman *et al.*, 2016). One of the hypotheses was born from the idea that, in addition to the evolutionarily conserved Ca^{2+} binding proteins Calmodulin (CaM), and syt-1, other synaptotagmin calcium sensor protein family members, with higher affinity to calcium, contribute to synaptic facilitation. Of all isoforms, synaptotagmin-7 (syt-7) has been found to have the highest affinity for calcium (Sugita *et al.*, 2001) and its role in synaptic facilitation at hippocampal mossy fibers, Schaffer collateral and lateral perforant path synapses, as well as corticothalamic synapses was shown later, as in syt-7 KO synaptic facilitation was eliminated or significantly decreased (Jackman *et al.*, 2016).

Synaptic facilitation is a hallmark of presynaptic plasticity at the mossy fiber-CA3 synapse (MF-CA3) (Nicoll and Schmitz, 2005), one of the most highly specialized excitatory synapses in the brain displaying a wide dynamic range of short-term plasticity (Rebola, Carta and Mulle, 2017). MF-CA3 synapses formed between giant boutons and thorny excrescences have several release sites (Chicurel and Harris, 1992), however, loose coupling between presynaptic Ca^{2+} channels and the release machinery limit the initial P_r, due to endogenous Ca^{2+} buffer activity (Vyleta, N. P. & Jonas, 2014), conferring a robust synaptic facilitation (Nicoll and Schmitz, 2005). In contrast to MF-CA3 synapses, Shaffer

collateral-CA1 synapses (SC-CA1) have only one release site for transmitter release producing different but similar plasticity. Although morphological examinations indicate that multiple vesicles are docked at the presynaptic active zones, minimal stimulation studies have reported that P_r at SC-CA1 synapses is restricted to one vesicle release per action potential (Stevens and Wang, 1995), implying that facilitation in CA1 is much less pronounced than CA3.

1.4.2 Long-term plasticity: presynaptic mechanisms in plasticity

Long-term synaptic plasticity is a major cellular substrate for learning, memory, and behavioral adaptation. Although several examples of long-term synaptic plasticity described a mechanism by which postsynaptic signal transduction was potentiated, it is now well established that there is a vast array of mechanisms for long-term synaptic plasticity that involve modifications to either or both the postsynaptic site and presynaptic terminal which offers a powerful means to modify neural circuits. A wide range of induction mechanisms has been identified. Some occur entirely in the presynaptic terminal or at the postsynaptic sites (Castillo, 2012; Nicoll, 2017), whereas others require the contribution of both, as retrograde signaling molecules arising from the postsynaptic neurons or astrocytes diffuse to presynaptic terminals triggering critical biochemical reactions (Monday, Younts and Castillo, 2018). In spite of different induction mechanisms, some common rules can be identified across synapses. Typically, Ca^{2+} influx generated via ligand-gated presynaptic receptor or VGCC triggers a downstream signaling cascade involving kinases and phosphatases modulating pre- and postsynaptic changes. One well-characterized mechanism involves presynaptic cyclic adenosine monophosphate (cAMP) and protein kinase A (PKA) signaling. Activation of cAMP induces presynaptic LTP at the hippocampal mossy fiber to CA3 pyramidal cell (MF-CA3) synapse and at many other synapses throughout the brain (Castillo, 2012). In contrast, presynaptic inhibition of the cAMP pathway via Gi/o protein-coupled receptors, like the cannabinoid-1 receptor (CB1R), μ-opioid receptor (MOR), dopamine-2 receptor (D2R), results in presynaptic LTD, which is also a widespread phenomenon (Atwood, 2014). The precise process by which

neurotransmitter release is altered in a long-lasting manner remains largely unknown. This is likely due to the difficulty associated with visualizing and manipulating the axon and involved presynaptic terminals. In addition, neurotransmission is a particularly complex phenomenon that involves multiple steps and molecular players (Monday and Castillo, 2017).

1.4.3 Long-term potentiation (LTP): post-synaptic mechanisms

LTP is one of the most well-studied forms of long-lasting activity-dependent changes in synaptic strength following the Hebbian rules. Such forms of plasticity typically function in an input-specific manner, are rapidly induced and long-lasting, and require correlated firing of the pre- and post-synaptic neurons (Malenka and Bear, 2004; Citri and Malenka, 2008; Nicoll, 2017; Diering and Huganir, 2018). Because these hallmark features facilitate the reinforcement of precise synaptic connections, which is fundamental for information storage in the brain, these Hebbian mechanisms are thought to be the cellular correlates of learning and memory. Indeed, LTP in postsynaptic cells is a requirement for the integration of new experience (i.e. learning) and is generally divided in two distinct phases: early (E-LTP) and late (L-LTP). LTP mechanisms have been extensively investigated in the CA3 and CA1 regions of the hippocampus, in which different inductors of plasticity have been discovered. In general, synchronous activation of presynaptic glutamate release and postsynaptic AMPARs activation, which results in a robust depolarization, is the critical step for LTP induction. Indeed, at negative membrane potentials, the pore of NMDAR is blocked by Mg^{2+}. Depolarization induced by AMPARs displaces Mg^{2+} from the pore, allowing Na^{+}, K^{+}, and mainly Ca^{2+} to pass and activate the biochemical process of potentiation. At SC-CA1 synapses, the triggering of LTP is dependent on NMDARs leading to a calcium increase, which has to reach a critical threshold value to activate specific biochemical processes, primarily leading to the addition of surface AMPARs to the postsynaptic membrane (Malenka and Nicoll, 1993). Experimentally, this is usually achieved by applying high-frequency tetanic stimulation (TBS 100 Hz, 1s) or high-frequency train stimulation (HFS) of Schaffer collaterals, although it is not suitable for

physiological activity. More appropriate and physiological measurements of LTP expression can be achieved by using spike-timing-dependent plasticity (STDP), which is based on the matching of the action potential of presynaptic neurons and the firing of postsynaptic neurons with an appropriate timing (Dan and Poo, 2006). In general, the mechanisms that result in AMPARs insertion by Ca^{2+} influx in response to NMDARs activation are regulated mainly by CaMKII. CaMKII binds the NR2B subunit of NMDARs and phosphorylates a large number of proteins in the post synaptic density, including AMPARs and transmembrane AMPAR-regulatory proteins (TARPs), which has profound effects on both basal transmission and LTP induction (Baltaci, Mogulkoc and Baltaci, 2019). This increase of AMPARs at the surface of the postsynaptic membrane stems from extra-synaptic loci containing pools of functional receptors and from exocytosis of AMPAR-containing endosomes into perisynaptic sites (Makino and Malinow, 2009). Interestingly, AMPARs are highly mobile, and diffuse along the membrane until they are captured by scaffolding proteins, mainly PSD95, at the PSD, and translocate into the synapse by lateral diffusion (Penn *et al.*, 2018). Other than CaMKII, many other molecular players are involved in AMPAR mediated plasticity, including the Ca^{2+} dependent enzyme calpain, different kinases like PKA, PKC and MAPK tyrosine kinase (Boehm *et al.*, 2006; Makino and Malinow, 2009). These signaling pathways are extremely complex and precisely regulated, as their correct functioning is crucial for the adaptation of the strength of synaptic transmission, which can vary during different phases of LTP depending on the rates of endocytosis, exocytosis, and retention of AMPARs. All those modifications, and many others not described here, contribute to the activity-dependent functional potentiation of synaptic transmission (Nicoll, 2017).

The plasticity at mossy fibers synapses onto CA3 pyramidal cells is fundamentally different. Whereas LTP at CA1 synapses is dependent on NMDARs, at CA3 synapses, LTP is independent of NMDAR activity (Nicoll and Schmitz, 2005), as blockade of NMDARs has no effect on mossy fibers LTP (Harris and Cotman, 1986), pointing to an exclusive contribution of presynaptic mechanisms, including an increase in presynaptic calcium currents and the activation of adenylyl cyclase-cAMP CaMKII cascade. The lack of

NMDAR-dependent LTP is most likely due to the low number of NMDARs observed in immunohistochemical studies (Watanabe *et al.*, 1998). However, it is possible that increasing influx of Ca^{2+} in the postsynaptic compartment by a specific mechanism required for mossy fibers LTP is occurring. Due to the extraordinary degree of diversity in process specificity at MF-CA3 synapses, and the lack of highly precise technical approaches while maintaining physiological conditions, the exact molecular mechanisms that underlie the maintenance of long-lasting enhancement of synaptic transmission at MF-CA3 pathways remain to be elucidated. Nevertheless, multiple studies have the common evidence that phosphorylated CaMKII is a key molecular substrate in the process of LTP induction and maintenance at MF-CA3 synapses (Juárez-Muñoz *et al.*, 2017).

1.4.4 A Disintegrin and Metalloproteinase 10 (ADAM10) at glutamatergic synapses

As discussed in the previous chapters, several proteins are recognized as modulators of glutamatergic synapse organization and function. One of the multiple modulators composing the excitatory PSD is the protease ADAM10 (Marcello *et al.*, 2007), the α-secretase that governs the nonamyloidogenic pathway of β-amyloid precursor protein metabolism (Wan *et al.*, 2012). Its role is primarily centered around the proteolytic processing of several proteins including Prion proteins (PrP), NCAM, Amyloid Precursor Protein (APP) and N-cadherin (Figure 4), that are instrumental in the formation and maintenance of excitatory synapses as well as their structure and function (Saftig and Lichtenthaler, 2015). In regards of glutamatergic postsynaptic sites, ADAM10 has a key role in the processing of N-Cadherin, a cell-cell adhesion molecule importantly involved during dendritic arborization, axon guidance, and synaptogenesis. N-Cadherin can be cleaved by ADAM10 and its processing can be altered by impairing its localization leading to an accumulation of the full-length N-Cadherin. This causes an increase in spine head width, and modifications of the number and function of glutamate receptors of AMPA type, affecting spine maturation, structure and function of glutamatergic synapses in vitro and in vivo (Malinverno *et al.*, 2010). The regulation of ADAM10 activity controlled by NMDA

receptor activation has been demonstrated to be a critical step of glutamatergic synaptic function (Wan *et al.*, 2012). Furthermore, the loss of ADAM10 resulted in decreased neuromotor abilities and reduced learning performance, which were associated with altered LTP and in vivo network activities in the hippocampal CA1 region (Prox *et al.*, 2013). Recently, proteins implicated in the presynaptic organization, vesicle and organelle trafficking have been demonstrated to interact with ADAM10, suggesting that it may act as a hub protein at the excitatory pre-synapse (Cozzolino *et al.*, 2021). It is therefore an interesting candidate that could be involved in presynaptic functions in addition to the modulation, developmental and plastic processes of the glutamatergic post-synapse that underlie important synaptic functions. Despite the recent advanced discoveries, due to the lack of appropriate antibodies suitable for immunostainings, the precise subcellular localization of ADAM10 has been challenging to be resolved. Filling this gap, it would be very important step towards better understanding of the contribution of ADAM10 as a molecular player in the function as well as stability and plasticity of glutamatergic synapses.

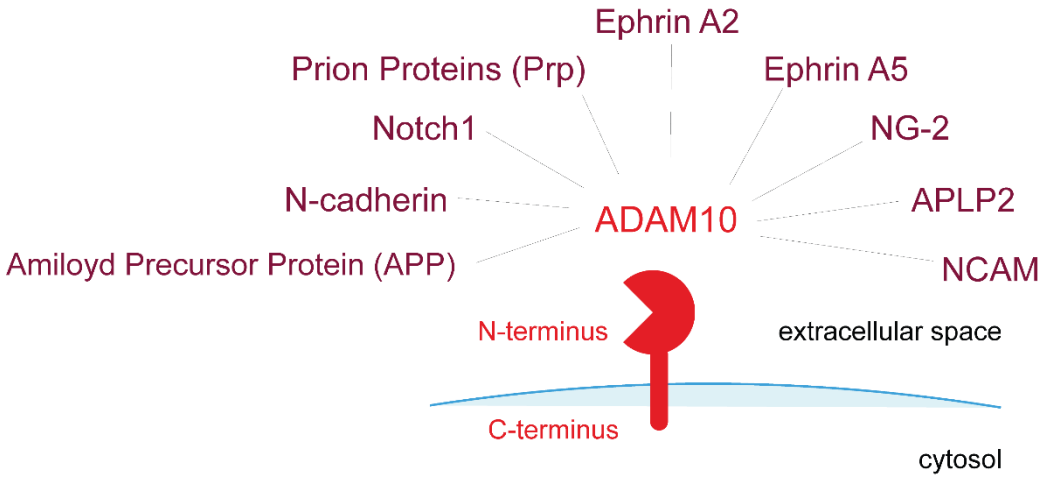

Figure 4: ADAM10 interaction partners in the Central Nervous System (CNS).
ADAM10 is a transmembrane protein that possesses a distinct extracellular domain capable of protease activity. This proteolytic function is accountable for the cleavage and subsequent removal of the extracellular domain of diverse cell surface proteins. This biological process is commonly recognized as "ectodomain shedding". Within the central nervous system (CNS), numerous substrates of ADAM10 have been identified at the postsynaptic site, playing essential roles in both embryonic brain development and maintaining the homeostasis of adult neuronal networks.

1.4.5 Structural plasticity and stability of dendritic spine synapses

It is widely acknowledged that synaptic structure and function are closely linked due to the strong association between spine head volume, PSD area, number of postsynaptic AMPARs, and presynaptic active zone. Consequently, alterations in synaptic strength typically coincide with modifications in synapse structure. In simpler terms, variations in dendritic spine size are tightly related to fluctuations of synaptic efficacy. The stability and dynamic nature of glutamatergic synapses are mediated by scaffolding proteins such as SHANKs and PSD95 associated with dendritic actin filaments (F-actin) trough interaction with F-actin-binding proteins like cortactin and α-actinin. This complex function is crucial for organizing the synaptic structure in response to synaptic activity (Mikhaylova et al, 2018; Bucher, Fanutza and Mikhaylova, 2020). The correlation between functional potentiation and structural enlargement of stimulated spines was demonstrated for the first time by the Matsuzaki lab, thanks to the development of two-photon glutamate uncaging (Matsuzaki et al, 2001). Enlargement of the spine structure induced by glutamate required a significant increase in AMPAR-mediated responses and activation of NMDARs and CaMKII. Although the initial expansion of the stimulated spine was massive but transient, it eventually stabilized at a level that exceeded its original size and remained like this for several hours. After this groundbreaking study, several other labs confirmed the correlation between function and structural changes induced by LTP at the single spine level (Harvey and Svoboda, 2007; Lee et al, 2009b; Bosch et al, 2014), suggesting that enlargement of the spine can potentially create more space for AMPA receptors to be inserted into the synapse, resulting in a sensitivity increase of the postsynaptic neuron to glutamate. The fact that glutamatergic receptors are expressed also at excitatory shaft synapses together with presynaptic proteins like VAMP2 and bassoon (Reilly, Hanson and Phillips, 2011; van Bommel *et al.*, 2019) suggests they represent active synapses. In line with this, excitatory shaft synapses are found to be functional in dopamine neurons (Jang *et al.*, 2015) or can be initially silent and become active upon plasticity induction in hippocampal primary cultures (Xu *et al.*, 2020). Since glutamatergic shaft synapses are enriched in both branched and linear F-actin (van Bommel *et al.*, 2019), it might be that similar mechanisms of plasticity

occurring in glutamatergic spine synapses are also taking place on shaft synapses. Advances in imaging techniques have revealed that CaMKII-dependent activation of small GTPases leads to actin polymerization and stabilization, which regulate spine structure expansion (Harvey et al, 2008; Murakoshi, Wang and Yasuda, 2011; Hedrick et al, 2016). It is believed that several actin-binding proteins (ABP) like the actin depolymerization factor (ADF), cofilin and profilin promote actin polymerization after LTP induction, a mechanism regulated by small GTPases such as Cdc42, Rac1, RhoA and Ras. Furthermore, in a recent study our laboratory has shown that the postsynaptic Ca^{2+} sensor caldendrin orchestrates nano-domain actin dynamics that are essential for actin remodeling in the early phase of LTP as caldendrin gene knockout results in higher synaptic actin turnover and impairment of structural spine plasticity (Mikhaylova *et al.*, 2018). Collectively, these results suggest that in spines activity-dependent remodeling of the actin cytoskeleton in combination with increased AMPAR expression are Ca^{2+}-dependent mechanisms regulated by several molecular players essential for the neurons to stabilize their synaptic strength in response to synaptic plasticity. Are similar mechanisms occurring in glutamatergic shaft synapses as well? A more in-depth characterization of glutamatergic shaft synapses is needed to determine if they represent a new type of independent synaptic structure and to delve deeper into the molecular mechanisms regulating their function, stability, plasticity, and morphology, under physiological conditions and in response to synaptic activity changes. The molecular components that comprise glutamatergic shaft synapses, such as receptors, transporters, and scaffolding proteins, should be extensively characterized to better comprehend the molecular machinery that mediates synaptic transmission and plasticity at these synapses. Also, comparing the properties of glutamatergic shaft synapses to those of dendritic spine synapses will provide insight into whether these sites, as they are formed next to each other, take part in heterosynaptic plasticity commonly seen in complex neural circuits involved in learning and memory, where synaptic plasticity is crucial for neural adaptation and behavior (Jenks *et al.*, 2021).

Aims of the thesis

The glutamatergic system is a highly specialized and fast signaling system used by excitatory neurons for communication. It is involved in many aspects of brain function, including learning, memory, and synaptic plasticity. The focus of this thesis is to explore the possible impact of glutamatergic synapse heterogeneity on neuronal transmission and plasticity of principal cells giving particular attention to hippocampal pyramidal neurons and excitatory synapses. Specifically, I aim

1. to identify molecular players which mediate plasticity of mossy fibers-CA3 synapses. I mostly focus on A Disintegrin And Metalloproteinase 10 (ADAM10), a protein highly expressed in the central nervous system which regulates the activity of many membrane-spanning proteins and plays critical roles in synaptic structure and function of excitatory synapses. I concentrate on the impact of ADAM10 in the short-term plasticity and synaptic transmission of the mossy fiber synapses, investigate the subcellular localization and novel presynaptic functions using microscopy and electrophysiological techniques.
2. to decipher the structure, localization, and molecular composition of the excitatory shaft synapses, compare them to spine synapses of CA1 pyramidal neurons and test the plasticity of the excitatory shaft synapses in response to long-term synaptic activity changes.

2 Results

2.1 Exploring the heterogeneity of glutamatergic synapses in the hippocampus

The data presented here has been generated with the help of different collaborators. Electron microscopy experiments were performed at the EM facility at the Center for Molecular Neuroscience Hamburg (ZMMH) headed by Michaela Schweizer. Electrophysiology measurements were assisted by technicians Sabine Gräf and Jan Schröder who helped with slice preparation and the maintenance of electrophysiological equipment. I would like to thank Dr. Christine Gee and Prof. Thomas G. Oertner at the ZMNH for access the synchroslice device. Fixed and live cell confocal microscopy imaging were performed under the guidance of Dr. Roland Thuenauer, head of the microscopy facility, at the Center for Structural System Biology (CSSB) located at German Electron Synchrotron DESY in Hamburg. Some of the microscopy data were provided by Dr. Julia Bär, a postdoc in our group with whom I collaborated on the ADAM10 project and are included for completeness of the story.

Synapses represent the smallest computational unit of the brain, exhibiting a wide range of structural, protein expression, and functional varieties that enable the formation of highly specialized connections between neurons (Zucker and Regehr, 2002; Harris and Littleton, 2015; Wichmann and Kuner, 2022). Synapses in the CNS can be broadly divided into two categories: excitatory and inhibitory, both of which play an important role in the formation of neuronal networks. (Wichmann and Kuner, 2022). Over the past few decades, extensive studies have been dedicated to the characterization of synapses. Despite significant progress made in this field, numerous aspects require further elucidation. In the following chapter, I will center my focus on the glutamatergic synapses formed between the dentate gyrus granule cells (DGCs) and CA3 pyramidal cells (PCs) through the mossy fibers (MFs). I will describe the impact of ADAM10 activity, a protein highly enriched in MF-CA3 synapses, on synaptic transmission and plasticity.

In a second chapter I will mainly focus on excitatory synapses formed between Schaffer collateral and CA1 pyramidal neurons. I will discuss structural morphology, molecular composition, stability, and plasticity of glutamatergic synapses formed directly in the dendritic shaft and compare them with spine synapses.

2.1.1 ADAM10 is highly expressed at hippocampal mossy fiber glutamatergic terminals where it localizes to presynaptic vesicles.

ADAM10 is a transmembrane protein that belongs to the ADAM protein family. ADAM10 is a protease that cleaves a variety of cell surface proteins, including adhesion molecules and receptors, and plays a crucial role in various physiological processes of development, tissue homeostasis, hippocampal neurogenesis and many others (Saftig and Lichtenthaler, 2015). Although the function of ADAM10 is well investigated at the postsynaptic compartment of hippocampal synapses (Malinverno *et al.*, 2010; Marcello *et al.*, 2019), recent studies suggest ADAM10 may also have presynaptic functions (Lundgren *et al.*, 2015, 2020; Cozzolino *et al.*, 2021). To address the question of subcellular ADAM10 localization in the hippocampus, immunofluorescence and DAB staining were performed using an antibody, which specifically binds to the C-terminus of ADAM10 that is oriented towards the cytosol (Fig. 5A). DAB staining for electron microscopy (EM) performed in a wild type (wt) mouse brain revealed that ADAM10 is strongly enriched in MFs (Fig.5B). The MF axons are characterized by their giant presynaptic mossy fiber bouton (MFB) typically coupled to a postsynaptic component known as thorny excrescence. EM of MF terminals shows ADAM10-DAB staining localized at the presynaptic MFB opposing the postsynaptic thorny excrescence (Fig. 5C, pink arrows), and cannot be found when using an ADAM10 antibody-lacking control (Fig. 5D, yellow arrows). Next, to get better localization of ADAM10 at the glutamatergic MF terminals, immunogold-EM labeling was performed. ADAM10 was found on synaptic vesicles with the cytosolic side oriented outside as the gold particle was located on the outer part of the vesicle membrane (Fig. 5E).

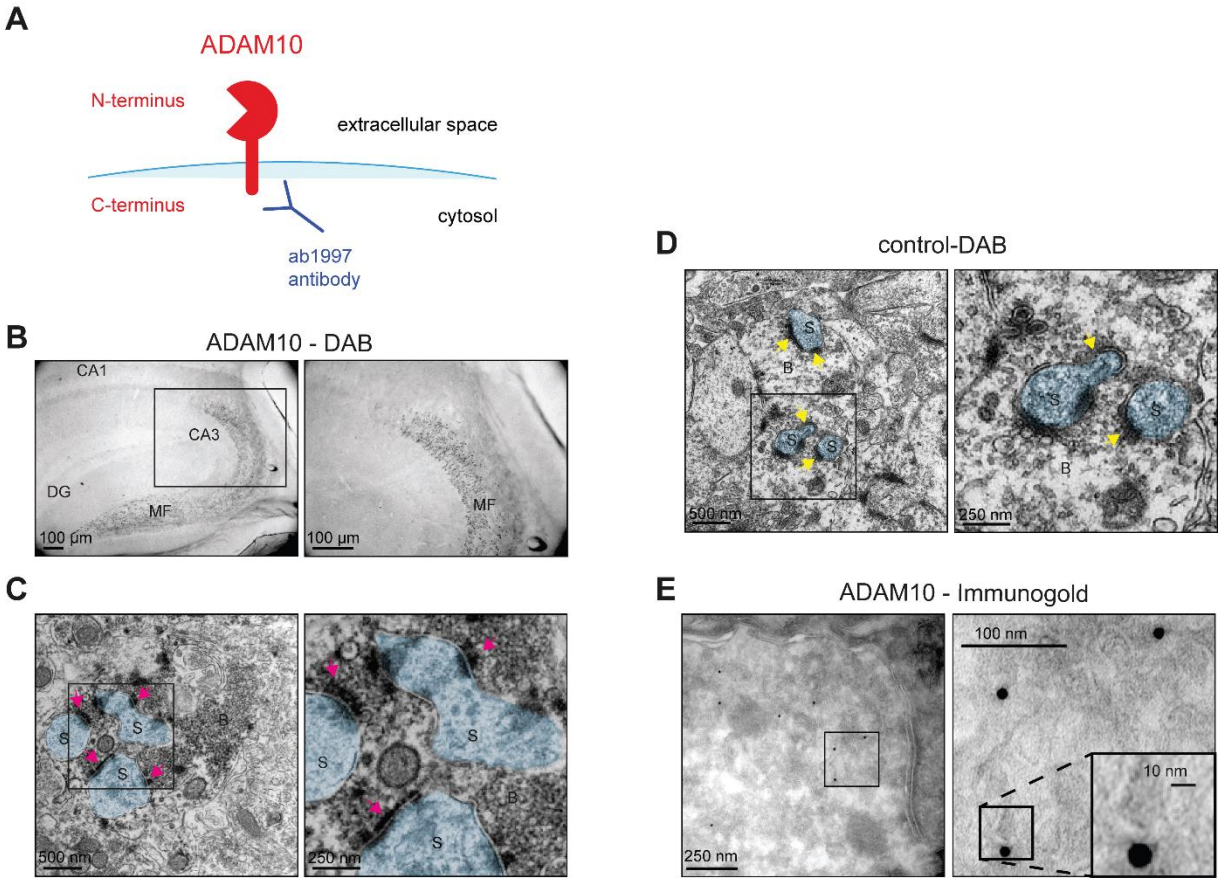

Figure 5: ADAM10 is enriched in hippocampal mossy fibers and localized at presynaptic vesicles.
(A) Scheme of ADAM10 at the synaptic membrane with indicated ADAM10 antibody ab1997 binding epitope. **(B)** DAB staining of ADAM10 in adult wt mouse hippocampus shows strong enrichment of ADAM10 in mossy fibers. DG: dentate gyrus; MF: mossy Fibers. **(C)** High magnification of ADAM10 DAB staining in MF-CA3 synapses. Note the strong ADAM10 localization to the presynaptic site (pink arrow). S: dendritic spine. B: mossy fiber bouton. **(D)** High magnification of control DAB staining (without primary antibody) in MF-CA3 synapses. Note the lack of DAB staining at presynaptic membrane (yellow arrowhead). S: dendritic spine. B: mossy fiber bouton. **(E)** Immunogold EM of P21 wt mouse hippocampal mossy fibers. Gold particles localize to the outside of vesicles, as the antibody detects ADAM10's C-terminus.

To gather additional information regarding the association of ADAM10 with excitatory synapses, immunostainings of ADAM10 in combination with different pre- and postsynaptic markers in mature rat hippocampal cultures at DIV17 were conducted. Subsequent analysis of synaptic sites in mature neurons via stimulated emission depletion (STED) nanoscopy revealed that ADAM10 is primarily localized to the presynapse, as

indicated by its strong co-localization with the presynaptic marker bassoon and opposing postsynaptic scaffolding protein SHANK3 (Fig. 6A). Line profile analysis, a method employed to examine the spatial correlation between two or more signals along a particular axis or line, was used to further investigate the localization of ADAM10 in relation to pre- and postsynaptic components. This analysis suggests that ADAM10 is situated closer to the presynaptic site compared to the postsynaptic site, as there is a pronounced spatial intensity correlation between ADAM10 and bassoon, while the spatial intensity correlation between ADAM10 and SHANK3 is less strong (Fig. 6B). In summary, the colocalization analysis provides relevant evidence for the presynaptic localization of ADAM10 at the MF-CA3 excitatory synapses, which may aid in the understanding of its role in synaptic signaling.

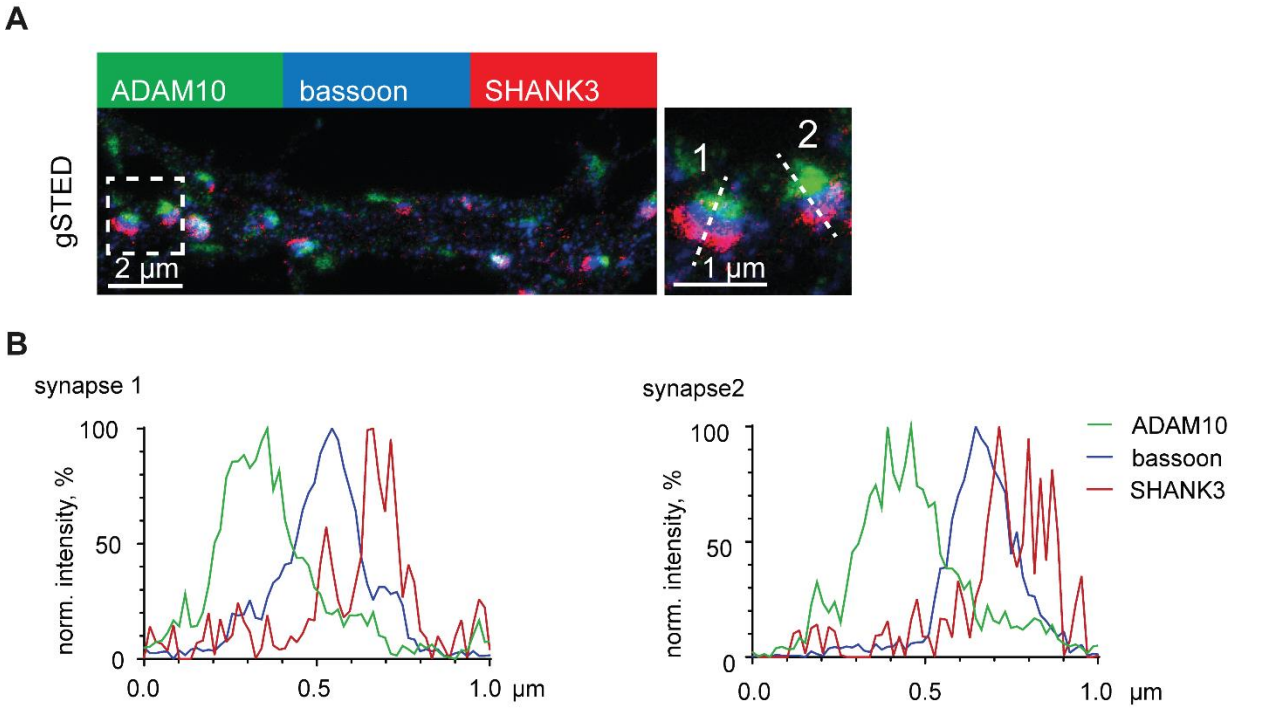

Figure 6: ADAM10 is strongly enriched at presynaptic sites and is present at the excitatory synapses.
(A) Representative gated STED image of mature rat hippocampal primary neurons (DIV17) stained for ADAM10 (green), the presynaptic scaffold protein bassoon (blue), and the postsynaptic scaffold SHANK3 (red). Box indicates position of zoom-ins. **(B)** Line profiles showing co-localization of ADAM10 and SHANK3 with the presynaptic (bassoon, blue) site. 0.5 px Gaussian blur filter applied to gated STED image to remove speckle noise without major change in signal intensities. Figure is provided by Dr. Julia Bär.

2.1.2 ADAM10 is required for expression of presynaptic plasticity at hippocampal MF-CA3 PC glutamatergic synapses

MF-CA3 PC glutamatergic synapses are known to exhibit a low probability of neurotransmitter release (Lawrence, Grinspan and McBain, 2004) and significant facilitation (Salin *et al.*, 1996; Rebola, Carta and Mulle, 2017), which distinguishes them from other hippocampal synapses and allows for sparse coding and pattern separation. Because ADAM10 is highly expressed at MF terminals, the question of its contribution in presynaptic plasticity comes up. To test this, I performed a series of *ex vivo* electrophysiological extracellular recordings using hippocampal acute slices of P20 ADAM10 conditional knock out (cKO) and wt mice.

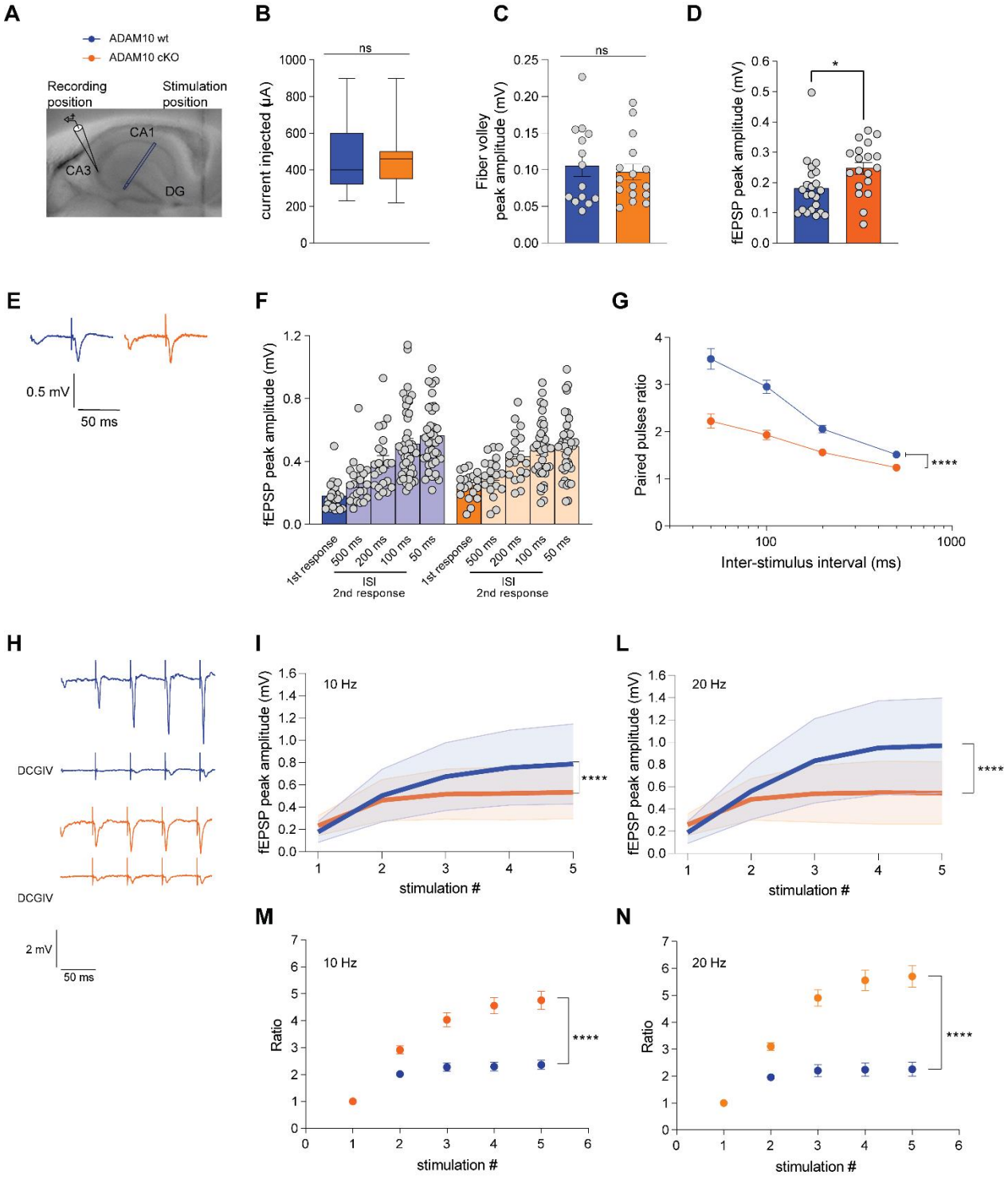

Figure 7: Lack of ADAM10 leads to impairment of hippocampal mossy fiber short term plasticity.

(A) Image of an acute hippocampal slice with indicated electrode positions for stimulating the mossy fibers (MF) in blue, and field excitatory extracellular recordings from dendritic region of CA3 area in black. **(B)** Box plots showing the average intensity current required to generate the Faction potentials. There is not a significant difference found between genotypes. Student's

unpaired t-test (p = 0.8716). n = 19 slices from 6 mice (wt); n = 19 slices from 5 mice (ADAM10 cKO). **(C)** Mean amplitude of fiber volley indicating the activation of presynaptic fibers. There was no significant difference between genotypes. Student's unpaired t-test. p = 0.6316. n = 14 slices from 6 mice (wt); n = 16 slices from 5 mice (ADAM10 cKO). Data are presented as mean +/- SEM. **(D)** field Excitatory Post Synaptic Potential (fEPSP) amplitude measured after the first stimulus was delivered. ADAM10 cKO mice show a slight increase of the initial synaptic response significantly different in comparison to wt mice. Student's unpaired t-test. *p = 0.0215. n = 22 slices from 6 mice (wt); n = 19 slices from 5 mice (ADAM10 cKO). Data are presented as mean +/- SEM. **(E)** Representative traces of fEPSP wt (blue) and ADAM10 cKO (orange) mice generated by pairing two stimuli at 50 ms apart from each other. **(F-G)** Amplitude of the first and the second fEPSP responses at different frequencies (F). The ADAM10 cKO show decreased short-term facilitation as also confirmed by quantitative analysis of the paired pulse ratio shown in (G). Two-way RM ANOVA with Šídák's multiple comparisons test. ****p < 0.0001. n = 18 slices from 6 mice (wt); n = 19 slices from 5 mice (ADAM10 cKO). Data are represented as mean +/-SEM. **(H)** Example traces of train facilitation at 20 Hz in wt (blue) and ADAM10 cKO (orange). Application of the group II mGluR agonist DCG-IV shows loss of response to prove mossy fiber origin of detected signal. **(I-L)** Plot of cumulative fEPSP amplitude in response to train facilitation at 10 Hz and 20 Hz frequencies. Two-way RM ANOVA with Šídák's multiple comparisons test. ****p < 0.0001. n = 18 slices from 6 mice (wt); n = 19 slices from 5 mice (ADAM10 cKO). **(M-N)** Quantification of the ratio calculated from the fEPSP amplitudes measured in response to train facilitation. ADAM10 cKO slices show depressed ratio calculated in response to train stimulation at 10 Hz and 20 Hz. Two-way RM ANOVA with Šídák's multiple comparisons test. ****p < 0.0001. n = 18 slices from 6 mice (wt); n = 19 slices from 5 mice (ADAM10 cKO). Data are represented as mean +/-SEM.

Action potentials were evoked at the MFs while field excitatory postsynaptic potentials (fEPSP) were recorded in the *stratum radiatum* of the CA3 region (Fig. 7A). The electrical current required to induce presynaptic depolarization at the MFs and evoke postsynaptic field potentials was found to be similar for both experimental groups (Fig. 7B). The amplitude of the fiber volley remained unchanged, indicating that there was likely no altered fiber excitability (Fig. 7C). However, after the first evoked stimulus, the amplitude of the fEPSPs was significantly increased in ADAM10 cKO compared to wt mice (wt mean: 0.8 mV, cKOs mean: 0.24 mV; Fig. 7D). To determine whether this increase was caused by presynaptic impairments, the probability of neurotransmitter release (P_r) was estimated by analyzing two forms of short-term $_p$lasticity: paired pulse facilitation (PPF) and train frequency facilitation (FF; Salin *et al.*, 1996; Jackman and Regehr, 2017). The

PPF was assessed using pairs of closely spaced presynaptic stimulations delivered at different interstimulus intervals (500, 200, 100, 50 ms). In both experimental groups, synaptic facilitation at different interstimulus intervals (ISI) was observed (Fig. 7E). However, ADAM10 cKO mice exhibit depressed facilitation in paired pulse (Fig. 7F) as well as in response to a stimulus train (5 stimuli delivered at 100-50 ms ISI; Fig. 7I-L). The ratio analysis confirmed that facilitation was strongly depressed in a way that was more than two-fold lower in ADAM10 cKOs compared to WT (two-way ANOVA test $p < 0.001$; Fig. 7G), as also observed in the ratio calculated from repetitive stimulation (two-way ANOVA test $p < 0.001$; Fig. 7M-N). The MF origin of the signal was systematically confirmed at the end of each experiment by the subsequent loss of response after the perfusion with the group II mGluR agonist DCG-IV (Yoshino *et al.*, 1996) (Fig. 7H). Overall, this data further suggests that ADAM10 plays a role in short term plasticity at MF-CA3 synapses and contributes to synaptic signaling. To evaluate if the proteolytic activity of ADAM10 is also necessary for presynaptic facilitation the enzymatic activity of ADAM10 was acutely inhibited in the wt mice by bath application of the selective ADAM10 inhibitor GI254023X (Hoettecke *et al.*, 2010) during slice equilibration (Fig. 8A). The experiment did not reveal any inhibitor-induced changes in fiber excitability (Fig. 8B), amplitude of fiber volley as well as fEPSP (Fig. 8C-D), suggesting that the presence of ADAM10 protein *per se* rather than the enzymatic activity is important for MF-CA3 short-term plasticity. Furthermore, the ratio measured from paired pulse (Fig. 8E-F) or train facilitation (Fig. 8I-L) as well as the fEPSP amplitudes (Fig. 8G-H) were also unchanged suggesting that proteolytic activity of ADAM10 is not contributing to synaptic facilitation mechanisms.

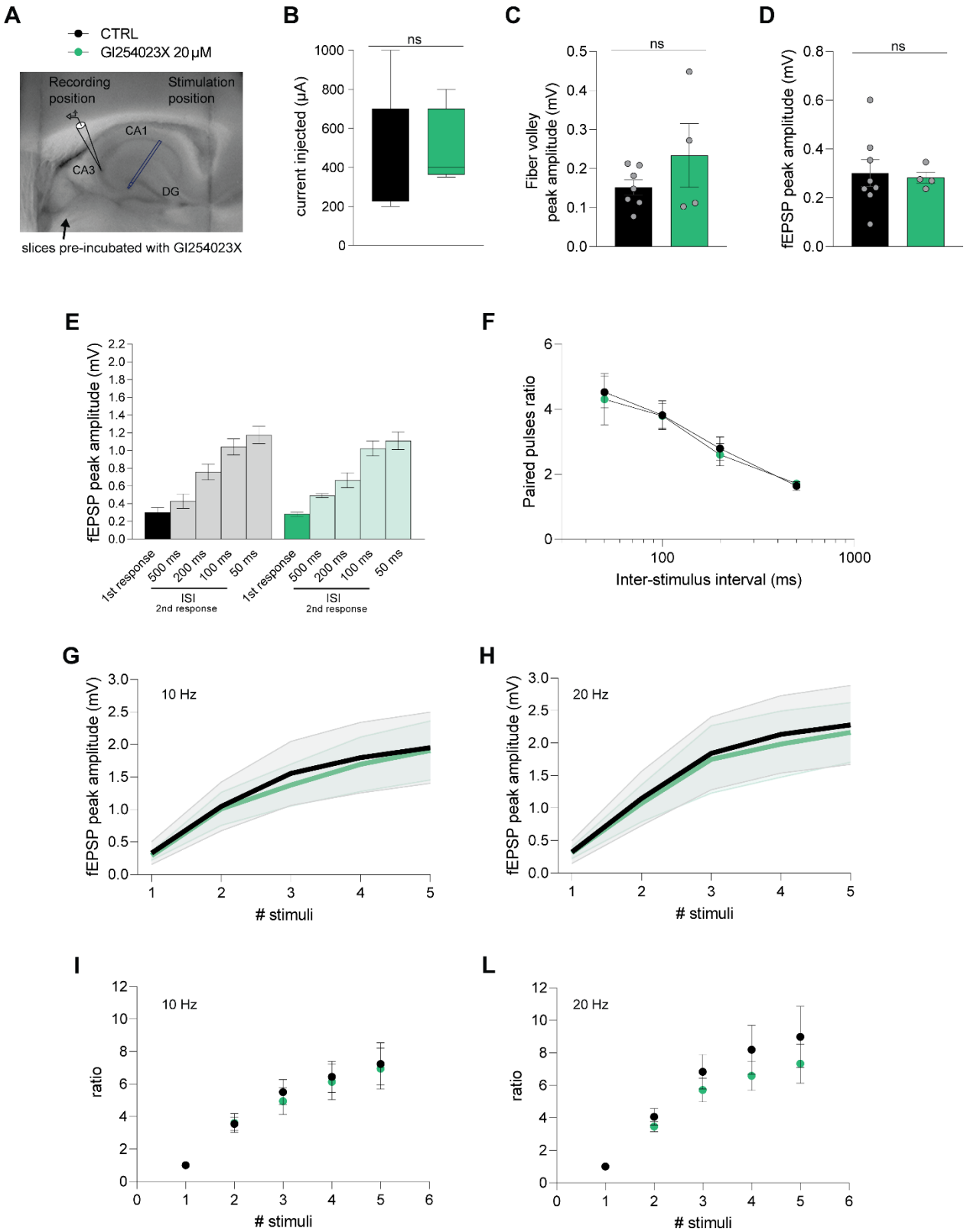
A
CTRL
GI254023X 20 µM
Recording position
Stimulation position
CA1
CA3
DG
slices pre-incubated with GI254023X
B
ns
current injected (µA)
C
ns
Fiber volley peak amplitude (mV)
D
ns
fEPSP peak amplitude (mV)
E
fEPSP peak amplitude (mV)
1st response
500 ms
200 ms
100 ms
50 ms
ISI
2nd response
F
Paired pulses ratio
Inter-stimulus interval (ms)
G
10 Hz
fEPSP peak amplitude (mV)
stimuli
H
20 Hz
fEPSP peak amplitude (mV)
stimuli
I
10 Hz
ratio
stimuli
L
20 Hz
ratio
stimuli

Figure 8: ADAM10 enzymatic inhibition does not influence mossy fiber short-term plasticity.

(A) Image of an acute hippocampal slice with indicated electrode positions for stimulating the mossy fibers (MF) in blue, and field excitatory extracellular recordings from dendritic region of CA3 area in black. The recordings were performed on the slices treated for 3 hours with 20 µM GI254023X (ADAM10 inhibitor). **(B)** Box plots showing the average of intensity currents required to generate action potentials. The current injected to evoke presynaptic action potentials is not significantly different after treatment. Student's unpaired t-test ($p = 0.8813$). n = 8 slices from 2 mice (CTRL); n = 4 slices from 1 mouse (CTRL-GI254023X). **(C)** Fiber volley amplitudes indicating the activation of presynaptic fibers. No difference is shown after treatment. Student's unpaired t-test ($p = 0.2359$). n = 8 slices from 2 mice (CTRL); n = 4 slices from 1 mouse (CTRL-GI254023X). **(D)** fEPSP amplitude measured after the first stimulus was delivered. No difference was shown at the initial synaptic response. Student's unpaired t-test ($p = 0.8156$). n = 8 slices from 2 mice (CTRL); n = 4 slices from 1 mouse (CTRL-GI254023X). **(E-F)** Amplitude of the first and the second fEPSP responses at different frequencies (E). Application of GI254023X ADAM10 inhibitor does not affect synaptic facilitation as also confirmed by quantitative analysis of the paired pulse ratio shown in (F). Two-way RM ANOVA with Šídák's multiple comparisons test. $p = 0.9346$. n = 8 slices from 2 mice (CTRL); n = 4 slices from 1 mouse (CTRL-GI254023X). Data are represented as mean +/-SEM. **(G-H)** Plot of cumulative fEPSP amplitudes in response to train facilitation at 10 Hz (M) and 20 Hz (N) frequencies. There is not difference in fEPSP amplitude between CTRL and CTRL treated with GI254023X. Two-Way repeated measures ANOVA [$p = 0.9087$ (10 Hz), $p = 0.9652$ (20 Hz)] with Šídák's post hoc analysis for multiple comparison. n = 8 slices from 2 mice (CTRL); n = 4 slices from 1 mouse (CTRL-GI254023X). Data are represented as mean +/-SEM. **(I-L)** Quantification of the ratio calculated from the fEPSP amplitudes measured in response to train facilitation. There is not difference in ratio between CTRL and CTRL-GI254023X. Two-Way repeated measures ANOVA [$p = 0.9843$ (10 Hz), $p = 0.8355$ (20 Hz)] with Šídák's post hoc analysis for multiple comparison. n = 4 slices from 1 mouse (CTRL-GI254023X). Data are represented as mean +/-SEM.

2.1.3 The cytosolic domain of ADAM10 is critical for presynaptic plasticity at MFs

These results raise the question of how ADAM10 could impact synaptic transmission at MFs-CA3PC synapses. The molecular structure of the protein is composed by a N-terminus domain facing the extracellular space and a short C-terminal tail formed by 55 amino acids located in the cytosol (Fig. 9A). This part of ADAM10 contains putative protein interaction sites, such as PxxP motifs (Ebsen *et al.*, 2014). We reasoned that the C-terminus domain of

ADAM10 could play an important role in MFs plasticity. Therefore, we disturbed the C-terminus interactions using a cell-permeable tat-peptide corresponding to mouse ADAM10 amino acids 709-730 (ADAM10-tat, Fig.9A) which contains the known PxxP motifs. In addition to ADAM10 tat-peptide we used a control tat-peptide where prolines were mutated to alanines to observe if ADAM10 cytosolic interactions are required in MF short-term plasticity. To this end, I performed a similar set of electrophysiological extracellular recordings as described above (Figure 7) using acute brain slices of P20-25 wt mice incubated either with ADAM10 tat or control tat-peptides. Thus, I systematically characterized the effect of the peptides on short-term plasticity at MFs-CA3 synapses. The experiments were performed as following: soon after preparation the brain slices were incubated in ~200 ml of artificial cerebrospinal fluid (aCSF) containing 3 µM concentration of either control-tat or ADAM10-tat peptides for about 3 hours, then the extracellular field recordings were performed. The electrical current required to induce depolarization at the MFs and evoke field potentials was similar in both treatments (Fig. 9B). The amplitude of the fiber volley and the fEPSP remained also unchanged, likely meaning that fiber excitability and P_r were unaffected (Fig. 9C-D). However, a significant short-term facilitation deficiency of MF-CA3 synapses in slices incubated with ADAM10-tat but not with control-tat peptides was observed (Fig. 9F), which was confirmed by the ratio analysis (Two-way ANOVA test $p < 0.0001$; Fig. 9G). As for the ADAM10 cKOs, the fEPSP amplitude was not properly facilitating after repetitive train stimulation in slices incubated with ADAM10 tat-peptide (Fig. 9I-L) generating a similar phenotype (Two-way ANOVA test $p < 0.0001$; Fig. 9M-N). The MF origin of the signal was systematically confirmed at the end of each experiment by the subsequent loss of response after the perfusion of the group II mGluR agonist DCG-IV (Fig. 9H).

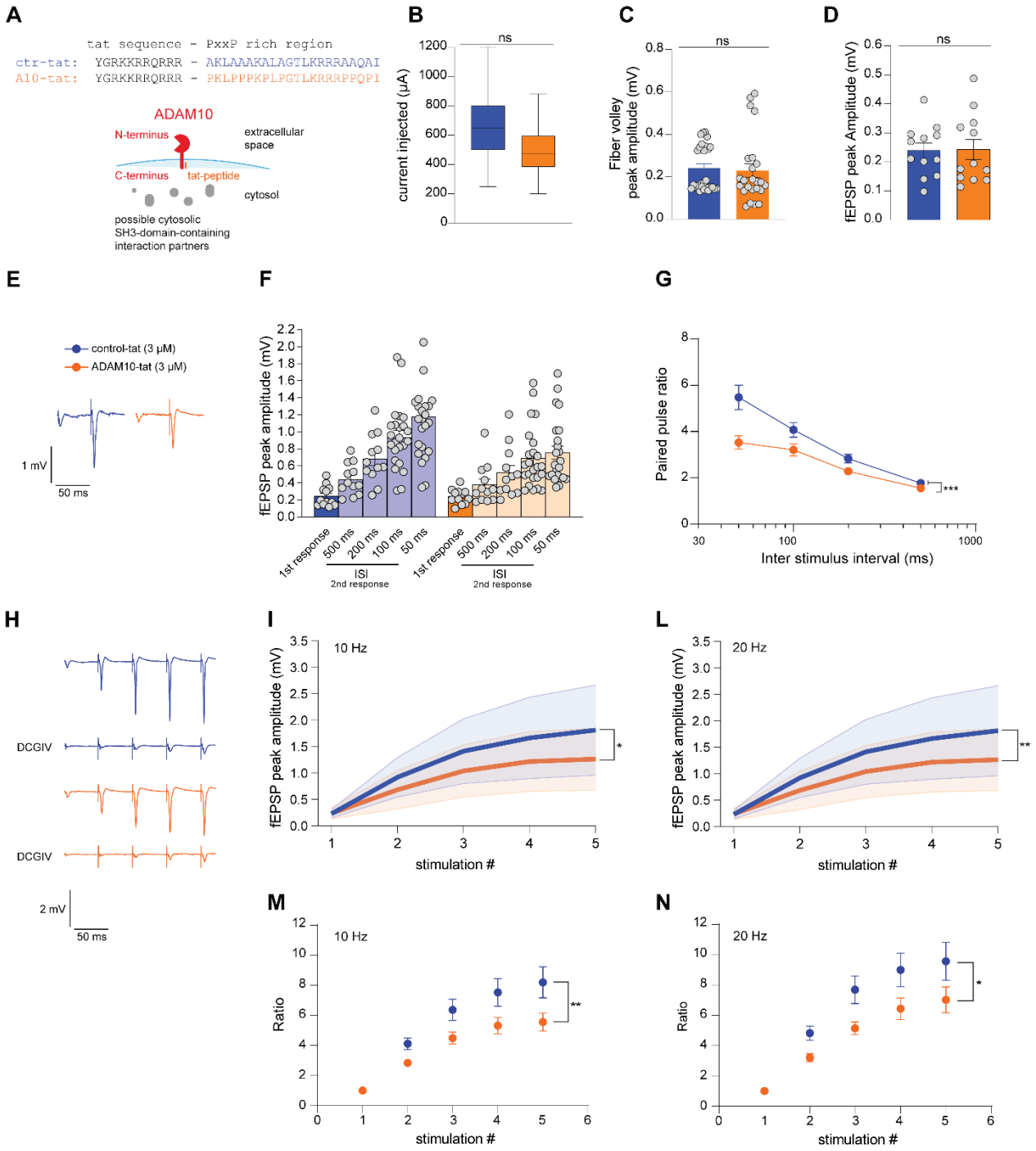

Figure 9: ADAM10 C-terminus is required for mossy fiber short-term plasticity.
(A) Experimental scheme: tat-peptide sequences used for acute hippocampal slices treatment to test plasticity at mossy fiber. **(B)** Box plots showing the average of intensity currents required to generate the action potentials. The current injected to evoke presynaptic action potentials is not significantly different after treatment. Student's unpaired t-test (p = 0.0962). n = 12 slices from 3 mice (CTRL-TAT); n = 12 slices from 3 mice (ADAM10-TAT). **(C)** Fiber volley amplitudes indicating the activation of presynaptic fibers. No difference is observed after treatment. Student's unpaired t-test. p = 0.7680. n = 12 slices from 3 mice (CTRL-TAT); n =

12 slices from 3 mice (ADAM10-TAT). Data are presented as mean +/- SEM. **(D)** field Excitatory Post Synaptic Potential (fEPSP) amplitude measured after the first stimulus was delivered. No difference was shown at the initial synaptic response. Student's unpaired t-test. p = 0.9493. n = 12 slices from 3 mice (CTRL-TAT); n = 12 slices from 3 mice (ADAM10-TAT). Data are presented as mean +/- SEM. **(E)** Representative traces of fEPSP CTRL-TAT (blue) and ADAM10-TAT (orange) mice generated by pairing two stimuli at 50 ms apart from each other. **(F-G)** Amplitude of the first and the second fEPSP responses at different frequencies (F). Application of ADAM10 C-terminus targeted tat-peptide leads to impairment in facilitation as also confirmed by quantitative analysis of the paired pulse ratio shown in (G). Two-way RM ANOVA with Šídák's multiple comparisons test. ***p < 0.0001. n = 12 slices from 3 mice (CTRL-TAT). n = 12 slices from 3 mice (ADAM10-TAT). Data are represented as mean +/-SEM. **(H)** Example traces of train facilitation at 20 Hz in CTRL-TAT (blue) and ADAM10-TAT (orange). Application of the group II mGluR agonist DCG-IV shows loss of response to prove mossy fiber origin of detected signal. **(I-L)** Plot of cumulative fEPSP amplitudes in response to train facilitation at 10 Hz (M) and 20 Hz (N) frequencies. Two-way RM ANOVA with Šídák's multiple comparisons test. *p = 0.0143 (10 Hz); **p = 0,0017 (20Hz). n = 12 slices from 3 mice (CTRL-TAT); n = 12 slices from 3 mice (ADAM10-TAT). **(M-N)** Quantification of the ratio calculated from the fEPSP amplitudes measured in response to train facilitation. ADAM10 tat-peptide treatment show lower ratio compared to CTRL-TAT treatment in response to train stimulation at 10 Hz (I) and 20 Hz (L). Two-Way repeated measures ANOVA [*p = 0.03 (10 Hz), *p = 0.04 (20 Hz)] with Šídák's post hoc analysis for multiple comparison (*p = 0.03 compared to control-tat). Data are represented as mean +/- SEM.

This acute interference indicates that presynaptic facilitation at MF-CA3 synapses could be perturbed by the interaction of ADAM10 C-terminus with presynaptic partners. Recently, several studies have shown impairments in synaptic facilitation caused by the absence or misfunction of syt-7 and, furthermore, it's role has been implicated in the regulation of presynaptic calcium dynamics at MF synapses (Jackman *et al.*, 2016; Huson and Regehr, 2020). Its importance in MFs plasticity can be explained by its special function as Ca^{2+} sensor engaged to facilitate the neurotransmitter release by increasing the probability of vesicle fusion (Sugita *et al.*, 2001; Bacaj *et al.*, 2013), or possibly promoting vesicle replenishment (Liu, Bai, Hui, *et al.*, 2014). Thus, a hypothetical model where ADAM10 interacting with syt-7 might regulate presynaptic processes at MF-CA3 synapses was developed (Figure 10), however, this needs to be investigated further.

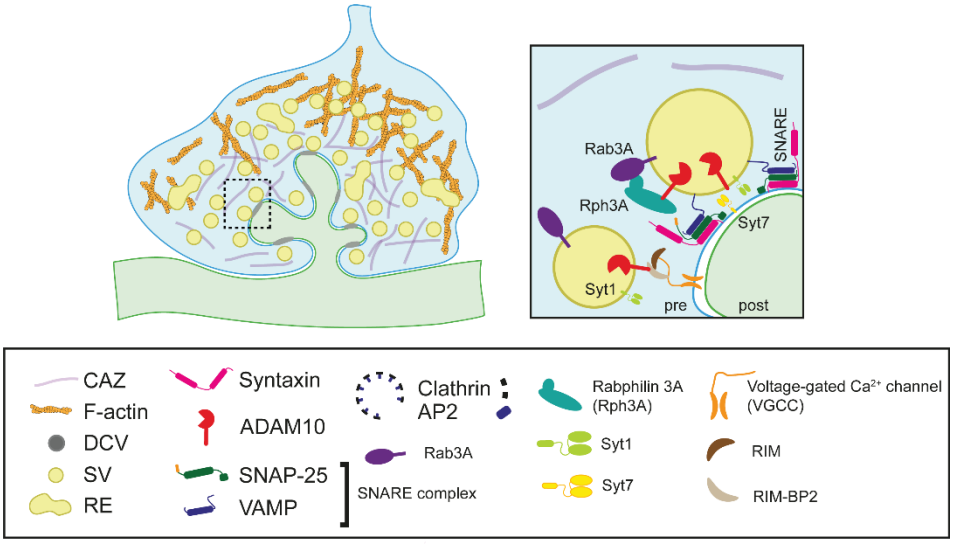

Figure 10: Schematic hypothetical facilitation model at the mossy fiber terminals which could depend on ADAM10 synaptotagmin-7 interaction.

The illustration shows the giant presynaptic MF bouton contacting the postsynaptic thorny excrescence containing multiple contact sites. A subset of proteins allocated to the synaptic contact is shown in the right panel. A summary legend is shown in the panel below. Interaction of syt-7 with ADAM10 could explain the observed deficits in facilitation when ADAM10 was missing or perturbed at the synapse.

2.2 Deciphering the structure and function of glutamatergic shaft synapses

The data presented here has been generated with the help of Arie Maeve Brückner, a bachelor internship student who contributed in developing the method of analysis for this part of the project.

Hippocampal glutamatergic synapses show a great degree of heterogeneity of their molecular composition, structural features, and functional properties. This diversity is important for the hippocampus to respond rapidly and efficiently to a multitude of stimuli, as well as to encode and consolidate complex information. I previously focused on the MF-CA3 synapses, and in the next chapter I will focus on glutamatergic synapses formed between the axons of the Schaffer collateral fibers (SCs) projecting from the CA3 PCs to the CA1 PCs. In contrast to MF-CA3 synapses, which exhibit multiple active zones per bouton, a typical hippocampal SC-CA1 synapse contains only one active zone per bouton (Wichmann and Kuner, 2022). In mature neurons, the majority of hippocampal excitatory synapses are located at the tip of dendritic spines, however, a small percentage can be found directly on the dendritic shafts (Richter *et al.*, 1999; Reilly, Hanson and Phillips, 2011; van Bommel *et al.*, 2019). One of the main key points of my project aims to further characterize the excitatory synapses located on the dendritic shafts of mature primary neurons in terms of their nanostructure organization and function.

To this end, I used mature (3-4 weeks in culture) organotypic hippocampal slices to estimate the frequency distribution of excitatory shaft synapses in analogy to spine synapses along the dendritic arbor of CA1 pyramidal neurons co-transfected with mRuby3 (volume marker) and PSD95.FingR-GFP (excitatory postsynaptic marker), a recombinant probe for visualizing endogenous PSD95 in living neurons (Gross *et al.*, 2013). The overexpression of mRuby3 allowed for the clear identification of the main apical shaft structure and for distinguishing two distinct morphological cell types, bifurcated and unidirectional, as previously observed by Benavides-Piccione and colleagues in human and mouse

(Benavides-Piccione *et al.*, 2020) (Fig. 11A). It further allowed the distinction of dendritic segments and aspinous shaft compartments, as well as dendritic spines (as seen in panel 13A-B) protruding from all dendritic branches. I counted the total number of dendritic spines and measured the density normalized to a dendritic length of 10 µm. Interestingly, bifurcated neurons exhibit a significantly greater number of dendritic spines compared to unidirectional neurons (Mann Whitney test $p = 0.0091$; Fig. 11B). The difference in the number of spines between the two neuronal types was also observed when examining each dendritic branch separately: basal, main, oblique and tuft dendrites (Two-way ANOVA basal dendrites: $p = 0.0024$; main dendrites: $p < 0.0001$; oblique dendrites: $p = 0.0080$; tuft dendrites: $p = 0.0002$; Fig.11D). Interestingly, the main apical shaft of unidirectional neurons is the segment where the fewest dendritic spines have been observed. Collectively, the significant difference in spine numbers between unidirectional and bifurcated neurons represents a novel morphological feature of this CA1 neuron subpopulation, raising the question of whether this might reflect to functional properties in transmission.

2.2.1 Distribution of glutamatergic synapses in dendrites of excitatory hippocampal CA1 neurons

The previous chapter established a comprehensive morphological analysis and classification of hippocampal CA1 neurons. However, a detailed description of the distribution of PSD95 throughout distinct neuronal morphologies and between different dendrites of CA1 pyramidal cells is largely missing. To provide such a description, CA1 neurons were transiently transfected with PSD95.FingR-GFP detecting endogenous PSD95 and the number of spine and shaft synaptic sites was analyzed in both types of neurons. Interestingly, the total number of spines containing PSD95 was overall higher in bifurcated neurons than in unidirectional neurons (Mann Whitney test $p = 0.0008$; Fig. 11C), and this observation was consistent for each analyzed dendritic segment (two-way ANOVA basal dendrites: $p = 0.0139$; main dendrites: $p < 0.0001$; oblique dendrites: $p = 0.0363$; tuft dendrites: $p = 0.0442$; Fig. 11E). Nevertheless, the majority of dendritic protrusions contain

PSD95 in all distinguished dendritic branches of both bifurcated and unidirectional cell types (Fig. 11F-G; data overview in table 1).

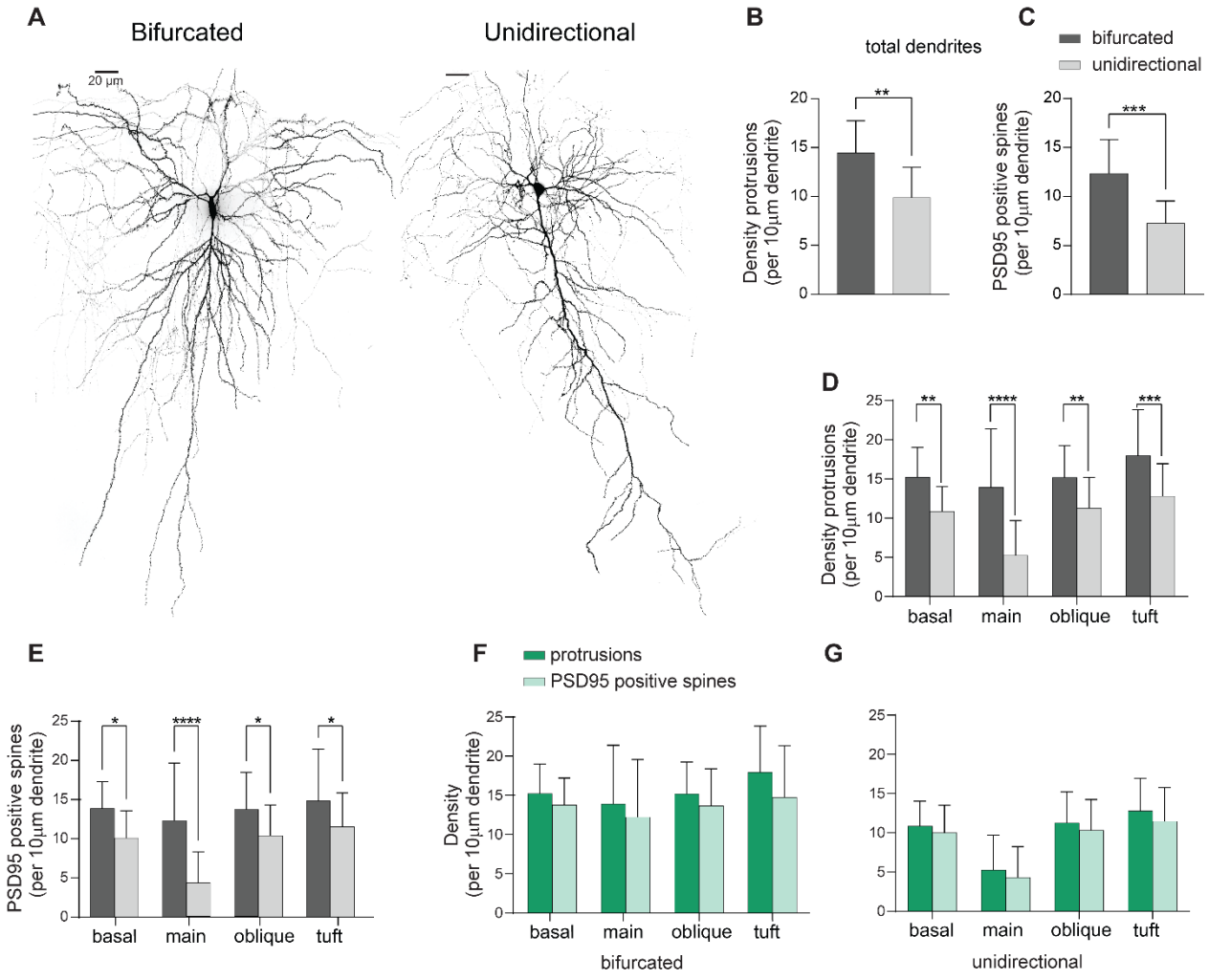

Figure 11: Distinct morphological pattern of hippocampal CA1 pyramidal neuron apical dendrites.

(A) Representative maximum z-projections of confocal images showing apical dendritic structures, with a branching main shaft namely bifurcated (left) and without branching main shaft namely unidirectional (right), of CA1 pyramidal neurons transiently co-transfected at DIV21 for 48-72 hours with mRuby3 (cell fill) by using single cell electroporation. Confocal images, objective X63 oil; voxel size 0,108 x 0,108 x 0,5µm3. Scale 20µm. **(B)** Description of overall spine density of bifurcated and unidirectional neurons. Bifurcated neurons show a higher degree of dendritic protrusions in comparison to unidirectional neurons. Mann–Whitney U-test. **P = 0.0091. n = 24 dendritic segments associated to 8 bifurcated neurons. n = 33 dendritic segments associated to 11 unidirectional neurons. **(C)** Quantification of overall spine containing PSD95 density of bifurcated and unidirectional neurons. The number of the spines containing PSD95 is much higher in bifurcated neurons than unidirectional neurons. Mann–Whitney U-test. ***P = 0.0008. n = 24 dendritic segments associated to 8 bifurcated neurons.

n = 33 dendritic segments associated to 11 unidirectional neurons. **(D)** Description of spine density in relation with distinct dendritic branches of bifurcated and unidirectional neurons. Two-way ANOVA with Šídák's multiple comparisons test. **P = 0.0024 (basal dendrites); ****P < 0.0001 (main shaft); **P = 0.0080 (oblique dendrites); ***P = 0.0002 (tuft dendrites). n = 24 dendritic segments associated to 8 bifurcated neurons. n = 33 dendritic segments associated to 11 unidirectional neurons. **(E)** Quantification of PSD95 positive spine density along dendritic segments with relation to bifurcated and unidirectional neurons. Two-way ANOVA with Šídák's multiple comparisons test. *P = 0.0139 (basal dendrites); **** P < 0.0001 (main dendrite); *P = 0.0363 (oblique dendrites); *P = 0.0442 (tuft dendrites). n = 24 dendritic segments associated to 8 bifurcated neurons. n = 33 dendritic segments associated to 11 unidirectional neurons. **(F-G)** Bar graphs showing density of protrusions and spines containing PSD95 across dendritic segments relative to bifurcated neurons in (F) and unidirectional neurons in (G); n = 24 dendritic segments associated to 8 bifurcated neurons. n = 33 dendritic segments associated to 11 unidirectional neurons. Data are presented as mean ± SD and no significant differences are present using Two-way ANOVA with Šídák's multiple comparisons test; P=0,8503 (bifurcated); P= 0,9878 (unidirectional).

Notably, a high rate of PSD95 expression in spines has been already reported in previous studies (Petralia *et al.*, 2005; Reilly, Hanson and Phillips, 2011; Mardones *et al.*, 2019), however, an additional description of how PSD95 is distributed throughout distinct neuronal morphologies and between different dendrites of CA1 pyramidal cells is largely missing. In contrast to dendritic spines, the analysis of shaft synapses presents the difficulty of distinguishing between PSD95 positive spines protruding in different z-dimension from the camera and PSD95-positive shaft postsynapses. Consequently, I developed a reliable method to achieve this discrimination by using 3D reconstruction as well as Z-axis plane analysis (see materials and methods). Shafts were identified as PSD95 signals expressing within aspinous dendritic compartments and visible as gray puncta (Fig. 12Aii). To confirm this spine/shaft identification method, representative 3D reconstructions of each dendritic compartment were constructed using the filament tracer tool (Fig. 12Bi), and the PSD95 puncta were detected using the spot detection tool of Imaris microscopy image analysis software (Fig. 12Bii). The rotation of the 3D reconstruction allowed the localization of PSD95 puncta (red spots) in relation to the dendritic body (Fig. 12C-D). The shaft-identifying arrows (filled arrow heads) indicate PSD95 puncta that occur within the dendritic body throughout the rotation of the reconstruction. The circular regions

highlighted prior or subsequently to the focal plane of the dendritic shaft were identified in the reconstruction as protruding dendritic spines (examples indicated by spine-identifying empty arrow heads). This validated the identification method of glutamatergic shaft synapses.

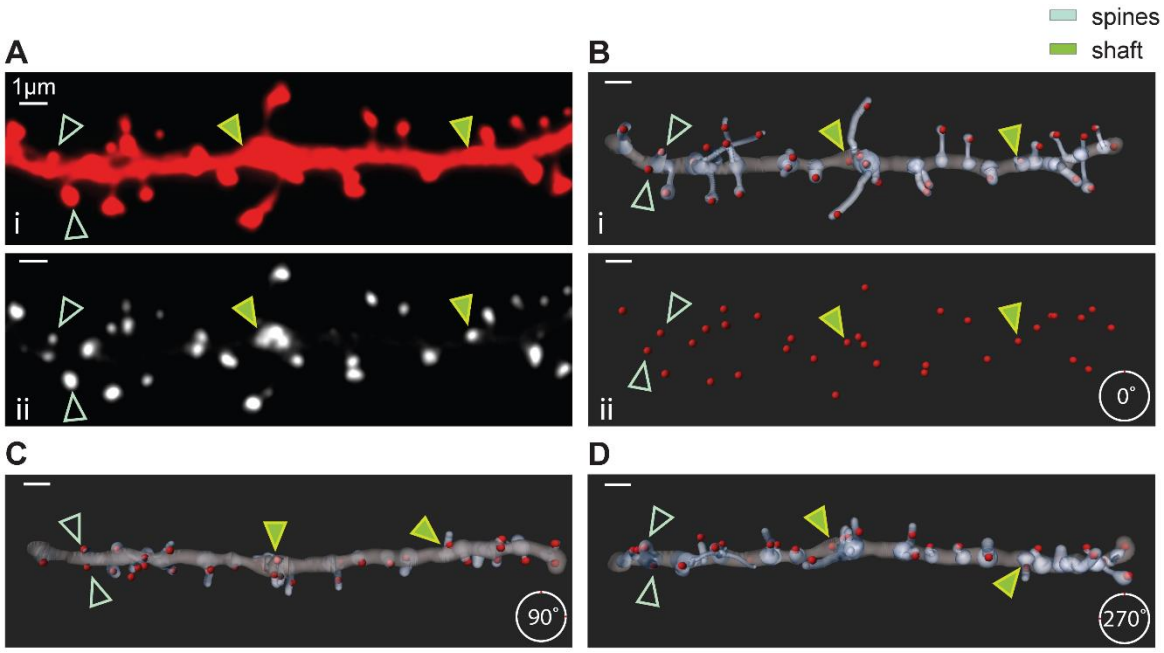

Figure 12: Method of PSD95 positive spine and shaft post-synapses identification validated using three-dimensional reconstruction.
PSD95 positive spine (empty arrow) and shaft postsynapses (filled arrow) are indicated. **(A)** Maximum z-projection of representative oblique dendritic segment from a CA1 pyramidal cell transiently co-transfected for 48-72 hours with mRuby3 (Ai) and PSD95.FingR-GFP (Aii) in organotypic slices at DIV21 by using single cell electroporation. Confocal images, objective X100 oil; voxel size 0,065 x 0,065 x 0,2 μm^3. Scale 1µm. **(B)** (Bi) 3D reconstruction of representative oblique section in image A using filament tracer tool in Imaris software. (Bii) Identification of PSD95 puncta of diameter 0.15-0.8µm with spot detection tool. Dendritic body (gray), spines (light gray) and PSD95 puncta (red). Scale 1µm. **(C)** 90-degree forward rotation of 3D reconstruction of representative oblique section in image A. Scale 1µm. **(D)** 270-degree forward rotation of 3D reconstruction of representative oblique section in image A. Scale 1µm.

Table 1. Density of dendritic spines and spine synapses averaged per 10 μm and distinguished by type of dendritic branches on bifurcated and unidirectional neurons.

Synaptic form	Protrusions		Spine synapses	
	Bifurcated	**Unidirectional**	**Bifurcated**	**Unidirectional**
Overall	14.46	9.88	12.36	7.27
Basal	15.23	10.86	13.92	10.02
Main	13.92	5.25	12.23	4.29
Oblique	15.19	11.28	13.68	10.32
Tuft	17.96	12.79	14.76	11.47

2.2.2 Comparison of shaft synapse densities in bifurcated versus unidirectional CA1 neurons

Next, to have an idea about the density of the shaft synapses in our model system and their distribution along the dendritic branches, I quantified the number of glutamatergic synapses on shafts across all dendritic compartments of both bifurcated and unidirectional neuronal subtypes. The frequency distribution of synaptic shafts overall was similar among neurons (Fig. 13C), and there were no significant differences across dendritic branches except in the main dendritic shaft of bifurcated neurons, where the number of synapses seemed to be generally higher than the main shaft of unidirectional neurons (Fig. 13D). These results raise the question whether the main apical branching pattern could alter the distribution ratio of spine to shaft postsynapses. Therefore, I calculated the percentage of all PSD95 detected signals in spines and shafts. The quantification showed similar distribution in both neuronal types with the ratio in bifurcated neurons approximately 1:4, whereas in unidirectional cells the percentage of shaft synapses was minimally higher. Of the total number of synapses counted approximately 71-74% were dendritic spine synapses and 26-29% were dendritic shaft synapses (Fig. 13E-F), in agreement with the fact that excitatory synapses in mature neurons tend to form synapses in spines and less in the shaft. Finally, I looked to the distribution of positive PSD95 spine and shaft synapses across dendritic

branches. Maximum z-projections of confocal images detected PSD95 signal predominantly from spines and significantly less from the shaft (Fig. 13G-H). However, PSD95 was evenly distributed between spines and shafts only in the main shaft of unidirectional neurons (Fig. 13H). All data are summarized in table 2.

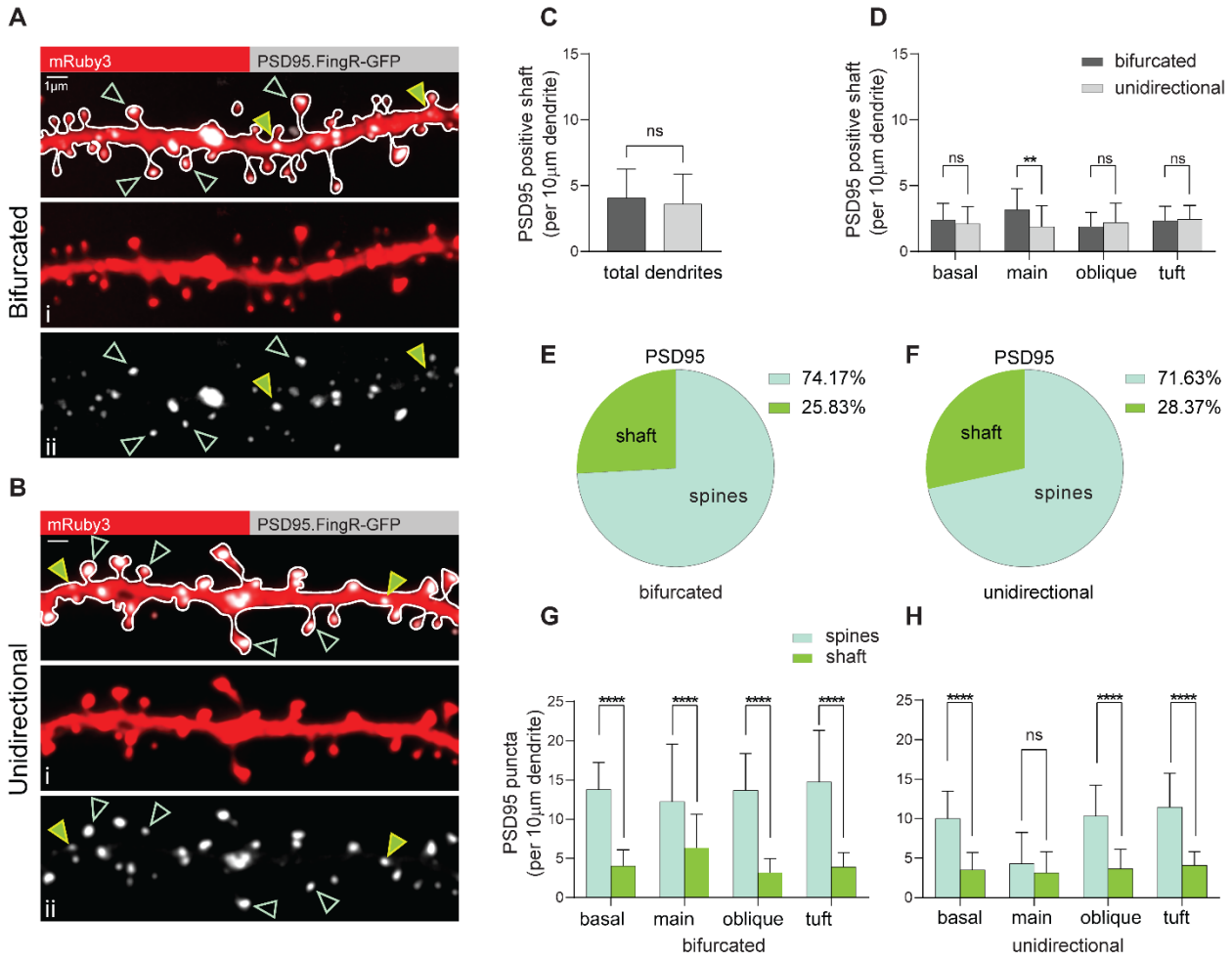

Figure 13: Glutamatergic synapses are mainly located in spines and much less within the shaft of mature CA1 pyramidal cell dendrites.

(A-B) Representative maximum z-projections of a confocal image displaying an oblique dendrite segment of bifurcated CA1 pyramidal neuron (A) and unidirectional neuron (B) transiently co-transfected for 48-72 hours with mRuby3 (Ai; Bi) and PSD95.FingR-GFP as excitatory marker (Aii, Bii) in organotypic slices at DIV21 by using single cell electroporation. PSD95 is distributed within dendritic spines as indicated with empty arrow heads, and shafts compartments indicated with filled arrow heads. Confocal images, objective X100 oil; voxel size 0,065 x 0,065 x 0,2µm^3. Scale 1µm. **(C)** Quantification of PSD95 positive shaft density in bifurcated versus unidirectional CA1 neurons. Bar graphs showing comparable shaft density among neurons. Data are presented as mean ± SD. No significant difference using student's t-test; P= 0,1340. **(D)** Bar graphs showing the average of shaft containing PSD95 density with

relation to different dendrites in bifurcated and unidirectional CA1 neurons. Two-way ANOVA with Šídák's multiple comparisons test. **P = 0.0026 (main dendrite). Data are presented as mean ± SD. **(E, F)** Representation in percentage of the total PSD95 puncta on spines and shafts of mature dendrites of bifurcated and unidirectional CA1 neurons. Most postsynaptic targets are present in the dendritic spines compared to dendritic shafts in both bifurcated neurons (E) and unidirectional neurons (F). **(G)** Description of the PSD95 density on spines versus shafts in association with different dendritic branches of bifurcated neurons. Two-way ANOVA with Šídák's multiple comparisons test. ****P < 0.0001 (basal, main, oblique, tuft dendrites). Data are presented as mean ± SD. **(H)** Description of the PSD95 density on spines versus shafts in association with different dendritic branches of unidirectional neurons. Two-way ANOVA with Šídák's multiple comparisons test. ****P < 0.0001 (basal, oblique, tuft dendrites); P = 0.4923 (main dendrite). Data are presented as mean ± SD. All the quantifications have been performed on bifurcated neurons, from 27 dendritic segments in 8 cells. Unidirectional neurons, from 33 dendritic segment in 11 cells.

2.2.3 Comparison of PSD95.FingR-GFP fluorescence intensities in spine versus shaft synapses in bifurcated and unidirectional CA1 neurons

Upon seeing that the density of synapses on dendritic spines in all dendritic branches of bifurcated neurons, particularly in the main apical shaft, was significantly higher compared to unidirectional neurons, questions about the parameter of synaptic strength rise up. One hypothesis is that a reciprocal relationship exists between synaptic density and strength among different types of neurons. Furthermore, the size of the postsynaptic density (PSD) has been shown to be strongly associated with synaptic strength (Dosemeci *et al.*, 2016). Therefore, quantification of the intensity values was performed in 5 cells per type. A significant increase in fluorescence intensity of PSD95 puncta in both spine and shaft synapses of unidirectional neurons compared to bifurcated neurons was clearly observed. However, the increase was not statistically significant when I compared the intensity values in relation with different dendritic branches, despite the trend being the same, suggesting that this effect was overall cell type dependent (Two-way RM ANOVA p = 0.0358; Fig. 14B-C). Altogether, these results indicate that higher synaptic density correlates with lower fluorescence intensity as observed in bifurcated neurons, and the reverse was found in unidirectional neurons. To complete the overview, a comparison between synaptic forms

was evaluated. The spine and shaft synapses did not significantly differ in terms of intensity, although in spines the intensity was higher to a small extent (Fig. 14D-E); all data are summarized in table 3.

Overall, these results suggest that a compensatory mechanism could be implemented by the cells during synaptic transmission in relation to the level of PSD95 protein expression, maybe enabling the remodeling of the synaptic strength activity network in response to external inputs. This point needs to be investigated with further experiments.

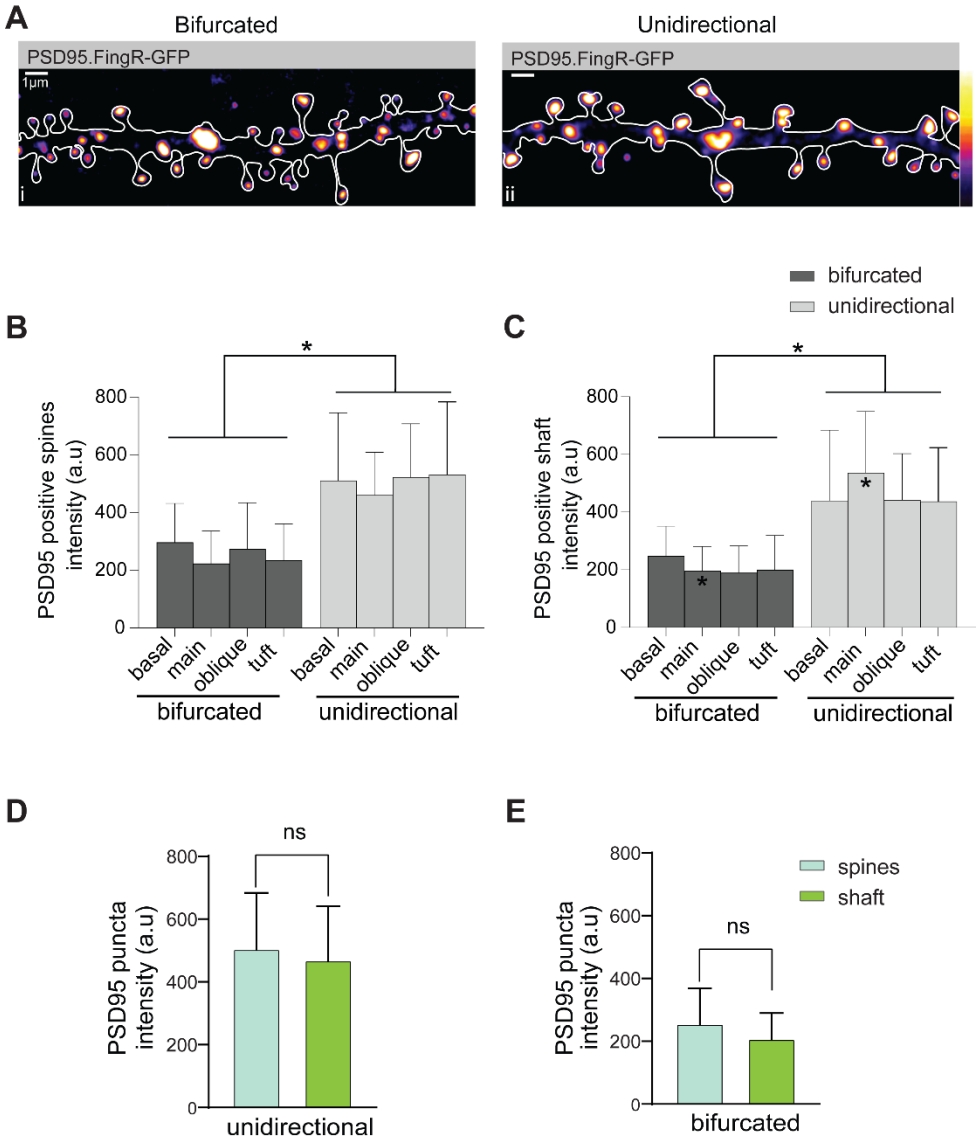

Figure 14: The CA1 pyramidal neurons with apical unidirectional pattern have high-rate expression of PSD95 in both spine and shaft synapses.

(A) Representative confocal maximum z-projection images showing the expression of PSD95 in synaptic spines and shaft from oblique dendrites of both bifurcated (Ai) and unidirectional

(Aii) CA1 neurons. **(B)** Quantitative intensity signals of PSD95 puncta in spines. The analysis shows there is a significant increase in overall dendritic spines of CA1 unidirectional neurons compared to bifurcated CA1 neurons. The difference is not significant comparing the intensities between different dendrites. Two-way ANOVA with Šídák's multiple comparisons test; P=0,4331 (basal); P = 0,0901 (main); P = 0,2571 (oblique); P = 0,1058 (tuft). Data are presented as mean ± SD. **(C)** Quantitative intensity signals of PSD95 puncta in shafts. The analysis shows there is a significant increase in overall dendritic shafts of CA1 unidirectional neurons compared to bifurcated CA1 neurons. The difference is not significant comparing the intensities between different dendrites, except for the main shaft. Two-way ANOVA with Tukey's multiple comparisons test; P = 0,5127 (basal); P = 0,0286 (main); P = 0,1950 (oblique); P = 0,2573 (tuft). Data are presented as mean ± SD. **(D-E)** Bar graphs showing the PSD95 intensity puncta located in spine and shaft synapses of unidirectional (D) and bifurcated (E) CA1 neurons. No significant changes in the PSD95 intensity mean distribution was found. Unpaired student's t-test; P = 0,7624 (unidirectional); P = 0,4870 (bifurcated). Data are presented as mean ± SD. All the quantifications have been performed on unidirectional neurons, from 15 dendritic segments in 5 cells. Bifurcated CA1 pyramidal neurons, from 15 dendritic segments in 5 cells.

Table 2: Mean density of shaft and spine synapses averaged per 10 µm and distinguished by dendritic branches.

Synaptic form	**Shaft synapses**		**Spine synapses**	
	Bifurcated	**Unidirectional**	**Bifurcated**	**Unidirectional**
Overall	4.06	3.60	12.36	7.27
Basal	4.03	3.50	13.79	10.02
Main	6.35	3.15	12.23	4.29
Oblique	3.17	3.66	13.68	10.32
Tuft	3.90	4.10	14.76	11.47

Table 3: Mean intensity values of the total shaft and spine synapses and the synapses distinguished by dendritic branches.

Synaptic form	Shaft synapses		Spine synapses	
	Bifurcated	**Unidirectional**	**Bifurcated**	**Unidirectional**
Total	208	469	256	505
Basal	277	439	302	510
Main	209	536	243	460
Oblique	207	442	281	522
Tuft	216	437	234	530

2.2.4 Protein expression profile of glutamatergic shaft and spine synapses in dissociated hippocampal neurons

The protein composition of glutamatergic synapses located in spines has been a subject of extensive investigation (Sell, Barrow and McAllister, 2020; Wichmann and Kuner, 2022). Immunolabeling of mature pyramidal neurons revealed that several proteins typically expressed in glutamatergic synapses within the spines are also present in the dendritic shaft (Reilly, Hanson and Phillips, 2011). However, a protein expression profile overview of the excitatory shaft synapses is still missing. To give key insights into the molecular composition of glutamatergic shaft of mature hippocampal neurons, I used rat primary neuron cultures at DIV17, and systematically analyzed the presence of several postsynaptic protein known to be enriched at the PSD. The neuronal cultures were prepared as previously described (*see methods for details protocol information*).

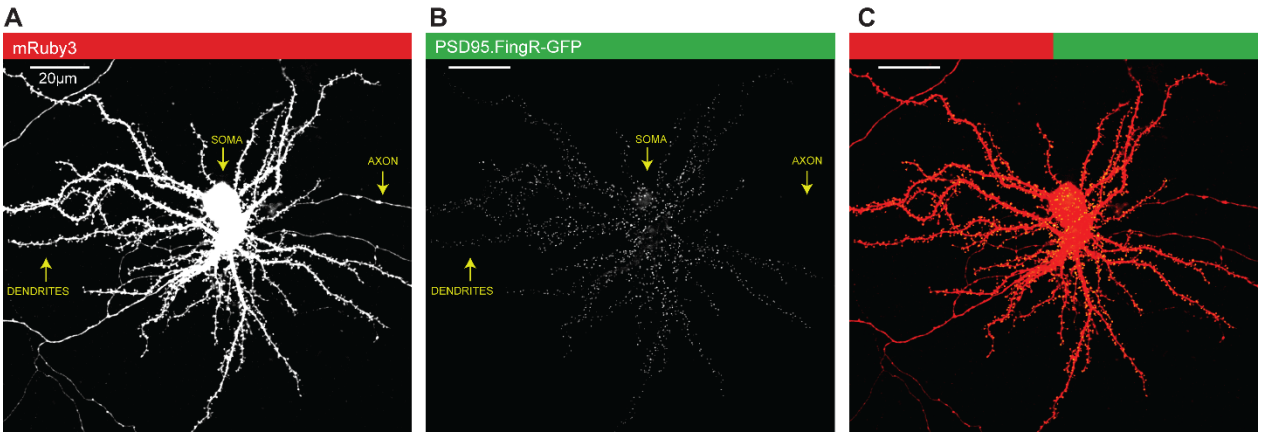

Figure 15: Representative images of DIV17 hippocampal primary neurons co-transfected with mRuby3 (cell fill) and PSD95.FingR-GFP (postsynaptic target).
(A) Representative maximum z-projections confocal images of mature hippocampal neurons transiently co-transfected for 24-48 hours with mRuby3 showing axon, somatic, and dendritic compartments **(B)** PSD95.FingR-GFP showing endogenous PSD95 a glutamatergic postsynaptic marker **(C)** Overlay of both fluorescent channels.

After the maturation process, DIV15 cells were co-transfected with mRuby3 (cell fill) (Fig. 15A), PSD95.FingR-GFP (postsynaptic excitatory marker) (Fig. 15B) plasmids, and then stained for several proteins associated with the glutamatergic postsynaptic density (PSD) like scaffolding proteins such as PSD95, Homer, SHANK1, SHANK2, SHANK3; auxiliary protein of NMDARs and AMPARs like SynGAP and Grip1 respectively; GluA1 containing AMPA receptor, GluN2B containing NMDA receptor, cytoskeletal protein like Cortactin, Synaptopodin cytoplasmic actin-associated protein, Cav 1.2 containing Ca^{2+} channel and adhesion molecules like Neuroligin (Fig. 16A). Firstly, the cumulative density (normalized to 10 µm of dendritic length) of dendritic spines (Fig. 16B dashed line) was calculated. Secondly, I estimated the frequency distribution of those proteins within dendritic spines (Fig. 16B) and shafts (Fig. 16C). Analysis of confocal maximum z-projection images showed that under basal conditions the scaffolding proteins Homer, SHANK2, SHANK3 and PSD95 as well as SynGAP and cortactin are preferentially located in spines rather than in the shaft. Synaptopodin is contained only in ~20-30% of the spines, consistent with previous studies (Konietzny *et al.*, 2019; Speranza *et al.*, 2022). The remaining protein targets SHANK1, Neuroligin, Cav 1.2, AMPA, NMDA and Grip1 are distributed in spines and shafts equivalently. All these proteins play a crucial role in synaptic function in

neurons. However, PSD95 is especially considered a pivotal marker of functional synapses as it is consistently found to be colocalizing to a presynaptic partner (Wiesner *et al.*, 2020), and its absence reduces the number and stability of glutamatergic synapses (Chen *et al.*, 2011; Cane *et al.*, 2014). Therefore, I consider the presence of a PSD95 signal as a reliable marker for functional synapses. Since the PSD95.FingR-GFP plasmid allows for the visualization of endogenous PSD95 protein, the combination with immunostaining facilitates a basal colocalization analysis of the abovementioned postsynaptic markers with PSD95 in both spine and shaft sites. As expected, PSD scaffolding proteins Homer, SHANK1, SHANK2, SHANK3 as well as the spine apparatus protein synaptopodin colocalize with PSD95 more significantly in spines than in shafts (Homer in spines: ~81%, in shafts: ~32%; SHANK1 in spines: ~60%, in shafts: ~34%; SHANK2 in spines: ~82%, in shafts: ~42%; SHANK3 in spines: ~83%, in shafts ~52%; synaptopodin in spines: ~28%, in shafts: ~12%). In contrast, the other postsynaptic targets like Neuroligin, Cav 1.2, SynGAP, AMPA, NMDA, cortactin and Grip1 nearly quantitatively colocalize in both spines and shafts. (Fig. 16D). All data are summarized in table 4.

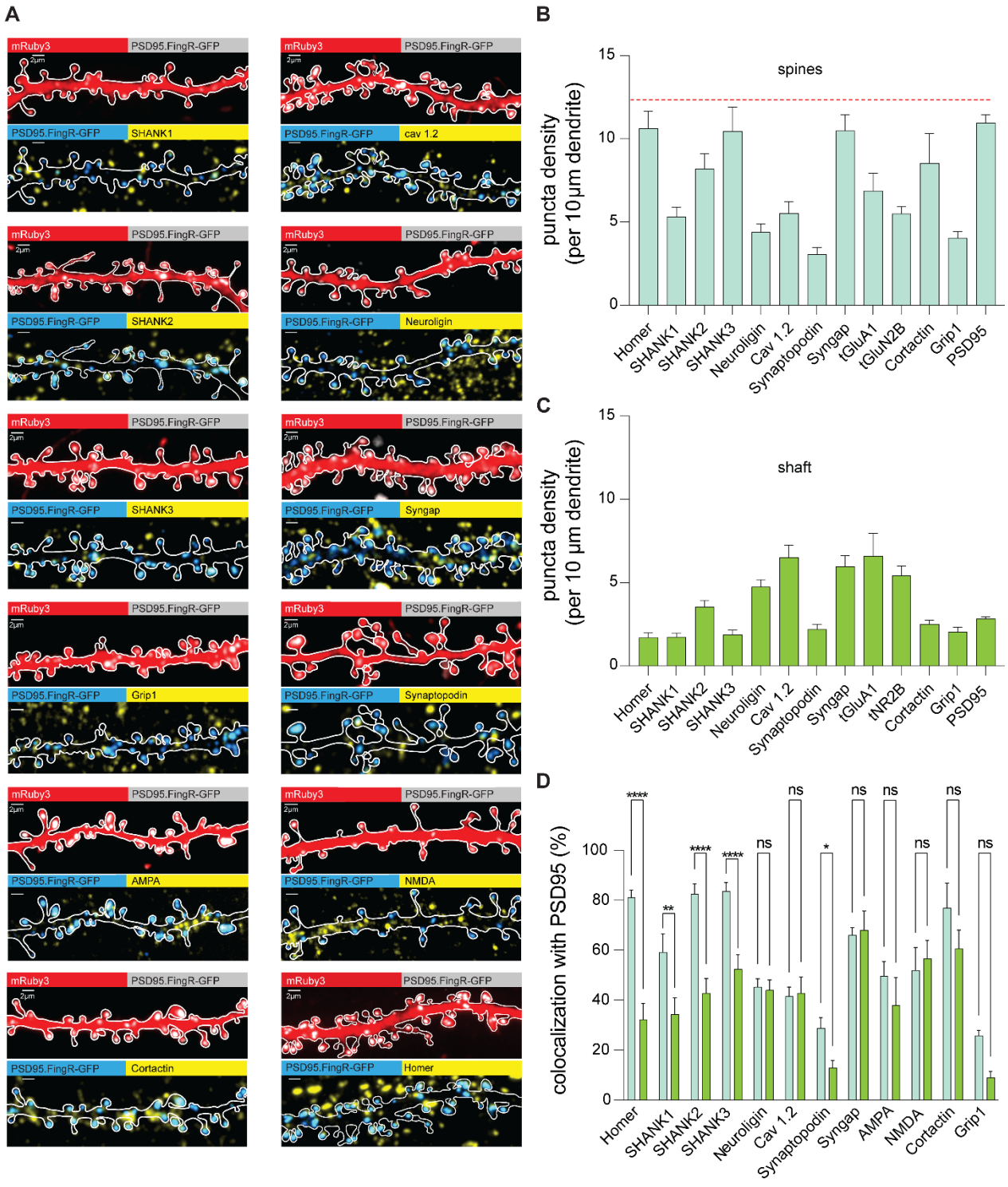

Figure 16: Diversity and commonalities of glutamatergic post-synaptic protein expression profile of dendritic spine and shaft synapses.

(A) Illustrative maximum z-projections confocal images of primary rat hippocampal neurons transiently co-transfected for 24-48 hours with mRuby3, PSD95.FingR-GFP and then immunolabeled against excitatory postsynaptic markers. **(B)** Quantification of glutamatergic synaptic markers distribution in spines. The number of protrusions was counted based on

mRuby3 signal and normalized to a dendritic length of 10 µm. The density of the overall protrusions is on average 12.518 per 10 µm dendrites (red dashed line). The number of spines associated with the excitatory postsynaptic markers was counted based on the PSD95.FingR-GFP puncta or 647-channel signal, and normalized to a dendritic length of 10 µm. **(C)** Quantification of glutamatergic synaptic markers distribution in aspinous dendritic segments. The number of shafts was counted based on the mRuby3 signal combined to the PSD95.FingR-GFP signal or 647-channel signal and normalized to a dendritic length of 10 µm. **(D)** Quantitative colocalization analysis of PSD95 associated with postsynaptic markers in dendritic spines (light green bar graphs) and shaft (green bar graphs). Two-way ANOVA with Bonferroni multiple comparisons test; ****P < 0.0001 (Homer); **P = 0.0033 (SHANK1); ****P < 0.0001 (SHANK2); ****P < 0.0001 (SHANK3); *P = 0.0209 (synaptopodin). Data are presented as SD. All the quantifications have been performed on 195 neurons.

To address whether shaft synapses are contacted by active presynaptic boutons in analogy with spine synapses, a syt-1 antibody uptake assay (Ivanova *et al.*, 2015; van Bommel *et al.*, 2019) was used (Fig. 17A). DIV17 cells, co-transfected one day before the assay with mRuby3 and PSD95.FingR-GFP, were incubated with syt-1 antibody for 30 minutes, then fixed and imaged with a spinning disk confocal system. As expected, both spine and shaft sites contain PSD95 colocalizing with syt-1 as shown by the intensity profiles measured from maximum z-projection images (Fig. 17B). Approximately 60% of all detected PSD95 puncta were also positive for syt-1 in spines, and their colocalization significantly decreased to ~40% when the antibody was applied to tetrodotoxin (TTX)-silenced cultures (Fig. 17C). On the other end, under basal conditions ~40% of all detected PSD95 puncta on the shafts were positive for syt-1, and the colocalization was significantly decreased to ~20% after TTX treatment (Fig. 17D). These results strongly indicate that PSD95 puncta oppose active presynaptic terminals on spines as well as on shafts although to some degree.

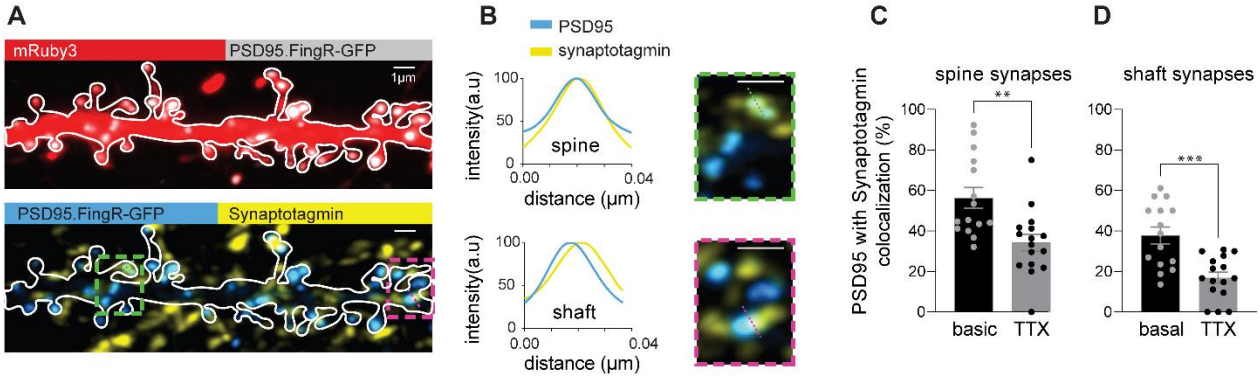

Figure 17: Active excitatory synapses are formed on dendritic shafts and spines of mature hippocampal primary neurons.
(A) Confocal images of DIV17 primary hippocampal neuron transiently co-transfected for 24-48 hours with mRuby3, PSD95.FingR-GFP and stained for syt-1 after live uptake of a syt-1 antibody by active presynaptic terminals. The presynaptic release sites co-localize with PSD95 within dendritic shafts and spines. **(B)** Fluorescent intensity line profile of PSD95 and synaptotagmin signals in both spines (indicated by green dashed square) and shafts (indicated by pink dashed square). **(C-D)** Silencing of neuronal activity by TTX application reduces synaptic release in dendritic spines (C) and shaft (D) synapses. Student's unpaired t-test. **P = 0.0022 (spine). ***P = 0.0002 (shaft). 16 neurons from 3 independent preparations. Data are presented as SD. All the quantifications have been performed on 15 neurons from 3 independent preparations.

In summary, based on these data, I propose a comprehensive schematic model that captures the molecular composition of glutamatergic shaft synapses in comparison to a spine synapse (Figure18). Notably, the molecular organization of glutamatergic shaft synapses is almost identical to that of spines with some proteins being more abundant in spine synapses. Among tested candidates, no protein could be identified yet which exclusively targets shaft synapses. In the future, it remains to be tested whether there are any specific proteins that exist in shaft synapses.

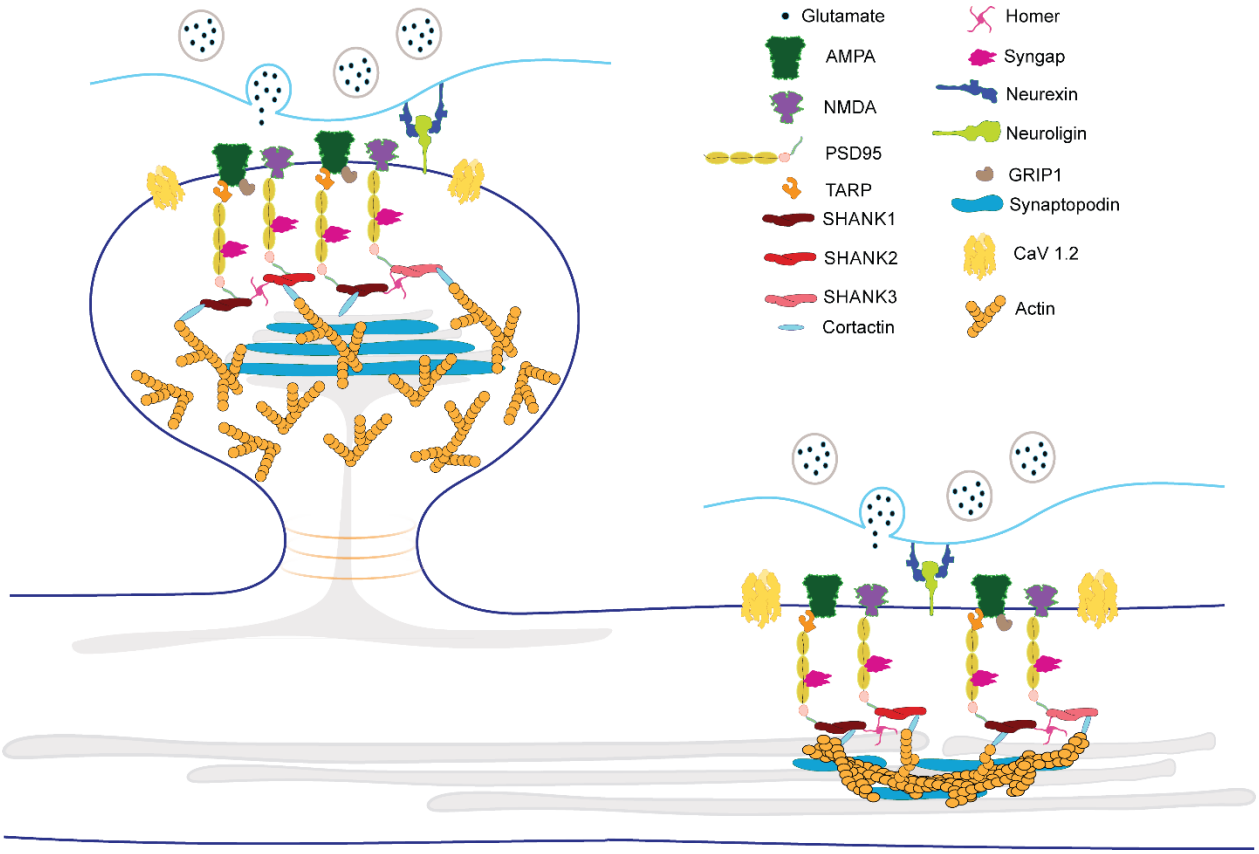

Figure 18: Illustration showing the protein profile of glutamatergic synapses on dendritic spine and shaft of mature hippocampal neurons.

Table 4: Mean density of postsynaptic proteins and colocalization with PSD95 within the shaft and spine compartments.

Synaptic target	Density		Colocalization with PSD95 (%)	
	Shaft synapses	Spine synapses	Shaft synapses	Spine synapses
Homer	1.69	10.62	32	81
SHANK1	1.73	5.32	34	59
SHANK2	3.55	8.19	43	82
SHANK3	1.86	10.47	52	84
Neuroligin	4.74	4.39	44	45
Cav 1.2	6.51	5.53	43	41
Synaptopodin	2.19	3.06	13	29

SynGAP	5.96	10.48	68	66
tGluA1	6.60	6.88	38	50
tGluN2B	5.42	5.50	57	52
Cortactin	2.51	8.52	61	77
Grip1	2.03	4.04	9	26
PSD95	2.83	10.95	-	-

2.2.5 Structural plasticity of excitatory shaft synapses

In non-stimulated primary neurons, shaft synapses can persist over long periods of time and rarely transform into spines (Reilly, Hanson and Phillips, 2011). However, it is possible that change in synaptic activity may trigger the transformation of shaft synapses into spine synapses. As most of the synaptic components are already there, such a transformation would be a way to rapidly increase the number of dendritic spines which has been observed for example in LTP conditions. To investigate plasticity-related changes of excitatory shaft synapse structures, I performed long-term live cell imaging on cultured neurons at DIV17-18. The cells were co-transfected with PSD95.FingR-GFP and with mRuby3 as a cell fill. Transfected neurons were imaged for ~30 min under basal conditions, and for up to 5 hours after short-term application of a glycine-based chemical LTP (cLTP) induction solution (magnesium-free aCSF supplemented with glycine, TTX and bicuculline; Fig. 19A), a method already used in previous studies (Musleh *et al.*, 1997; Bae *et al.*, 2012; Xu *et al.*, 2020). The analysis of potentiated neurons showed that a large fraction of PSD95 remained stable at the synapse locations over time (green arrow). However, a certain amount of PSD95 was shifting position along the dendritic shaft, sometimes clustering and sometimes relocating to the base of the spines. Moreover, maximum z-projections of confocal images showed widespread remodeling of the dendrites upon cLTP induction. Interestingly, I noticed membrane structural changes at PSD95 positive shaft synapses and observed spine-like structures protruding from existing excitatory shaft synapses (indicated by yellow arrow in Fig. 19B). Collectively, different fractions of PSD95-positive shaft synapses

exhibit distinct behavioral patterns after plasticity induction. Analysis revealed, that approximately 6% of the total detected PSD95 puncta in the shaft transform into spines, whereas, approximately 20% of the PSD95 puncta shift their position along dendritic segment, and the remaining puncta, which account for approximately 70% of the total, remain stable and do not exhibit any changes in terms of their location (Fig. 19C). Quantification of PSD95 signal intensities as expected showed a significant increase in expression over time in response to cLTP (Fig. 19D, blue curve), but not under basal conditions (Fig. 19D, dark red curve), where a decrease in fluorescence of the PSD95 signal was actually observed. The photobleaching effect was measured and the resulting values were used to correct the intensity detected during the potentiation (Fig. 19D, black curve). The frequency distribution of intensities fractions upon chemical induction of LTP and at basic conditions are represented by the cumulative plots (Fig. 19E-F). In summary, these results provide new key insights into the plasticity-related changes of excitatory shaft synapse structures and highlight the potential for pre-existing shaft synapses to transform into dendritic spine synapses under certain activity conditions.

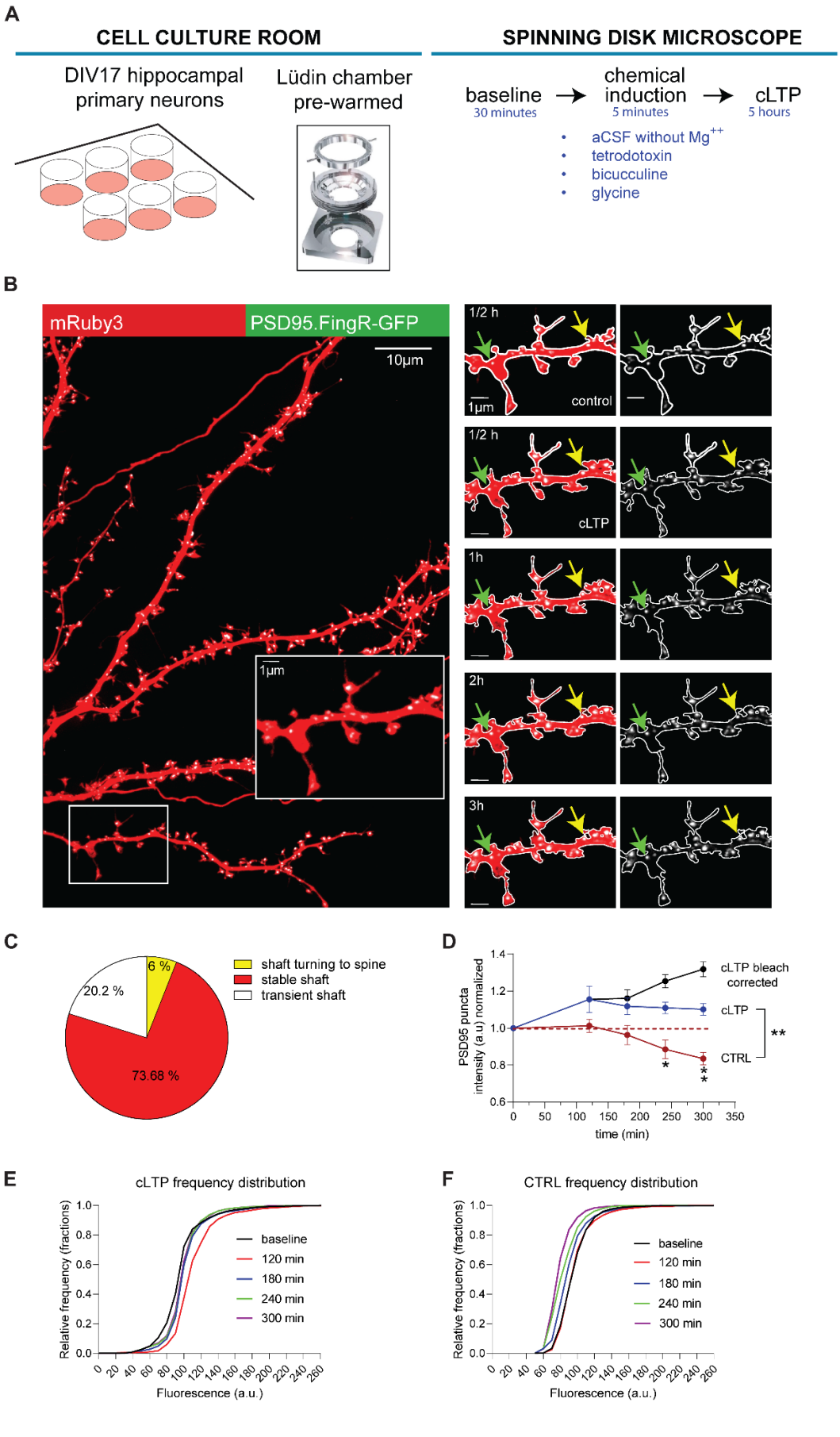
A
CELL CULTURE ROOM
SPINNING DISK MICROSCOPE
DIV17 hippocampal primary neurons
Lüdin chamber pre-warmed
baseline
30 minutes
chemical induction
5 minutes
cLTP
5 hours
aCSF without Mg++
tetrodotoxin
bicucculine
glycine
B
mRuby3
PSD95.FingR-GFP
10µm
1µm
1/2 h
control
cLTP
1h
2h
3h
C
6 %
20.2 %
73.68 %
shaft turning to spine
stable shaft
transient shaft
D
PSD95 puncta intensity (a.u) normalized
time (min)
cLTP bleach corrected
cLTP
CTRL
**
E
cLTP frequency distribution
Relative frequency (fractions)
Fluorescence (a.u.)
baseline
120 min
180 min
240 min
300 min
F
CTRL frequency distribution
Relative frequency (fractions)
Fluorescence (a.u.)
baseline
120 min
180 min
240 min
300 min

Figure 19: A subset of glutamatergic shaft synapses can turn into spine synapses after long-term potentiation chemically induced by glycine (cLTP).
(A) Schematic pipeline of the method used to induce long-term potentiation plasticity in hippocampal primary neurons. **(B)** Confocal images of a DIV17 primary hippocampal neuron transiently co-transfected for 24-48 hours with mRuby3 and PSD95.FingR-GFP (left panels). Dendritic segment imaged before and after cLTP induction (right panels) showing stable glutamatergic shaft synapses indicated with green arrows and shaft synapses transforming into spine indicated with yellow arrows tracked over 5 hours after long-term plasticity. **(C)** Graph cake showing the total number in percentage of shafts turning into spines, stable and dynamic shafts. **(D)** Normalized intensity of PSD95 signal after cLTP induction. PSD95 increases for about 5 hours (blue curve) upon 5 minutes application of the induction solution. In contrary, in normal conditions neurons show decrease PSD95 intensity over 5 hours time frame (red curve) suggesting that a bleaching effect is occurring. The amount of bleaching signal detected without stimulation could be added to the PSD95 signal measured after cLTP induction generating better indication of the PSD95 intensity (black curve). Two-way ANOVA with Šídák's multiple comparisons test; **P = 0.0031. Quantification of cLTP was performed in 10 neurons from 4 independent preparations. Quantification of normal condition (control) was performed in 6 neurons from 1 preparation. Data are presented as mean +/- SEM. **(E-F)** Cumulative frequency distribution plot showing the PSD95 fluorescent signal fractions over time after cLTP induction and in absence of chemical stimulation.

3 Discussion and perspective

3.1 Revealing the impact of ADAM10 in the short-term plasticity of mossy fibers-CA3 glutamatergic synapses

Over the past few decades, the glutamatergic hippocampal synapses formed between mossy fibers and CA3 pyramidal cells have received considerable attention as an unique type of synaptic site where special plasticity occurs during memory formation (Castillo, 2012; Jackman and Regehr, 2017; Rebola, Carta and Mulle, 2017; Carta *et al.*, 2018). While significant progress has been made on this topic, many questions regarding the contribution of the molecular players involved in mechanisms of plasticity in these special synapses remain unanswered. ADAM10 is a protein critically important for glutamatergic synaptic function as well as for neuronal differentiation during development, and it is associated with multiple diseases, including Alzheimer's (Jorissen *et al.*, 2010; Saftig and Lichtenthaler, 2015). Experimental evidence suggests ADAM10 plays a critical role in both postsynaptic and presynaptic functions (Lundgren *et al.*, 2015; Bruyère *et al.*, 2020). This metalloprotease has multiple substrates located at the postsynaptic compartment, including neuroligins, APP, and prion proteins, which further underlines its important contribution to postsynaptic functions (Saftig and Lichtenthaler, 2015) (Fig.4). Recently, an association with the pre-synaptic protein piccolo and novel pre-synaptic substrates of ADAM10 have been identified (Cozzolino *et al.*, 2021). Thus, it is becoming very important to provide a reliable account for the cellular localization of ADAM10 and its role in presynaptic functions. Mass spectrometry profiling of the ADAM10 complex isolated from the striatum of a Huntington’s mouse model indicated the presence of important proteins composing the active zone (Cozzolino *et al.*, 2021). ADAM10 was already suggested to be released from SVs in an activity dependent manner in cortical mouse slices (Venkatesh *et al.*, 2017), and later, the importance of ADAM10-dependent cleavage of the presynaptic adhesion molecule neurexin-1 for the organization of the synapse has been reported (Trotter *et al.*, 2019). Despite the extensive study of ADAM10 cellular functions in CA1 hippocampal neurons (Khezri, Mohebalizadeh and Ghasemnejad-Berenji, 2023), the impact of ADAM10

as a molecular player mediating the plasticity of glutamatergic MF-CA3 synapses remains unknown. In the present study, a direct presence of ADAM10 at the intact presynaptic MF bouton opposing thorny excrescences was experimentally observed by conducting DAB staining for electron microscopy and using a specific antibody targeting the cytosolic C-terminus of ADAM10. This approach allowed to uncover a substantial expression of ADAM10 at the MF glutamatergic terminals of the CA3 region. As these contacts are vital for hippocampal function and memory formation, the function of ADAM10 at MFs has been investigated in more detail. Next, immunogold-EM labeling was performed to better localize ADAM10 at MF-CA3 synapses and we found that it localizes to presynaptic vesicles of mature neurons from hippocampal sections of wt animals. In parallel, the colocalization of ADAM10 with pre-and postsynaptic markers, like bassoon and SHANK3, respectively, has been revealed by using super-resolution microscopy. Follow up experiments of electrophysiology fEPSP measurements were conducted to further investigate the role of ADAM10 in synaptic glutamatergic transmission and short-term plasticity. Paired pulse facilitation and train facilitation are two of the most traditional short-term plasticity paradigms used to test mossy fibers plasticity (Salin *et al.*, 1996; Nicoll and Schmitz, 2005; Jackman *et al.*, 2016). Surprisingly, MF-CA3 synapses of ADAM10 cKO mice showed a strong impairment in facilitation of both types of plasticity, and this reduction was not dependent on ADAM10 proteolytic activity. In fact, its pharmacological inhibition in wt slices had no influence in both excitatory basal transmission and in synaptic facilitation. Importantly, incubation of a tat-peptide mimicking the cytosolic tail of ADAM10 in wt hippocampal acute slices reproduced the deficit in short-term facilitation resembling the phenotype of the ADAM10 cKO mice. These findings suggest that the observed deficiency in plasticity is due to a role of ADAM10's C-terminus and it is independent of its enzymatic activity, highlighting that cytosolic interactions rather than the proteolytic function of ADAM10 are essential in a short-term plasticity paradigm. Furthermore, the lack of facilitating responses, after the low initial release characterizing the mossy fibers, in absence of ADAM10 can be likely explained by a possible disruption of the mechanisms regulating the release of the vesicle pools or a disfunction in pre-synaptic

calcium signaling. Mechanistically, we can speculate that ADAM10 might be involved in SV recycling machinery, most likely interacting with other membrane proteins that promote vesicle fusion and replenishment, which can be also regulated by signaling molecules activated by calcium. Recently, several groundbreaking studies have shown impairments in synaptic facilitation of multiple glutamatergic synapses in different brain regions caused by the deletion or perturbation of syt-7 (Jackman *et al.*, 2016). Syt-7 is a member of the synaptotagmin protein family broadly expressed in the central nervous system (Li et al, 1995). Syt-7, like other isoforms, is known for its tandem C2 functional domains. However, this particular isoform stands out with its high Ca^{2+} sensitivity, and its ability to bind anionic phospholipids and induce membrane fusion in vitro at Ca^{2+} concentrations of <1 μM (Sugita *et al.*, 2001; Bhalla et al, 2005). These unique properties have led to its implication in various aspects of SV release and short-term synaptic plasticity, particularly in glutamatergic hippocampal synapses (Jackman *et al.*, 2016; Huson and Regehr, 2020). Syt-7 has been demonstrated to have high affinity for Ca^{2+} and slow intrinsic kinetics, making this isoform very important as a Ca^{2+} sensor for asynchronous release (Bacaj *et al.*, 2013; Vevea *et al.*, 2021). Importantly, syt-7 was found to mediate Ca^{2+}-dependent SV replenishment in response to a high-frequency stimulation paradigm (Liu, Bai, Xue, *et al.*, 2014), and be required for short-term facilitation (Jackman *et al.*, 2016; Vevea *et al.*, 2021). Finally, 'zap-and-freeze' electron microscopy revealed that a loss of syt-7 diminishes docking of synaptic vesicles after a stimulus and inhibits the recovery of depleted synaptic vesicles after a stimulus train, supporting these functions from the axonal plasma membrane, where its localization and stability require both γ-secretase-mediated cleavage and palmitoylation (Vevea *et al.*, 2021). Experimental studies of immunohistochemistry shows that syt-7 is highly enriched in MF terminals of hippocampal CA3 (Jackman *et al.*, 2016). As the phenotype of syt-7 KO mice very much resembles the facilitation phenotype of the ADAM10 KO, we can speculate that the direct or indirect interaction of ADAM10 with syt-7 could be a potential mechanism regulating presynaptic processes at MF-CA3 synapses. For instance, the lack of ADAM10 could possibly cause syt-7 to diffuse away from the presynaptic site, reducing the triggering of the neurotransmitter release, which

could explain the similar phenotype observed in ADAM10 KO and syt-7 KO mice. However, this aspect needs to be investigated with further experiments. Thus, we proposed a hypothetical mechanism shown in a schematic cartoon model (Fig.10).

3.2 Branching of CA1 apical dendrites correlates with altered density of dendritic spine but not shaft synapses

Another well characterized hippocampal glutamatergic synapse is represented by the Schaffer collaterals projecting to pyramidal neurons of CA1 region. Beyond the overall neuronal polarity established between the axon-dendritic axis, pyramidal neurons exhibit additional intrinsic dendritic compartmentalization conferred by their apical and basal structures which receive different inputs from the CA3 region contributing to specific biophysical and computational properties (Yuan *et al.*, 2015; Benavides-Piccione *et al.*, 2020). A typical CA1 pyramidal neuron is positioned in the CA1 in such way that its basal dendrites occupy the space in the *stratum oriens*, directly above the *stratum pyramidale*. Its apical dendritic structures are positioned in the *stratum radiatum* and *lacunosum moleculare*, where the main, oblique, and tuft dendrites are highly organized. These dendritic segments receive numerous axonal inputs from the CA3 region, which form synaptic contacts on both the medial and distal parts of each individual dendrite. This organization allows for efficient integration of information across multiple synapses and enables the CA1 pyramidal neurons to play a crucial role in the processing of spatial and episodic memory in the hippocampus (Dimsdale-Zucker *et al.*, 2018). Interestingly, two different neuronal subpopulations presenting distinct apical dendritic configurations, namely bifurcated and unidirectional, have been recently described in the mature hippocampus in mice and in humans (Benavides-Piccione *et al.*, 2020). In the current study, single cell electroporation of two plasmids with different transgenes were introduced into individual CA1 cells of organotypic hippocampal slices for visualization of cell morphology (mRuby3) and for detection of the postsynaptic glutamatergic marker PSD95 (PSD95.FingR-GFP). The combination of these two markers allowed the localization of detected PSD95 in shaft or spine sites and enabled us to estimate the density distribution in

dendrites, as well as to characterize different CA1 neuronal subpopulations present in hippocampus. Thus, bifurcated and unidirectional apical patterns were identified also in mature CA1 pyramidal neurons from rats, and an interesting correlation between the apical structure and the number of spines protruding from the dendrites was observed. The bifurcating neurons had overall a significantly higher spine density and spine synapses compared to unidirectional neurons in all distinguished dendritic branches. Since the synapses are the fundamental computational units of the brain, synaptic density is an essential indicator linked to development and functioning of the neural system. Furthermore, the parameter of proximal main apical branching has thus far gone relatively unexplored, and the impact of this feature on the distribution, functional and morphological properties of glutamatergic synapses is unknown. Recent progress has shown differences in molecular, structural, physiological, and connectivity properties between CA1 pyramidal cells that are dependent on how deep the cells are localized in different layers, suggesting that CA1 pyramidal cells are a more heterogeneous population than previously expected (Soltesz and Losonczy, 2018; Cavalieri *et al.*, 2021). Although the number of spine synapses was different relative to the apical branching pattern, the distribution of excitatory shaft synapses was similar between bifurcated and unidirectional neurons, suggesting that mature CA1 pyramidal cell morphology of the apical dendrites does not correlate with the number of excitatory shaft synapses as shown for spine synapses. Moreover, the density ratio between synapses located on spine and shaft sites was very similar in both neuronal branching patterns, showing that, overall, glutamatergic synapses are mainly formed in spines and much less on dendritic shafts. RNA-sequencing and genetic-fate mapping of unidirectional and bifurcated cells could be pursued to determine whether these neurons code for differing marker genes or represent different age-groups of pyramidal cells, presenting a new property for the heterogeneity of CA1 cells.

3.3 Reciprocal relationship between PSD95.FingR-GFP mean fluorescence intensity and PSD95 expression

The postsynaptic ionic currents and intracellular second messenger signals produced and controlled by the postsynaptic density (PSD) are crucial for regulating neuronal transmission (Dosemeci et al, 2016). PSD95 serves as a major scaffold protein in the PSD and is involved in anchoring and organizing a variety of proteins, including NMDA and AMPA receptors, ion channels, signaling molecules, and cytoskeletal components. PSD95 helps to cluster and stabilize these proteins in the postsynaptic membrane, contributing to the proper functioning and regulation of synaptic transmission (Berry and Nedivi, 2017; Mardones *et al.*, 2019). The density in expression of PSD95 molecules in the PSD can be measured by using the mean intensity parameter, and the significant difference in PSD95.FingR-GFP fluorescence intensity between spine and shaft synapses of unidirectional and bifurcated cells could be indicative for the functional differences possibly discriminating the bifurcated and unidirectional cell types. Despite demonstrating a significantly higher density of spine synapses over shaft synapses, the overall fluorescence intensity of PSD95.FingR-GFP in bifurcated cells was significantly lower in both synaptic locations compared to unidirectional cells. An *in vivo* study reported a linear, proportional relationship between PSD95.FingR-GFP brightness (fluorescence intensity) and the size of the PSD, determined via electron microscopy reconstructions (Cane *et al.*, 2014). The exact dimension of the post-synaptic compartments could not be determined, but the intensity of PSD95.FingR-GFP fluorescence gives an initial indicator of the potential PSD sizes. Between the two cell types, a reciprocal regulatory mechanism could be present between synaptic density and PSD95 expression and thus potentially also PSD size. Due to the correlation of PSD size with synaptic strength, these results could signify a compensatory action of unidirectional cells. The indication of significantly higher expression of PSD95 in the PSD of spine and shaft synapses suggests that unbranched cells may compensate for their lower synaptic density with larger, stronger synapses, as in cortical neurons it has been observed that larger synapses tend to have higher basal levels of synaptic strength compared to smaller synapses (Holler *et al.*, 2021). However, there are

no indicative results showing differences in terms of intensity between shaft and spine synapses of the same cell type. It would be interesting to know about the expression level of AMPARs on shaft synapses of hippocampal neurons. This could be achieved experimentally in future studies by targeting endogenous glutamatergic receptors and performing advanced microscopy techniques such as super resolution imaging. Currently, there exist multiple methods that can be used for this purpose. One possible strategy would be employing specific ligands or antibodies that have high affinity and selectivity for the target receptor at the extracellular side of the cell membrane. Receptor surface labeling would allow to investigate the spatial distribution, density, and changes in receptor expression on cell surfaces. It is particularly useful for studying receptor trafficking, internalization, and localization within specific cellular compartments and better understanding of receptor dynamics in various physiological and pathological processes. An alternative strategy would be using CRISPR-based approaches such as pORANGE, which combines the power of CRISPR-Cas9 technology with the ability to introduce specific genetic modifications and trace them, also at the level of receptor subunit composition, through the expression of fluorescent proteins (Willems *et al.*, 2020). Furthermore, since real glutamatergic synapses should not only have glutamate receptors, but should also respond to glutamate, it could be helpful to test the functionality of the shaft synapses by employing single cell patch-clamp electrophysiology and glutamate uncaging at the same time in order to measure the AMPARs and NMDARs currents. Another aspect which might be important to investigate is if the size of the PSD, and so the synaptic strength, varies along the same dendritic segment, for instance in relation to distal or proximal dendrites, which is another possible compensatory mechanism utilized by the neurons to maintain a certain stability of transmission (Katz *et al.*, 2009).

3.4 Molecular composition, activity and plasticity of excitatory shaft and spine synapses in dissociated hippocampal neurons

To gain a better understanding of the molecular composition of glutamatergic shaft synapses in mature hippocampal neurons, a protein expression profile analysis of these

synapses under basal conditions was conducted. The analysis was designed to provide insights into the excitatory shaft synapses in comparison to spine synapses. Although several proteins commonly found at glutamatergic spine synapses are also present at shaft synapse sites, there is also a differential expression of excitatory postsynaptic markers between these two synaptic locations. More specifically, the scaffolding proteins at glutamatergic synapses, such as PSD95, Homer and SHANK family member proteins, along with glutamate receptor interacting protein-1 (GRIP1), were predominantly found in spine rather than in shaft synapses. Conversely, other excitatory markers such as AMPARs and NMDARs, as well as adhesion molecules like neuroligins and postsynaptic voltage-gated calcium channels, exhibited comparable expression levels at both spine and shaft synaptic sites. Furthermore, the actin-binding proteins cortactin and SynGAP were highly expressed in both compartments. These results may suggest that under basal conditions, mature hippocampal neurons tend to establish synaptic contacts primarily on spines, as the most critical postsynaptic molecular players required for the formation of functional synapses are highly distributed in spine structures and less on dendritic shaft. This could imply that spines may have a more significant role in the establishment and maintenance of functional synapses in mature hippocampal neurons. However, the same glutamatergic protein expression profile is also present in shaft structures, albeit in different amounts, therefore, it would suggest hippocampal dendritic shafts being potential sites where active synapses could be formed. In line with this, we observed the functional activity of glutamatergic shaft synapses after silencing the neuronal cultures by perfusing tetrodotoxin, which inhibits the generation of action potentials. The glutamatergic transmission was clearly decreased in both spine and shaft sites (Fig.17), demonstrating excitatory shaft synapses, like for spine sites, can participate in the neurotransmission.

Active glutamatergic shaft synapses have been previously reported in dopaminergic neurons where distinct morphological and functional properties in comparison to glutamatergic spine synapses were observed (Jang *et al.*, 2015). Moreover, silent hippocampal excitatory shaft synapses became active by recruiting more AMPARs after LTP induced by glycine, suggesting that silent shaft synapses may represent a synaptic state

in developing neurons with enhanced capacity of activity-dependent potentiation (Xu *et al.*, 2020). Furthermore, one can speculate that the presence of NMDARs on shaft synapses would allow for direct Ca^{2+} dependent synaptic control of organelle exocytosis, e.g. exocytosis of lysosomes. This raises the question whether and how activation of shaft synapses influences organelle transport. Considering the architecture of the cytoskeleton, shaft synapses might contribute more strongly to regulating organelle trafficking in comparison to spine synapses, as they lack the limited space defined by the neck. Finally, synaptic glutamatergic inputs directly to the dendritic shaft of cortical pyramidal cells from mouse, macaque, and human have been very recently analyzed in detail by using three-dimensional EM reconstructions (Loomba *et al.*, 2022).

The present study demonstrates dynamic changes occurring in excitatory shaft synapses upon LTP induced by pharmacological treatment with glycine, which enlarged spine dimensions and increased PSD95 expression in both spine and shaft synapses, showing that excitatory shaft synapses are modulated by plasticity. In potentiated neurons, the majority of excitatory shaft synapses are stable as a synapse type, however, a small fraction of PSD95 positive shaft synapses is redistributed along the dendrites and sometimes form clusters which localize to the base of the spines. There they could potentially act as a hub of reserve synaptic proteins which can be recruited into spines in order to stabilize their initial activity-induced potentiation. An effective strategy to delve deeper into this aspect could involve the targeting of endogenous proteins, whose expression typically increases in correlation with long-term potentiation, by employing fluorescent probes which can ensure minimal interference with the physiological functioning. For instance, by using CRISPR-based approaches for precise genome editing in neurons such as pORANGE or TKIT (Fang *et al.*, 2021). The latter is a new optimized method to assess the mobility of endogenous proteins or receptors, which in combination with advanced imaging techniques such as two-photon imaging or super-resolution microscopy in living cells can provide detailed insights into the dynamic behavior of the targeted proteins within the synaptic sites. It may be valuable to conduct quantitative analyses, such as tracking the movement of individual proteins or measuring their diffusion coefficients in spines and shafts, in order to establish the specific

effects of potentiation on protein localization and diffusion at these synapses. Notably, I have also observed that another very small fraction of glutamatergic shaft synapses turns into spine synapses, and it is maintained up to 5 hours post induction. It is still unclear whether newly formed spines could retract back to the shaft, an additional aspect that could be further investigated by imaging the cells for longer periods of time.

Although the density of excitatory shaft synapses significantly decreases after maturation, these synapses can still have a remarkable cellular impact during synaptic transmission and plasticity in mature glutamatergic neurons. In the last twenty years, most studies addressing the molecular composition, physiological properties, and activity pattern of excitatory synapses focus mainly on glutamatergic spines (Matsuzaki et al, 2001; Matsuzaki *et al.*, 2004; Bourne and Harris, 2008, 2011; Mikhaylova et al, 2018; Kruijssen and Wierenga, 2019; Wichmann and Kuner, 2022) and not many research studies focused on glutamatergic shaft synapses (Fiala et al, 1998; Aoto *et al.*, 2007; Reilly, Hanson and Phillips, 2011; Jang *et al.*, 2015; van Bommel *et al.*, 2019; Xu *et al.*, 2020). However, the role of the active shaft synapses in neuronal circuits has been increasingly recognized, and it is becoming clear that excitatory shaft synapses are a functional component of synaptic networks as they actively contribute to synaptic transmission in rat, mouse, macaque and human brains (Loomba *et al.*, 2022). Follow up experiments need to be conducted to measure the local strength of excitatory shaft synapses and how it changes in response to different stimulations. This can be achieved *in vitro* or more importantly *in vivo* by using for instance glutamatergic activity sensor tools in combination with advanced imaging techniques, which can allow visualization of fluorescent signals originating from the glutamatergic activity specifically on the dendritic shaft. Also, the question of whether pyramidal neurons recruit functional glutamatergic shaft synapses to adapt their synaptic strength during synaptic scaling remains open. These findings would help to uncover further mechanisms utilized by glutamatergic neurons during plasticity. By continuing to investigate the role of excitatory shaft synapses, we may deepen our understanding of the complex and dynamic nature of neuronal circuits and elucidate their contribution to brain function in addition to related brain disorders.

Materials and methods

Animals

Wistar rats Crl:WI (Han; Charles River) and Wistar Unilever HsdCpb:WU (Envigo) rats were used in this study. Pregnant rats (E18) for primary hippocampal cultures and male rat pups aged between P4-P7 for organotypic hippocampal slice cultures were sacrificed in accordance with the Animal Welfare Law of the Federal Republic of Germany (Tierschutzgesetz der Bundesrepublik Deutschland, TierSchG) and with the approval of local authorities of the city-state Hamburg (Behörde für Gesundheit und Verbraucherschutz, Fachbereich Veterinärwesen, from 21.04.2015) and the animal care committee of the University Medical Center Hamburg-Eppendorf.

Conditional ADAM10 knockout mice (ADAM10$^{flox/flox}$ Cre$^{+/-}$ and ADAM10$^{flox/flox}$ Cre$^{-/-}$ controls; (Prox *et al.*, 2013)) were obtained by breeding ADAM10$^{flox/flox}$ Cre$^{-/-}$ or ADAM10$^{flox/+}$ Cre$^{-/-}$ with ADAM10$^{flox/+}$ Cre$^{+/-}$ mice. Male P21-23 mice and littermate controls were used for this study. Mice were bred and maintained at CAU, Kiel, Schleswig-Holstein. Animals were housed in individually ventilated cages with a capacity of five animals per cage. The room temperature was kept at 19-22°C and humidity at 45-60%. Alternating light-dark cycles of 12 h were applied and animals were fed with water and laboratory animal food (Ssniff Spezialdiäten) ad libitum. The animals were kept in accordance with (Behörde für Gesundheit und Verbraucherschutz, Fachbereich Veterinärwesen) and the animal care committee of the University Medical Center Hamburg-Eppendorf.

Electron microscopy: perfusion, DAB and immunogold staining

Perfused brains were dissected and 100 µm thick sagittal sections were cut with a vibratome (Leica VT 1000S). Thereafter, pre-embedding immunoelectron microscopy was performed as follows: vibratome sections with the hippocampal formation were selected and

cryoprotected in 2.3 M sucrose and subjected to two cycles of freeze-thaw in liquid nitrogen. After rinsing in PBS, the sections were incubated with 10 % horse serum (HS) containing 0.2 % bovine serum albumin (BSA; blocker) for 15 min and incubated with anti-ADAM10 antibody diluted 1:250 in PBS containing 1 % HS and 0.2 % BSA (carrier) over night. The sections were washed with PBS, then further incubated with biotinylated goat anti-rabbit IgG (Vector laboratories, Burlingame, CA) diluted 1:1000 in carrier for 90 min. After rinsing, they were incubated with Avidin Biotin Complex (ABC) (Vector Labs) diluted 1:100 in PBS for 90 min. Sections were washed again in PBS and reacted in diaminobenzidine (DAB)-H_2O_2 solution (Sigma St. Louis, USA) for 10 min. Thereafter, the sections were rinsed three times in 0.1 M sodium cacodylate buffer (pH 7.2-7.4; Sigma-Aldrich, Buchs, Switzerland) and incubated with 1 % osmium tetroxide (Science Services, Munich, Germany) in cacodylate buffer for 20 minutes on ice. The osmication of sections was followed by dehydration through ascending ethyl alcohol concentration steps and sections were subsequently rinsed twice in propylene oxide (Sigma-Aldrich, Buchs, Switzerland). Infiltration of the embedding medium was performed by immersing the sections first in a mixture of 2:1 of propylene oxide and Epon (Carl Roth, Karlsruhe, Germany) then in a 1:1 mixture and finally in neat Epon and hardened at 60 °C for 48 h. For post-embedding immunogold labeling, small pieces of cryoprotected hippocampal CA3 region (2.3 M sucrose) were mounted on specimen holders immersed in liquid nitrogen and ultrathin sections (70 nm) were cut and labeled according to (Slot and Geuze, 2007). Briefly, sections were collected on Carbon-Formvar-coated nickel grids (Science Services GmbH, Germany), labeled with rabbit anti-ADAM10 antibody (dilution 1:1000) that was recognized by protein A secondary antibody conjugated with 10 nm large gold particle (purchased from G. Posthuma, University Medical Center Utrecht). Ultrathin sections were examined in an EM902 (Zeiss, Germany) or JEM-2100Plus (JEOL, Germany). Pictures were taken with a TRS 2K digital camera (A. Tröndle, Moorenweis, Germany) and XAROSA (EMSIS), respectively.

Electrophysiology: field extracellular recordings

C57BL6/J Wt or ADAM10 cKO male mice aged 3 weeks were used. The experimenter was blind to the mouse genotype. Transversal brain slices containing the hippocampal formation were prepared as follows. Animals were anesthetized with CO_2 followed by decapitation. Brains were rapidly removed from the skull and placed in an ice-cold modified artificial cerebrospinal fluid solution (aCSF) containing (in mM): 110 Choline Chloride, 25 $NaHCO_3$, 25 D-Glucose, 11.6 Na-L-Ascorbate, 7 $MgSO_4$, 1.25 NaH_2PO_4, 2.5 KCl, 0.5 $CaCl_2$ (pH 7.4 equilibrated with 95% O_2 and 5% CO_2). Transversal brain slices (400 µm thick) were prepared with a microtome vf-200 tissue slicer (Compresstome, Precisionary Instruments, USA) and then incubated at 30°C for approximately 90 minutes in a physiological aCSF containing (in mM): 124 NaCl, 26 $NaHCO_3$, 10 D-Glucose, 1 $MgSO_4$, 1 NaH_2PO_4, 4 KCl, 2.4 $CaCl_2$ (pH 7.4 equilibrated with 95% O_2 and 5% CO_2). Subsequently, the hemi-slices were transferred to the Synchroslice (Lohmann Research Equipment) recording chambers perfused with aCSF at a flow rate of ~2 ml/min using a peristaltic pump (minipulse 3, Gilson, USA). All experiments were conducted at a temperature of 30°C and recordings were performed by using a 2-channel Miniature Preamplifier (multichannel systems, Germany). The field excitatory post-synaptic potential (fEPSP) extracellular recordings were performed by using a single fiber electrode (Lohmann Research Equipment, Germany) placed in the CA3 pyramidal cell body layer. fEPSPs were evoked by stimulating the mossy fibers using a semi-micro concentric bipolar electrode (Lohmann Research Equipment, Germany) placed nearby the granule cell layer or in the hilus region. Square-wave current pulses were generated by a stimulus generator (multichannel systems STG 4008, Germany) and delivered to evoke action potentials. The recorded mossy fiber-CA3 signal was routinely verified by the following procedures: 1) synaptic response amplitudes were largely increased when the 'frequency facilitation' protocol was applied (5 pulses, frequency 20Hz), 2) fEPSPs were only accepted if responses showed an exponential increase in synaptic facilitation after each pulse, 3) application of the group II mGluR agonist (2S,2′R)-2-(2′,3′-Dicarboxycyclopropyl) glycine (DCG-IV, 1µM) at the end of the experiment had to block synaptic transmission responses.

Experiments were discarded if they did not match these three criteria. Paired-Pulse ratio (PPR) was measured by delivering two stimuli at 50, 100, 200, 500 ms inter-stimulus intervals. Synaptic facilitation was examined by repetitive stimulation (5 times) for each inter-stimulus interval, and the resulting potentials were averaged. The PPR was calculated by dividing the amplitude of the second EPSP by the amplitude of the first EPSP. Train facilitation was measured by delivering five pulses at 50 and 100 ms inter-stimulus intervals. Synaptic facilitation was examined by repetitive stimulation (5 times) for each inter-stimulus interval, and potentials were averaged. The facilitation was calculated by dividing the amplitude of each EPSP response by the amplitude of the first EPSP response.

Data acquisition and statistical analysis: all signals were low-pass filtered at 2 kHz and digitized at 10 kHz. Recordings were analyzed by using SynchroSlice (Lohmann Research Equipment) software. Statistical comparisons of pooled data were performed by ANOVA (two-way) using Prism software (GraphPad, San Diego,CA, USA). A p- value of <0.05 was considered statistically significant.

Organotypic slice cultures and single cell electroporation

Organotypic hippocampal slices were prepared from male Wistar rats at post-natal day 4 - 7 as described previously (Gee *et al.*, 2017). Briefly, dissected hippocampi were cut into 400 µm slices with a tissue chopper (McIlwain Tissue Chopper; Model TC752) and cultured on a hydrophilic polytetrafluoroethylene (PTFE) membrane (Millicell CM, Millipore). Cultures were maintained at 37 °C, 5% CO_2 in a medium containing 78.8 % MEM, 20% heat-inactivated horse serum supplemented with 1 mM L-glutamine, 0.00125% ascorbic acid, 0.01 mg/ml insulin, 1 mM $CaCl_2$, 2 mM $MgSO_4$, 13 mM D-glucose and 20 mM HEPES. No antibiotics were added to the culture medium. Individual CA1 pyramidal cells were transfected by single-cell electroporation (Wiegert, Gee and Oertner, 2017a, 2017b) using pAAV-synapsin-mRuby3 and PSD95.FingR_eGFP_CCR5TC plasmids at a final concentration of 1 ng/µL. During electroporation, slices were perfused with a solution containing in mM: 145 NaCl, 10 HEPES, 12.5 D-glucose, 1.2 NaH_2PO_4, 2.5 KCl, 1 $MgCl_2$ and 2 $CaCl_2$. The pH was adjusted to 7.4. 2-4 days after transfection, electroporated slices

were fixed with 4% Roti-Histofix/4% sucrose for 15 min at room temperature (RT), washed 3 x 10 min with phosphate-buffered saline (PBS), and mounted on microscope slides with Mowiol mounting media. Mowiol (Carl Roth) was prepared by following the protocol provided by the manufacturer. This was necessary to assess whether the density of glutamatergic shaft and spine synapses along CA1 neuronal branches was comparable to previously reported literature, and to test the efficacy of the system. In my preparations, the overexpression of mRuby3 allowed for the clear identification of the all distinguished dendrites namely basal, main, oblique and tuft dendrites (Supplemental fig.1).

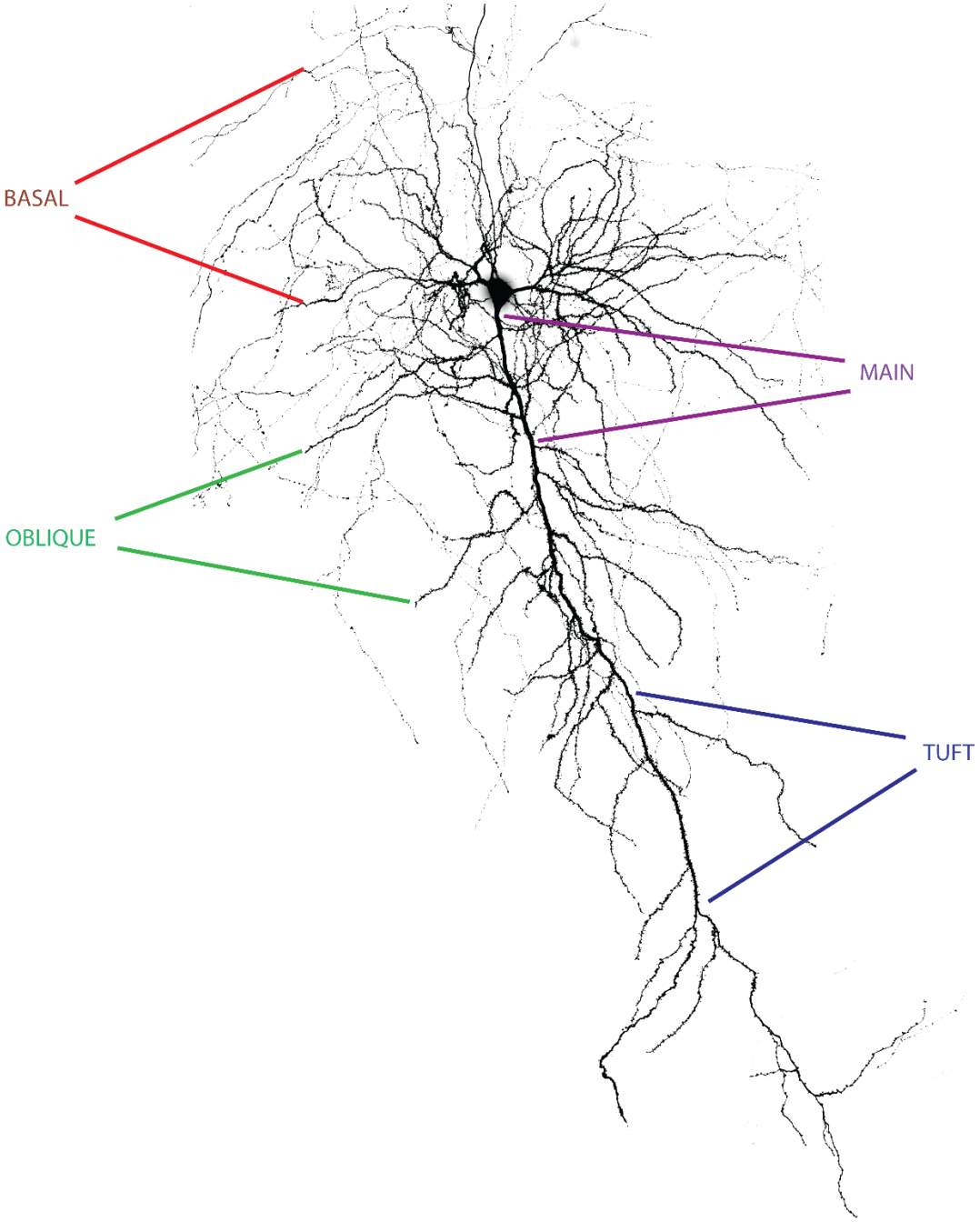

Supplemental figure 1: classification of primary and secondary dendrites namely basal, main, oblique and tuft dendrites.

Hippocampal primary cultures, transfections

Rat primary hippocampal cultures were prepared as described previously with minor adjustments (van Bommel *et al.,* 2019). In brief, hippocampi were isolated from E18 embryos in ice cold HBSS and mechanically dissociated after 10 minutes of 0.25 % trypsin treatment at 37°C of temperature, then plated on poly-L-lysine-coated glass coverslips (18mm) at a density of 40.000-60.000 cells / mL suspended in DMEM supplemented with 10 % fetal bovine serum and penicillin/streptomycin antibiotic (Thermo Fisher Scientific, #15140122). The plating medium was replaced after 1 h by BrainPhys neuronal medium supplemented with SM1 and 0.5 mM glutamine. Primary neurons were grown in an incubator at 37 °C, 5 % CO_2 and 95 % humidity. Cells were transfected at DIV15 by using lipofectamine 2000 and a total DNA/lipofectamine ratio of 1:2. The ratio of the co-transfected DNA constructs was defined and adjusted depending on the combination of the plasmids. Before transfection, the original neuronal medium was removed and kept at 37 °C. BrainPhys medium without additional supplements was added to the cells for the transfection. To this medium, the pre-mixed and pre-incubated transfection mix consisting of plasmid DNA, lipofectamine 2000 and BrainPhys, was added. After 60-75 minutes the transfection medium was exchanged back to the original BrainPhys containing supplements. The pAAV-synapsin-mRuby3 and pCAG_PSD95.FingR-eGFP-CCR5TC plasmids were transfected at a concentration of (1µg/well). 2 days after the transfection the experiments were conducted.

Chemical LTP induction

For chemical LTP induction, neurons grown on coverslips were transferred to Mg^{2+}-free extracellular solution containing in mM: 145 NaCl, 10 HEPES, 12.5 D-glucose, 1.2 NaH_2PO4, 2.5 KCl and 2 CaCl2, pH adjusted to 7.4. Stimulation was given by 5-min exposure to 200µM glycine in combination with 1µM tetrodotoxin and 50µM bicuculline methiodide. After glycine stimulation, the neurons were placed back to the original Mg^{2+}-free extracellular solution followed by imaging sessions.

Immunocytochemistry

Dissociated primary neurons were fixed with 4% Roti-Histofix / 4% sucrose for 20 min at room temperature (RT), washed 3 x 10 min with phosphate-buffered saline (PBS), and permeabilized with 0,2 % Triton X-100 in PBS for 15 min at RT. The neurons were then washed 3 times in PBS and blocked for 60 minutes at RT with blocking buffer (10% horse serum, 0.1 % Triton X-100 in PBS). Primary antibodies were diluted in blocking buffer solution and added to the cells for overnight incubation at 4°C. Subsequently, the neurons were washed 3 x 10 min and secondary antibodies were then diluted in blocking buffer, added to the cells, and incubated for 1 h at RT. Finally, cells were washed 3 x 10 min in PBS and mounted on microscope slides with Mowiol. Mowiol (Carl Roth) was prepared by following the protocol provided by the manufacturer.

Fixed cell imaging: spinning disk confocal microscopy

Cell imaging of fixed samples was performed by using two different confocal microscopy systems. First system: Nikon Eclipse Ti-E inverted microscope controlled by VisiView software (Visitron System). Samples were kept in focus with the built-in Nikon perfect focus system. The microscope was equipped with 488, 561 and 647 nm excitation lasers, coupled to a CSU-W1 spinning disc unit (Yokogawa) via a single-mode fiber. Emission was collected on an Orca flash 4.0LT CMOS camera (Hamamatsu) through a quad-band filter (Chroma, ZET 488/561/647 m). Z-plane images with 0.2 µm intervals of fixed hippocampal slices and primary neurons were taken with either a 60× (Nikon, ApoTIRF 60×/1.49) or a 100× (Nikon, CFI Plan Apochromat Lambda 100×/1.45) objective. The pixel size was set to 65 nm^2.

The second system was provided by the microscopy facility at the German Electron Synchrotron (DESY) center of research. Fixed cell imaging of primary hippocampal cultures was performed with a Nikon Eclipse Ti2 inverted microscope controlled by the NIS-Elements software. As for system one, the samples were kept in focus with the built-in Nikon perfect focus system. The microscope was equipped with 488, 561 and 647 nm

excitation lasers, coupled to a CSU-W1 spinning disc unit (Yokogawa) via a single-mode fiber. Z-plane images with 0.2 µm intervals of fixed primary neurons were acquired with a 100x (Nikon, CFI Plan Apochromat Lambda 100x/1.45) objective.

Live cell Imaging: spinning disk confocal microscopy

Live cell imaging was performed with the same spinning disk microscopy systems described in the previous paragraph. Live imaging of primary neurons was performed for 6 hours by using a Ludin chamber (Life Imaging Services) and µ-Dish 35 mm, or high Glass Bottom (Ibidi). Images and movies were acquired at 2 Hz. At both systems, correct temperature (37°C), CO_2 (5%) and humidity (90%) were maintained with a top stage incubator (Okolab). Pharmacological treatments were performed during live imaging by adding the drugs manually to the culture medium.

Data analysis and Statistics

Distinction of dendritic compartment and main apical branching

Maximum projections and z-planes, utilized for the analysis, were processed, and evaluated using ImageJ software. The analysis aims to quantify the total number of PSD95-positive spine and shaft synapse within different dendritic compartments of two morphologically distinct CA1 hippocampal neuronal types as classified by Benavides-Piccione and colleagues (Benavides-Piccione et al., 2020; Fig. 11A). Benavides-Piccione and colleagues did not provide a precise definition of main apical branching, therefore an initial classification was devised. CA1 cells were classified as bifurcated if a branching point was observed in the main apical shaft, within approximately 200 µm away from the soma, producing two continuing shafts of approximately equal diameter post bifurcation. CA1 cells in which no branching point was observed, or where a branching point produced two morphologically different shafts, were classified as unidirectional. Synaptic density was quantified for unidirectional neurons (no bifurcation of main apical shaft) compared to bifurcated neurons (singular bifurcation of main apical shaft). The distinguished dendritic

compartments were main apical shaft, basal dendrites, tuft dendrites and oblique dendrites (supplemental figure 1). Only primary and secondary branches were considered for analysis. In total, 11 unidirectional and 8 bifurcated neurons were analyzed.

Identification of glutamatergic spine and shaft synapses

Spines were identified as mRuby3-positive protrusions extending from the dendritic body. Spines of different morphologies (filopodia, mushroom, stubby etc.) were included in the analysis. PSD95 was use as a post-synaptic marker and was detected with PSD95.FingR-GFP, a probe based on an intrabodies against PSD95 fused to a GFP (for method see (Gross *et al.*, 2013)). PSD95.FingR-GFP reports localization and amount of the endogenous target protein. Spines were defined as "protrusions" or "PSD95-positive" depending on the presence of PSD95. Synapses appearing before or after dendritic shaft being in focus were identified as protrusions growing in Z dimension and therefore not considered as shaft synapses. To confirm this spine identification method, 3D reconstructions of representative dendritic segments were constructed using the filament tracer tool in Imaris microscopy image analysis software (see next Chapter). This method allowed for the differentiation of indistinguishable protrusions and PSD95-positive shaft synapses. Shafts were identified as puncta of PSD95 signal within the dendritic segment (Fig. 12). Spines and shafts were counted manually using the ImageJ cell counter tool and then normalized to a dendritic length of 10 µm. In every neuron, three separate dendritic segments (15- 60 µm in length) were analyzed for each type of dendrite.

Three-dimensional reconstruction of dendritic segments

Representative three-dimensional (3D) reconstructions of five dendritic segments were created using the filament tracer tool of Imaris microscopy image analysis software (Fig. 12B-D). Z-planes were converted from tif. to IMS (Imaris file format) and imported into the software. mRuby3 and PSD95 were selected as two different channels. Scrolling through the individual planes of the mRuby3-positive Z-planes, certain circular regions were visible prior or subsequently to the illumination of the dendritic shaft. As mRuby3

was employed as a morphological marker we hypothesized that these circular regions were protruding spines perpendicular to the dendritic shaft, illuminated independently to the cell body due to protrusion into a different Z-plane. mRuby3 signal was reconstructed in three dimensions with the filament tracer tool using automatic detection and adjusted manually with reference to the Z-plane. PSD95 puncta were detected with the spot detected tool set to identify puncta with a diameter between 0.15 to 0.8µm. The rotation of the 3D reconstructions allowed for determination of the localization of the PSD95 puncta within the dendritic shaft or a protrusion. The reconstructions served as a comparative method to determine whether indistinguishable protrusions and PSD95-positive shafts were being correctly identified from Z-planes. This method serves as independent validation for the 2D analysis done with ImageJ and additionally contributes to reduce the number of wrongly detected or assigned PSD95-signals. The voxel size was x: 0.065, y: 0.065 and z: 0.2 for all reconstructions.

Analysis of signal intensity of PSD95.FingR-GFP in hippocampal slices

The intensity of PSD95.FingR-eGFP signal, detecting endogenous PSD95 in spine and shaft synapses was determined for five previously analyzed unidirectional and bifurcated neurons. The transcriptional control system of the GFP-fused recombinant probe is matched to the expression of the target protein, therefore the intensity of PSD95.FingR-GFP fluorescence indicates the amount of PSD95 in an individual PSD (Gross *et al.*, 2013). Three dendritic segments (15-60 µm in length) per dendritic segment type of each neuron were analyzed. Maximum z-plane projections of the 488 nm channel were used as source images for the analysis in ImageJ. The elliptical and polygon selection tools were employed to trace the perimeter of the PSD95 puncta. The ‘mean gray value’ was determined and the background intensity subtracted (available method already used previously (Montenegro-Venegas *et al.*, 2022)).

Determination of PSD95.FingR-GFP intensity signals in hippocampal primary cultures

The intensity of PSD95.FingR-GFP signal, detecting endogenous PSD95 in spine and shaft, was determined for 12 primary neurons in total. Dendritic sections of imaged neurons were analyzed using the ComDet plugin of ImageJ, and four independent preparations were quantified. The analysis was performed using maximum intensity z-projections of the 488 nm channel, and "mean gray values" were determined after background intensity subtraction.

Overview of materials for conducted experiments

Table 5. Chemicals/Reagents used

Name	Manufacturer	Reference Number
Choline Chloride	Sigma-Aldrich	C7017
Sodium Dihydrogen phosphate (NaH_2PO_4)	Sigma-Aldrich	S5011
Hydrogen Chloride (HCl)	Merck	109057
Sodium-L-ascorbate	Sigma-Aldrich	A7631
D (+)-Saccharose, 1 kg (D-Sucrose)	Carl Roth Karlsruhe, Germany	9286.1
Sodium bicarbonate ($NaHCO_3$)	Carl Roth Karlsruhe, Germany	6885.1
D-Glucose	Carl Roth	X997.2
Potassium chloride (KCl)	Honey Well	60121
Magnesium chloride ($MgCl_2$)	Honey Well	63020
Calcium chloride ($CaCl_2$)	Sigma-Aldrich	21115
Phenol red (0.5%)	Honeywell Charlotte, USA	32661
Kynurenic acid sodium salt	Tocris Bioscience Bristol, UK	3694
Gibco™ MEM	Thermo Fischer Scientific Waltham, USA	21090-022
Gibco™ DMEM	Thermo Fischer Scientific Waltham, USA	41966-029

Gibco™ horse serum	Thermo Fischer Scientific Waltham, USA	16050122
Gibco™ fetal bovine serum	Thermo Fischer Scientific Waltham, USA	10270
Tripsin	Thermo Fischer Scientific Waltham, USA	25200-056
Antibiotic	Thermo Fischer Scientific Waltham, USA	15140122
SM1	Stem Cell Kit	5792
Lipofectamine 2000	Thermo Fischer Scientific Waltham, USA	11668019
Poly-L-lysine	Sigma-Aldrich	P2636
L-glutamine (200 mM)	Thermo Fischer Scientific Waltham, USA	25030024
Insulin from bovine pancreas (1 mg/mL)	Sigma-Aldrich St Louis, USA	I6634
Sodium chloride (NaCl) (5 M)	Sigma-Aldrich St Louis, USA	S5150
Magnesium Sulphate ($MgSO_4$) (1 M)	Honeywell Charlotte, USA	63126
Ascorbic acid (25%)	Honeywell Charlotte, USA	11140
Egtazic acid (EGTA)	Sigma-Aldrich St Louis, USA	E0396
Potassium gluconate	Sigma-Aldrich St Louis, USA	G45000
HEPES	Sigma-Aldrich St Louis, USA	H4034
Adenosine 5′-triphosphate disodium salt hydrate (Na_2-ATP)	Sigma-Aldrich St Louis, USA	A3377
Guanosine 5′-triphosphate sodium salt hydrate (Na-GTP)	Sigma-Aldrich St Louis, USA	G8877
QIAGEN Plasmid Midi Kit (25)	Qiagen Hilden, Germany	12143

Phosphocreatine disodium salt hydrate (Na_2-phosphocreatine	Sigma-Aldrich St Louis, USA	P7936
L-Ascorbic acid	Sigma-Aldrich St Louis, USA	A5960
ROTI®Histofix 10 %, 10 l, pH7 (Formaldehyde)	Carl Roth	A146.1
BrainPhys + supplement	Stem cell	5792
DCG-IV	Tocris bioscience	0975
Glycine	Carl Roth	3790.3
Bicuculline methiodide	Tocris bioscience	2503
Tetrodotoxin	Carl Roth	6973.1

Table 6: Pharmacological treatment compounds

Name	Manufacturer	Solubility	Reference Number
Control tat-peptide (YGRKKRRQRRRAKLAAAKALA GTLKRRRAAQ AI)	Genosphere Biotechnologies (France)	Water	N/A
A10 tat-peptide (A10 aa 709-730) (YGRKKRRQRRRPKLPPPKPLPGT LKRRRPPQP I)	Genosphere Biotechnologies (France)	Water	N/A
GI254023X	Sigma-Aldrich	DMSO	SML0789-5MG

Table 7: Plasmids

Name	Manufacturer	Reference Number
pCAG_PSD95.FingR-eGFP-CCR5TC	Addgene Watertown, USA	46295
pAAV-synapsin-mRuby3	Gifted by Bas van Bommel	-
CMV-SnFR gamma 2	Gifted by Andrew Plested or Addgene	165495

Table 8: Primary antibodies

Name	Designation	Manufacturer	Dilution	Reference Number
Homer 1/2/3	Rabbit, polyclonal	Synaptic system	1:500	160103
Neuroligin	Mouse, polyclonal	Synaptic system	1:400	129 111

Shank 1	Rabbit, polyclonal	Synaptic system	1:500	162 002
Shank 2	Rabbit, polyclonal	Synaptic system	1:500	162 202
Shank 3	Guinea pig, polyclonal	Synaptic system	1:500	162 304
Synaptopodin	Mouse, monoclonal	Synaptic system	1:500	163 011
SynGAP	Rabbit, polyclonal	Synaptic System	1:100	157 003
Grip1	Rabbit, polyclonal	Synaptic system	1:100	151 003
Cav 1.2	Mouse, monoclonal	Thermo Fisher	1:500	MA5-27717
GluR1 (AMPA)	Rabbit, polyclonal	Sigma-Aldrich	1:500	ABN241
GluN2B (NMDA)	Mouse, monoclonal	Santa cruz	1:500	sc-515148
Cortactin	Mouse, monoclonal	Merck Millipore	1:500	05-180
Synaptotagmin-1	Rabbit, polyclonal	Synaptic system	1:100	105103C5

Table 9: Secondary antibodies

Name	Designation	Manufacturer	Dilution	Reference Number
Alexa 647	Rabbit, polyclonal	Life Technologies	1:500	A21245
Alexa 647	Mouse, polyclonal	Life Technologies	1:500	A21235
Alexa 635	Guinea pig, polyclonal	Abberior	1:500	st635p

Table 10: equipment

Name	Manufacturer	Reference Number
McIlwain Tissue Chopper	Campden Instruments Loughborough, England	Model TC752
Millicell cell culture insert (30-mm, hydrophilic PTFE [polytetrafluoroethylene], 0.4-µm)	Merck Darmstadt, Germany	PICMORG50
Axoporator 800A with pipette holder	Molecular Devices San Jose, USA	
LN Mini Motorized micromanipulator	Luigs & Neumann Feinmechanik und Elektrotechnik Ratingen, Germany	
20X-40X water immersion objective	Olympus	
Upright microscope with motorized stage, charge-coupled device/complementary metal oxide semiconductor		
Heracell 150i CO_2-incubator	Thermo Fischer Scientific Waltham, USA	16496629
Nikon Eclipse Ti-E inverted microscope	Nikon Tokyo, Japan	
CSU-X1 confocal scanner unit	Yokogawa Tokyo, Japan	

Orca flash 4.0LT CMOS camera	Hamamatsu Photonics Shizuoka, Japan	C13440-20CU

Table 11: software

Name	Developer	Application
VisiView	Visitron Systems Puchheim, Germany	Imaging session
Image J	National Institute of Health Bethesda, USA	Imaging Analysis
Imaris microscopy image analysis software	Oxford Instruments Abingdon, UK	3D reconstruction
GraphPad Prism	Dotmatics Boston	Statistics
Adobe Ilustrator	Adobe Inc. San Jose, California	Figures
Microsoft Office	Microsoft Corporation Washington, US	Word, excel
Synchroslice	Lohmann Research Equipment	Electrophysiology

References

Ahmari, S.E., Buchanan, J.A. and Smith, S.J. (2000) 'Assembly of presynaptic active zones from cytoplasmic transport packets', *Nature Neuroscience*, 3(5), pp. 445–451. Available at: https://doi.org/10.1038/74814.

Aoki, C. *et al.* (1994) 'Cellular and subcellular localization of NMDA-R1 subunit immunoreactivity in the visual cortex of adult and neonatal rats', *Journal of Neuroscience*, 14(9), pp. 5202–5222. Available at: https://doi.org/10.1523/jneurosci.14-09-05202.1994.

Aoto, J. *et al.* (2007) 'Postsynaptic ephrinB3 promotes shaft glutamatergic synapse formation', *Journal of Neuroscience*, 27(28), pp. 7508–7519. Available at: https://doi.org/10.1523/JNEUROSCI.0705-07.2007.

Araya, R., Vogels, T.P. and Yuste, R. (2014) 'Activity-dependent dendritic spine neck changes are correlated with synaptic strength', *Proceedings of the National Academy of Sciences of the United States of America*, 111(28). Available at: https://doi.org/10.1073/pnas.1321869111.

Atwood (2014) 'Presynaptic long-term depression mediated by Gi/o-coupledreceptors', *Trends in Neurosciences*, 37(11), pp. 663–673. Available at: https://doi.org/10.1016/j.tins.2014.07.010.Presynaptic.

Bacaj, T. *et al.* (2013) 'Synaptotagmin-1 and Synaptotagmin-7 Trigger Synchronous and Asynchronous Phases of Neurotransmitter Release', *Neuron*, 80(4), pp. 947–959. Available at: https://doi.org/10.1016/j.neuron.2013.10.026.

Bae, J. *et al.* (2012) 'F-actin-dependent regulation of NESH dynamics in rat hippocampal neurons', *PLoS ONE*, 7(4). Available at: https://doi.org/10.1371/journal.pone.0034514.

Baltaci, S.B., Mogulkoc, R. and Baltaci, A.K. (2019) 'Molecular Mechanisms of Early and Late LTP', *Neurochemical Research*, 44(2), pp. 281–296. Available at: https://doi.org/10.1007/s11064-018-2695-4.

Bekkers, J.M. (2011) 'Pyramidal neurons', *Current Biology*, 21(24), p. R975. Available at: https://doi.org/10.1016/j.cub.2011.10.037.

Benavides-Piccione, R. *et al.* (2020) 'Differential Structure of Hippocampal CA1 Pyramidal Neurons in the Human and Mouse', *Cerebral Cortex*, 30(2), pp. 730–752. Available at: https://doi.org/10.1093/cercor/bhz122.

Berry, K.P. and Nedivi, E. (2017) 'Spine Dynamics: Are They All the Same?', *Neuron*, 96(1), pp. 43–55. Available at: https://doi.org/10.1016/j.neuron.2017.08.008.

Bhalla et al (2005) 'Synaptotagmin Isoforms Couple Distinct Ranges of Ca2+, Ba2+, and Sr2+ Concentration to SNARE-mediated Membrane Fusion', *Molecular Biology of the Cell*, 16(November), pp. 5356–5372. Available at: https://doi.org/10.1091/mbc.E05.

Bliss and Lomo (1973) ‘Long-lasting potentiation of synaptic transmission in the dentate area of the unanaesthetized rabbit following stimulation of the perforant path’, *The Journal of Physiology*, 232(2), pp. 357–374. Available at: https://doi.org/10.1113/jphysiol.1973.sp010274.

Boehm, J. *et al.* (2006) ‘Synaptic Incorporation of AMPA Receptors during LTP Is Controlled by a PKC Phosphorylation Site on GluR1’, *Neuron*, 51(2), pp. 213–225. Available at: https://doi.org/10.1016/j.neuron.2006.06.013.

van Bommel, B. *et al.* (2019) ‘F-actin patches associated with glutamatergic synapses control positioning of dendritic lysosomes’, *The EMBO Journal*, 38(15). Available at: https://doi.org/10.15252/embj.2018101183.

Bosch et al (2014) ‘Structural and molecular remodeling of dendritic spine substructures during long-term potentiation’, *Neuron*, 23(1), pp. 1–7. Available at: https://doi.org/10.1016/j.neuron.2014.03.021.Structural.

Bourne, J.N. and Harris, K.M. (2008) ‘Balancing structure and function at hippocampal dendritic spines’, *Annual Review of Neuroscience*, 31, pp. 47–67. Available at: https://doi.org/10.1146/annurev.neuro.31.060407.125646.

Bourne, J.N. and Harris, K.M. (2011) ‘Coordination of size and number of excitatory and inhibitory synapses results in a balanced structural plasticity along mature hippocampal CA1 dendrites during LTP’, *Hippocampus*, 21(4), pp. 354–373. Available at: https://doi.org/10.1002/hipo.20768.

Boyer, C., Schikorski, T. and Stevens, C.F. (1998) ‘Comparison of hippocampal dendritic spines in culture and in brain’, *Journal of Neuroscience*, 18(14), pp. 5294–5300. Available at: https://doi.org/10.1523/jneurosci.18-14-05294.1998.

Bruyère, J. *et al.* (2020) ‘Presynaptic APP levels and synaptic homeostasis are regulated by akt phosphorylation of huntingtin’, *eLife*, 9, pp. 1–30. Available at: https://doi.org/10.7554/eLife.56371.

Bucher, M., Fanutza, T. and Mikhaylova, M. (2020) ‘Cytoskeletal makeup of the synapse: Shaft versus spine’, *Cytoskeleton*. John Wiley and Sons Inc., pp. 55–64. Available at: https://doi.org/10.1002/cm.21583.

Buzsáki, G. and Chrobak, J.J. (1995) ‘Temporal structure in spatially organized neuronal ensembles: a role for interneuronal networks’, *Current Opinion in Neurobiology*, 5(4), pp. 504–510. Available at: https://doi.org/10.1016/0959-4388(95)80012-3.

Cane, M. *et al.* (2014) ‘The relationship between PSD-95 clustering and spine stability In Vivo’, *Journal of Neuroscience*, 34(6), pp. 2075–2086. Available at: https://doi.org/10.1523/JNEUROSCI.3353-13.2014.

Carta, M. *et al.* (2018) ‘Activity-dependent control of NMDA receptor subunit composition at hippocampal mossy fibre synapses’, *Journal of Physiology*, 596(4), pp. 703–716. Available at: https://doi.org/10.1113/JP275226.

Castillo, P.E. (2012) 'Presynaptic LTP and LTD of excitatory and inhibitory synapses', *Cold Spring Harbor Perspectives in Biology*, 4(2). Available at: https://doi.org/10.1101/cshperspect.a005728.

Cavalieri, D. *et al.* (2021) 'Ca1 pyramidal cell diversity is rooted in the time of neurogenesis', *eLife*, 10, pp. 1–30. Available at: https://doi.org/10.7554/eLife.69270.

Chang, S., Trimbuch, T. and Rosenmund, C. (2018) 'Synaptotagmin-1 drives synchronous Ca 2+ -triggered fusion by C 2 B-domain-mediated synaptic-vesicle-membrane attachment', *Nature Neuroscience*, 21(1), pp. 33–42. Available at: https://doi.org/10.1038/s41593-017-0037-5.

Chen, X. *et al.* (2011) 'PSD-95 is required to sustain the molecular organization of the postsynaptic density', *Journal of Neuroscience*, 31(17), pp. 6329–6338. Available at: https://doi.org/10.1523/JNEUROSCI.5968-10.2011.

Chicurel, M.E. and Harris, K.M. (1992) 'Three-dimensional analysis of the structure and composition of CA3 branched dendritic spines and their synaptic relationships with mossy fiber boutons in the rat hippocampus', *Journal of Comparative Neurology*, 325(2), pp. 169–182. Available at: https://doi.org/10.1002/cne.903250204.

Chiu et al (2013) 'Compartmentalization of GABAergic Inhibition by Dendritic Spines', *Science*, 23(1), pp. 1–7. Available at: https://doi.org/10.1126/science.1234274.Compartmentalization.

Citri, A. and Malenka, R.C. (2008) 'Synaptic plasticity: Multiple forms, functions, and mechanisms', *Neuropsychopharmacology*, 33(1), pp. 18–41. Available at: https://doi.org/10.1038/sj.npp.1301559.

Clifton, N.E. *et al.* (2019) 'Regulation and Function of Activity-Dependent Homer in Synaptic Plasticity', *Complex Psychiatry*, 5(3), pp. 147–161. Available at: https://doi.org/10.1159/000500267.

Cobb S.R et al. (1995) 'Synchronization of neuronal activity in hippocampus by individual GABAergic interneurons', *Nature* [Preprint].

Colonnier, M. (1968) 'Synaptic patterns on different cell types in the different laminae of the cat visual cortex. An electron microscope study', *Brain Research*, 9(2). Available at: https://doi.org/10.1016/0006-8993(68)90234-5.

Contreras, A., Hines, D.J. and Hines, R.M. (2019) 'Molecular specialization of GABAergic synapses on the soma and axon in cortical and hippocampal circuit function and dysfunction', *Frontiers in Molecular Neuroscience*, 12(June), pp. 1–9. Available at: https://doi.org/10.3389/fnmol.2019.00154.

Cornejo, V.H., Ofer, N. and Yuste, R. (2022) 'Voltage compartmentalization in dendritic spines in vivo', *Science*, 375(6576), pp. 82–86. Available at: https://doi.org/10.1126/science.abg0501.

Cozzolino, F. *et al.* (2021) 'ADAM10 hyperactivation acts on piccolo to deplete synaptic vesicle stores in Huntington's disease', *Human Molecular Genetics*, 30(13), pp. 1175–1187. Available at: https://doi.org/10.1093/hmg/ddab047.

Craig, A.M. *et al.* (1993) 'The distribution of glutamate receptors in cultured rat hippocampal neurons: Postsynaptic clustering of AMPA selective subunits', *Neuron*, 10(6), pp. 1055–1068. Available at: https://doi.org/10.1016/0896-6273(93)90054-U.

Crosby, K.C. *et al.* (2019) 'Nanoscale Subsynaptic Domains Underlie the Organization of the Inhibitory Synapse', *Cell Reports*, 26(12), pp. 3284–3297. Available at: https://doi.org/10.1016/j.celrep.2019.02.070.Nanoscale.

Dan, Y. and Poo, M.M. (2006) 'Spike timing-dependent plasticity: From synapse to perception', *Physiological Reviews*, 86(3), pp. 1033–1048. Available at: https://doi.org/10.1152/physrev.00030.2005.

DeFelipe, J. and Fariñas, I. (1992) 'The pyramidal neuron of the cerebral cortex: Morphological and chemical characteristics of the synaptic inputs', *Progress in Neurobiology*, 39(6), pp. 563–607. Available at: https://doi.org/10.1016/0301-0082(92)90015-7.

Dichter and Ayala (1987) 'Cellular mechanisms of epilepsy: A status report.', *Science* [Preprint].

Diering, G.H. and Huganir, R.L. (2018) 'The AMPA Receptor Code of Synaptic Plasticity', *Neuron*, 100(2), pp. 314–329. Available at: https://doi.org/10.1016/j.neuron.2018.10.018.

Dimsdale-Zucker, H.R. *et al.* (2018) 'CA1 and CA3 differentially support spontaneous retrieval of episodic contexts within human hippocampal subfields', *Nature Communications*, 9(1). Available at: https://doi.org/10.1038/s41467-017-02752-1.

Dingledine, R. *et al.* (1999) 'The glutamate receptor ion channels', *Pharmacological Reviews*, 51(1), pp. 7–61.

Dosemeci, A. *et al.* (2016) 'The postsynaptic density: There is more than meets the eye', *Frontiers in Synaptic Neuroscience*, 8(AUG), pp. 1–8. Available at: https://doi.org/10.3389/fnsyn.2016.00023.

Dosemeci et al (2016) 'The Postsynaptic Density : There Is More than Meets the Eye', *Frontiers in Synaptic Neuroscience*, 8(August), pp. 1–8. Available at: https://doi.org/10.3389/fnsyn.2016.00023.

Dudek, S.M. and Bear, M.F. (1992) 'Homosynaptic long-term depression in area CA1 of hippocampus and effects of N-methyl-D-aspartate receptor blockade', *Proceedings of the National Academy of Sciences of the United States of America*, 89(10), pp. 4363–4367. Available at: https://doi.org/10.1073/pnas.89.10.4363.

Ebsen, H. *et al.* (2014) 'Identification of SH3 domain proteins interacting with the

cytoplasmic tail of the a Disintegrin and Metalloprotease 10 (ADAM10)', *PLoS ONE*, 9(7). Available at: https://doi.org/10.1371/journal.pone.0102899.

Essrich, C. *et al.* (1998) 'Postsynaptic clustering of major GABAA receptor subtypes requires the γ2 subunit and gephyrin', pp. 563–571.

Falcón-Moya, R., Losada-Ruiz, P. and Rodríguez-Moreno, A. (2019) 'Kainate receptor-mediated depression of glutamate release involves protein kinase a in the cerebellum', *International Journal of Molecular Sciences*, 20(17), pp. 1–12. Available at: https://doi.org/10.3390/ijms20174124.

Fang, H. *et al.* (2021) 'An optimized CRISPR/Cas9 approach for precise genome editing in neurons', *eLife*, pp. 1–25.

Fiala et al (1998) 'Synaptogenesis via dendritic filopodia in developing hippocampal area CA1', *Journal of Neuroscience*, 95(6), pp. E5–E11.

Freund, T.F. (1996) 'Interneurons of the Hippocampus', *Hippocampus*, 470.

Gee, C.E. *et al.* (2017) 'Preparation of slice cultures from rodent hippocampus', *Cold Spring Harbor Protocols*, 2017(2), pp. 126–130. Available at: https://doi.org/10.1101/pdb.prot094888.

Geiger, J.C. *et al.* (2014) 'The GRIP1/14-3-3 pathway coordinates cargo trafficking and dendrite development', *Developmental Cell*, 28(4), pp. 381–393. Available at: https://doi.org/10.1016/j.devcel.2014.01.018.

Geiger, J.R.P. *et al.* (1995) 'Relative abundance of subunit mRNAs determines gating and Ca2+ permeability of AMPA receptors in principal neurons and interneurons in rat CNS', *Neuron*, 15(1), pp. 193–204. Available at: https://doi.org/10.1016/0896-6273(95)90076-4.

Goo, M.S. *et al.* (2017) 'Activity-dependent trafficking of lysosomes in dendrites and dendritic spines', *Journal of Cell Biology*, 216(8), pp. 2499–2513. Available at: https://doi.org/10.1083/jcb.201704068.

Gray EG. (1959) 'Axo-somatic and axo-dendritic synapses of the cerebral cortex: An electron microscope study', *J. Anatomy*, pp. 15–17. Available at: https://doi.org/10.1016/B978-0-12-801426-4.05001-X.

Gross, G.G. *et al.* (2013) 'Recombinant Probes for Visualizing Endogenous Synaptic Proteins in Living Neurons', *Neuron*, 78(6), pp. 971–985. Available at: https://doi.org/10.1016/j.neuron.2013.04.017.

Grunditz, Å. *et al.* (2008) 'Spine neck plasticity controls postsynaptic calcium signals through electrical compartmentalization', *Journal of Neuroscience*, 28(50), pp. 13457–13466. Available at: https://doi.org/10.1523/JNEUROSCI.2702-08.2008.

Harris, E.W. and Cotman, C.W. (1986) 'Long-term potentiation of guinea pig mossy fiber responses is not blocked by N-methyl d-aspartate antagonists', *Neuroscience Letters*, 70(1), pp. 132–137. Available at: https://doi.org/10.1016/0304-3940(86)90451-9.

Harris, K.D. *et al.* (2018) *Classes and continua of hippocampal CA1 inhibitory neurons revealed by single-cell transcriptomics*, *PLoS Biology*. Available at: https://doi.org/10.1371/journal.pbio.2006387.

Harris, K.M. and Stevens, J.K. (1989) 'Dendritic spines of CA1 pyramidal cells in the rat hippocampus: Serial electron microscopy with reference to their biophysical characteristics', *Journal of Neuroscience*, 9(8), pp. 2982–2997. Available at: https://doi.org/10.1523/jneurosci.09-08-02982.1989.

Harris, K.P. and Littleton, J.T. (2015) 'Transmission, development, and plasticity of synapses', *Genetics*, 201(2), pp. 345–375. Available at: https://doi.org/10.1534/genetics.115.176529.

Harvey and Svoboda (2007) 'Locally dynamic synaptic learning rules in pyramidal neuron dendrites', *Nature*, 16(I), pp. 48109–48109. Available at: https://doi.org/10.1038/nature06416.Locally.

Harvey et al (2008) 'The Spread of Ras Activity Triggered by Activation of a Single Dendritic Spine', *Science*, 23(1), pp. 1–7. Available at: https://doi.org/10.1126/science.1159675.The.

Hebb, D.O. (1949) 'The Organization of Behavior; A Neuropsychological Theory', *Oxford, England: Wiley*, 63(4), p. 633. Available at: https://doi.org/10.2307/1418888.

Hedrick et al (2016) 'Rho GTPase complementation underlies BDNF-dependent homo- and heterosynaptic plasticity', *Science*, 538(80), pp. 678–687. Available at: https://doi.org/10.1038/nature19784.Rho.

Henze, D.A., Wittner, L. and Buzsáki, G. (2002) 'Single granule cells reliably discharge targets in the hippocampal CA3 network in vivo', *Nature Neuroscience*, 5(8), pp. 790–795. Available at: https://doi.org/10.1038/nn887.

Herculano-Houzel, S. (2009) 'The human brain in numbers: A linearly scaled-up primate brain', *Frontiers in Human Neuroscience*, 3(NOV), pp. 1–11. Available at: https://doi.org/10.3389/neuro.09.031.2009.

Hodapp, A. *et al.* (2022) 'Dendritic axon origin enables information gating by perisomatic inhibition in pyramidal neurons', *Science*, 377(6613), pp. 1448–1452. Available at: https://doi.org/10.1126/science.abj1861.

Hoettecke, N. *et al.* (2010) 'Improved synthesis of ADAM10 inhibitor GI254023X', *Neurodegenerative Diseases*, 7(4), pp. 232–238. Available at: https://doi.org/10.1159/000267865.

Holderith, N. *et al.* (2012) 'Release probability of hippocampal glutamatergic terminals scales with the size of the active zone', *Nature Neuroscience*, 15(7), pp. 988–997. Available at: https://doi.org/10.1038/nn.3137.

Holler, S. *et al.* (2021) 'Structure and function of a neocortical synapse', *Nature*,

591(7848), pp. 111–116. Available at: https://doi.org/10.1038/s41586-020-03134-2.

Hughes, R. (1958) 'Post Tetanic Potentiation', *Physiological Reviews* [Preprint].

Huson, V. and Regehr, W.G. (2020) 'Diverse roles of Synaptotagmin-7 in regulating vesicle fusion', *Current Opinion in Neurobiology*, 63, pp. 42–52. Available at: https://doi.org/10.1016/j.conb.2020.02.006.

Imig, C. *et al.* (2014) 'The Morphological and Molecular Nature of Synaptic Vesicle Priming at Presynaptic Active Zones', *Neuron*, 84(2), pp. 416–431. Available at: https://doi.org/10.1016/j.neuron.2014.10.009.

Ivanova, D. *et al.* (2015) ' Synaptic activity controls localization and function of Ct BP 1 via binding to B assoon and P iccolo ', *The EMBO Journal*, 34(8), pp. 1056–1077. Available at: https://doi.org/10.15252/embj.201488796.

Jackman, S.L. *et al.* (2016) 'The calcium sensor synaptotagmin 7 is required for synaptic facilitation', *Nature*, 529(7584), pp. 88–91. Available at: https://doi.org/10.1038/nature16507.

Jackman, S.L. and Regehr, W.G. (2017) 'The Mechanisms and Functions of Synaptic Facilitation', *Neuron*, 94(3), pp. 447–464. Available at: https://doi.org/10.1016/j.neuron.2017.02.047.

Jacob TC., et al (2008) 'GABAA receptor trafficking and its role in the dynamic modulation of neuronal inhibition', *Nature Reviews Neuroscience* [Preprint]. Available at: https://doi.org/10.1038/nrn2370.GABA.

Jang, M. *et al.* (2015) 'Coexistence of glutamatergic spine synapses and shaft synapses in substantia nigra dopamine neurons', *Scientific Reports*, 5. Available at: https://doi.org/10.1038/srep14773.

Jenks, K.R. *et al.* (2021) 'Heterosynaptic Plasticity and the Experience-Dependent Refinement of Developing Neuronal Circuits', *Frontiers in Neural Circuits*, 15(December), pp. 1–20. Available at: https://doi.org/10.3389/fncir.2021.803401.

Jorissen, E. *et al.* (2010) 'The disintegrin/metalloproteinase ADAM10 is essential for the establishment of the brain cortex', *Journal of Neuroscience*, 30(14), pp. 4833–4844. Available at: https://doi.org/10.1523/JNEUROSCI.5221-09.2010.

Juárez-Muñoz, Y. *et al.* (2017) 'CaMKII requirement for the persistence of in vivo hippocampal mossy fiber synaptic plasticity and structural reorganization', *Neurobiology of Learning and Memory*, 139, pp. 56–62. Available at: https://doi.org/10.1016/j.nlm.2016.12.015.

Katz and Miledi (1968) 'THE ROLE OF CALCIUM IN NEUROMUSCULAR FACILITATION', *Journal of Physiology*, pp. 357–361. Available at: https://doi.org/10.1016/b978-1-4832-8322-7.50066-2.

Katz, Y. *et al.* (2009) 'Synapse Distribution Suggests a Two-Stage Model of Dendritic

Integration in CA1 Pyramidal Neurons', *Neuron*, 63(2), pp. 171–177. Available at: https://doi.org/10.1016/j.neuron.2009.06.023.

Kennedy, M.B. (2016) 'Synaptic Signaling in Learning and Memory', *Cold Spring Harbor Perspectives in Biology* [Preprint].

Khezri, M.R., Mohebalizadeh, M. and Ghasemnejad-Berenji, M. (2023) 'Therapeutic potential of ADAM10 modulation in Alzheimer's disease: a review of the current evidence', *Cell Communication and Signaling*, 21(1), pp. 1–12. Available at: https://doi.org/10.1186/s12964-023-01072-w.

Kim, E. and Sheng, M. (2004) 'PDZ domain proteins of synapses', *Nature Reviews Neuroscience*, 5(10), pp. 771–781. Available at: https://doi.org/10.1038/nrn1517.

Knott, G.W. *et al.* (2006) 'Spine growth precedes synapse formation in the adult neocortex in vivo', *Nature Neuroscience*, 9(9), pp. 1117–1124. Available at: https://doi.org/10.1038/nn1747.

Konietzny, A. *et al.* (2019) 'Myosin V regulates synaptopodin clustering and localization in the dendrites of hippocampal neurons', *Journal of Cell Science*, 132(16). Available at: https://doi.org/10.1242/jcs.230177.

Kruijssen, D.L.H. and Wierenga, C.J. (2019) 'Single Synapse LTP: A Matter of Context?', *Frontiers in Cellular Neuroscience*, 13(November). Available at: https://doi.org/10.3389/fncel.2019.00496.

Kursula, P. (2019) 'Shanks — multidomain molecular scaffolds of the postsynaptic density', *Current Opinion in Structural Biology*, 54, pp. 122–128. Available at: https://doi.org/10.1016/j.sbi.2019.01.007.

Kwon, H.B. and Sabatini, B.L. (2011) 'Glutamate induces de novo growth of functional spines in developing cortex', *Nature*, 474(7349), pp. 100–104. Available at: https://doi.org/10.1038/nature09986.

Lawrence, J.J., Grinspan, Z.M. and McBain, C.J. (2004) 'Quantal transmission at mossy fibre targets in the CA3 region of the rat hippocampus', *Journal of Physiology*, 554(1), pp. 175–193. Available at: https://doi.org/10.1113/jphysiol.2003.049551.

Lee et al (2009a) 'Activation of CaMKII in single dendritic spines during long-term potentiation', *Nature*, 176(5), pp. 139–148. Available at: https://doi.org/10.1038/nature07842.Activation.

Lee et al (2009b) 'Activation of CaMKII in single dendritic spines during long-term potentiation', *Nature*, 176(3), pp. 139–148. Available at: https://doi.org/10.1053/j.gastro.2016.08.014.CagY.

Li et al (1995) 'Ca2+-dependent and -independent activities of neural and non-neural synaptotagmins', *Nature*, 246(5429), p. 170. Available at: https://doi.org/10.1038/246170a0.

Liu, H., Bai, H., Xue, R., *et al.* (2014) 'Linker mutations reveal the complexity of synaptotagmin 1 action during synaptic transmission', *Nature Neuroscience*, 17(5), pp. 670–677. Available at: https://doi.org/10.1038/nn.3681.

Liu, H., Bai, H., Hui, E., *et al.* (2014) 'Synaptotagmin 7 functions as a Ca2+-sensor for synaptic vesicle replenishment', *eLife*, 3, pp. 1–18. Available at: https://doi.org/10.7554/elife.01524.

Loomba, S. *et al.* (2022) 'Connectomic comparison of mouse and human cortex', *Science*, 377(6602). Available at: https://doi.org/10.1126/science.abo0924.

Lundgren, J.L. *et al.* (2015) 'ADAM10 and BACE1 are localized to synaptic vesicles', *Journal of Neurochemistry*, 135(3), pp. 606–615. Available at: https://doi.org/10.1111/jnc.13287.

Lundgren, J.L. *et al.* (2020) 'Proximity ligation assay reveals both pre- A nd postsynaptic localization of the APP-processing enzymes ADAM10 and BACE1 in rat and human adult brain', *BMC Neuroscience*, 21(1), pp. 1–12. Available at: https://doi.org/10.1186/s12868-020-0554-0.

Lüscher, B. and Keller, C.A. (2004) 'Regulation of GABAA receptor trafficking, channel activity, and functional plasticity of inhibitory synapses', *Pharmacology and Therapeutics*, 102(3), pp. 195–221. Available at: https://doi.org/10.1016/j.pharmthera.2004.04.003.

Luscher et al. (2011) 'GABAA R trafficking-mediated plasticity of inhibitory synapses', *Neuron* [Preprint]. Available at: https://doi.org/10.1016/j.neuron.2011.03.024.GABA.

Makino and Malinow (2009) 'AMPA receptor incorporation into synapses during LTP: the role of lateral movement and exocytosis', *Neuron*, 23(1), pp. 1–7. Available at: https://doi.org/10.1016/j.neuron.2009.08.035.AMPA.

Malenka, R.C. and Bear, M.F. (2004) 'LTP and LTD: An embarrassment of riches', *Neuron*, 44(1), pp. 5–21. Available at: https://doi.org/10.1016/j.neuron.2004.09.012.

Malenka, R.C. and Nicoll, R.A. (1993) 'NMDA-receptor-dependent synaptic plasticity: multiple forms and mechanisms', *Trends in Neurosciences*, 16(12), pp. 521–527. Available at: https://doi.org/10.1016/0166-2236(93)90197-T.

Malinverno, M. *et al.* (2010) 'Synaptic localization and activity of ADAM10 regulate excitatory synapses through N-cadherin cleavage', *Journal of Neuroscience*, 30(48), pp. 16343–16355. Available at: https://doi.org/10.1523/JNEUROSCI.1984-10.2010.

Marcello, E. *et al.* (2007) 'Synapse-associated protein-97 mediates α-secretase ADAM10 trafficking and promotes its activity', *Journal of Neuroscience*, 27(7), pp. 1682–1691. Available at: https://doi.org/10.1523/JNEUROSCI.3439-06.2007.

Marcello, E. *et al.* (2019) 'Amyloid-β Oligomers Regulate ADAM10 Synaptic Localization Through Aberrant Plasticity Phenomena', *Molecular Neurobiology*, 56(10),

pp. 7136–7143. Available at: https://doi.org/10.1007/s12035-019-1583-5.

Mardones, M.D. *et al.* (2019) 'PSD95 regulates morphological development of adult-born granule neurons in the mouse hippocampus', *Journal of Chemical Neuroanatomy*, 98(November 2018), pp. 117–123. Available at: https://doi.org/10.1016/j.jchemneu.2019.04.009.

Matsuzaki et al (2001) 'Dendritic spine geometry is critical for AMPA receptor expression in hippocampal CA1 pyramidal neurons', 18(9), pp. 1199–1216. Available at: https://doi.org/10.1038/nn736.Dendritic.

Matsuzaki, M. *et al.* (2004) 'Structural basis of long-term potentiation in single dendritic spines', *Nature*, 429(6993), pp. 761–766. Available at: https://doi.org/10.1038/nature02617.

Maus, L. *et al.* (2020) 'Ultrastructural Correlates of Presynaptic Functional Heterogeneity in Hippocampal Synapses', *Cell Reports*, 30(11), pp. 3632-3643.e8. Available at: https://doi.org/10.1016/j.celrep.2020.02.083.

Mikhaylova et al (2018) 'Caldendrin Directly Couples Postsynaptic Calcium Signals to Actin Remodeling in Dendritic Spines Article Caldendrin Directly Couples Postsynaptic Calcium Signals to Actin Remodeling in Dendritic Spines', *Neuron*, pp. 1110–1125. Available at: https://doi.org/10.1016/j.neuron.2018.01.046.

Mikhaylova, M. *et al.* (2018) 'Caldendrin Directly Couples Postsynaptic Calcium Signals to Actin Remodeling in Dendritic Spines', *Neuron*, 97(5), pp. 1110-1125.e14. Available at: https://doi.org/10.1016/j.neuron.2018.01.046.

Miles et al. (1996) 'Differences between Somatic and Dendritic Inhibition in the Hippocampus', *Ne* [Preprint].

Monday and Castillo (2017) 'Closing the gap: long-term presynaptic plasticity in brain function and disease', *Current Opinion in Neurobiology*, pp. 106–112. Available at: https://doi.org/10.1016/j.conb.2017.05.011.Closing.

Monday, H.R., Younts, T.J. and Castillo, P.E. (2018) 'Long-term plasticity of neurotransmitter release: Emerging mechanisms and contributions to brain function and disease', *Annual Review of Neuroscience*, 41(April), pp. 299–322. Available at: https://doi.org/10.1146/annurev-neuro-080317-062155.

Montenegro-Venegas, C. *et al.* (2022) ' Bassoon controls synaptic vesicle release via regulation of presynaptic phosphorylation and cAMP ', *EMBO reports*, 23(8). Available at: https://doi.org/10.15252/embr.202153659.

Mosbacher, J. *et al.* (1994) 'A molecular determinant for submillisecond desensitization in glutamate receptors', *Science*, 266(5187), pp. 1059–1062. Available at: https://doi.org/10.1126/science.7973663.

Mulkey, R.M. and Malenka, R.C. (1992) 'Mechanisms underlying induction of

homosynaptic long-term depression in area CA1 of the hippocampus', *Neuron*, 9(5), pp. 967–975. Available at: https://doi.org/10.1016/0896-6273(92)90248-C.

Murakoshi, H., Wang, H. and Yasuda, R. (2011) 'Local, persistent activation of Rho GTPases during plasticity of single dendritic spines', *Nature*, 472(7341), pp. 100–104. Available at: https://doi.org/10.1038/nature09823.Local.

Musleh, W. *et al.* (1997) 'Glycine-induced long-term potentiation is associated with structural and functional modifications of α-amino-3-hydroxyl-5-methyl-4-isoxazolepropionic acid receptors', *Proceedings of the National Academy of Sciences of the United States of America*, 94(17), pp. 9451–9456. Available at: https://doi.org/10.1073/pnas.94.17.9451.

Neher, E. (1998) 'Usefulness and limitations of linear approximations to the understanding of Ca++ signals', *Cell Calcium*, 24(5–6), pp. 345–357. Available at: https://doi.org/10.1016/S0143-4160(98)90058-6.

Nicoll, R.A. (2017) 'A Brief History of Long-Term Potentiation', *Neuron*, 93(2), pp. 281–290. Available at: https://doi.org/10.1016/j.neuron.2016.12.015.

Nicoll, R.A. and Schmitz, D. (2005) 'Synaptic plasticity at hippocampal mossy fibre synapses', *Nature Reviews Neuroscience*, 6(11), pp. 863–876. Available at: https://doi.org/10.1038/nrn1786.

Padamsey, Z. *et al.* (2017) 'Activity-Dependent Exocytosis of Lysosomes Regulates the Structural Plasticity of Dendritic Spines', *Neuron*, 93(1), pp. 132–146. Available at: https://doi.org/10.1016/j.neuron.2016.11.013.

Penn, A.C. *et al.* (2018) *Europe PMC Funders Group Hippocampal LTP and contextual learning require surface diffusion of AMPA receptors*, *Nature*. Available at: https://doi.org/10.1038/nature23658.Hippocampal.

Petralia, R.S. *et al.* (2005) 'Ontogeny of postsynaptic density proteins at glutamatergic synapses', *Molecular and Cellular Neuroscience*, 29(3), pp. 436–452. Available at: https://doi.org/10.1016/j.mcn.2005.03.013.

Prior, P. *et al.* (1992) 'Primary structure and alternative splice variants of gephyrin, a putative glycine receptor-tubulin linker protein', *Neuron*, 8(6), pp. 1161–1170. Available at: https://doi.org/10.1016/0896-6273(92)90136-2.

Prox, J. *et al.* (2013) 'Postnatal disruption of the disintegrin/metalloproteinase ADAM10 in brain causes epileptic seizures, learning deficits, altered spine morphology, and defective synaptic functions', *Journal of Neuroscience*, 33(32), pp. 12915–12928. Available at: https://doi.org/10.1523/JNEUROSCI.5910-12.2013.

Ramón y Cajal S. (1983) 'Neue darstellung vom histologischen bau des centralnervensystem.', *Arch. Anat.* [Preprint].

Rebola, N., Carta, M. and Mulle, C. (2017) 'Operation and plasticity of hippocampal CA3

circuits: Implications for memory encoding', *Nature Reviews Neuroscience*, 18(4), pp. 209–221. Available at: https://doi.org/10.1038/nrn.2017.10.

Reilly, J.E., Hanson, H.H. and Phillips, G.R. (2011) 'Persistence of excitatory shaft synapses adjacent to newly emerged dendritic protrusions', *Molecular and Cellular Neuroscience*, 48(2), pp. 129–136. Available at: https://doi.org/10.1016/j.mcn.2011.06.014.

Richards, S.E.V. and Van Hooser, S.D. (2018) 'Neural architecture: From cells to circuits', *Journal of Neurophysiology*, 120(2), pp. 854–866. Available at: https://doi.org/10.1152/jn.00044.2018.

Richter, K. *et al.* (1999) 'Is Localized at Both Excitatory and Inhibitory Synapses of Rat Brain', *The Journal of comparative neurology*, 448(January), pp. 437–448.

Risher, W.C. *et al.* (2014) 'Rapid golgi analysis method for efficient and unbiased classification of dendritic spines', *PLoS ONE*, 9(9). Available at: https://doi.org/10.1371/journal.pone.0107591.

Rollenhagen, A. *et al.* (2007) 'Structural determinants of transmission at large hippocampal mossy fiber synapses', *Journal of Neuroscience*, 27(39), pp. 10434–10444. Available at: https://doi.org/10.1523/JNEUROSCI.1946-07.2007.

Sabo, S.L., Gomes, R.A. and McAllister, A.K. (2006) 'Formation of presynaptic terminals at predefined sites along axons', *Journal of Neuroscience*, 26(42), pp. 10813–10825. Available at: https://doi.org/10.1523/JNEUROSCI.2052-06.2006.

Saftig, P. and Lichtenthaler, S.F. (2015) 'The alpha secretase ADAM10: A metalloprotease with multiple functions in the brain', *Progress in Neurobiology*, 135, pp. 1–20. Available at: https://doi.org/10.1016/j.pneurobio.2015.10.003.

Salin, P.A. *et al.* (1996) 'Distinct short-term plasticity at two excitatory synapses in the hippocampus', *Proceedings of the National Academy of Sciences of the United States of America*, 93(23), pp. 13304–13309. Available at: https://doi.org/10.1073/pnas.93.23.13304.

Schikorski, T. and Stevens, C.F. (1997) 'Quantitative Ultrastructural Analysis of Hippocampal excitatory synapses', *J. Neurosci.*, 17(15), pp. 5858–5867. Available at: https://pdfs.semanticscholar.org/6317/17f04ca52a47f6c909b5e614a4a2afa6c141.pdf.

Sell, G.L., Barrow, S.L. and McAllister, A.K. (2020) *Molecular composition of developing glutamatergic synapses, Synapse Development and Maturation: Comprehensive Developmental Neuroscience*. Elsevier Inc. Available at: https://doi.org/10.1016/B978-0-12-823672-7.00001-6.

Sheng, M. and Kim, E. (2011) 'The postsynaptic organization of synapses', *Cold Spring Harbor Perspectives in Biology*, 3(12), pp. 1–20. Available at: https://doi.org/10.1101/cshperspect.a005678.

Soltesz, I. and Losonczy, A. (2018) ‘CA1 pyramidal cell diversity enabling parallel information processing in the hippocampus’, *Nature Neuroscience*, 21(4), pp. 484–493. Available at: https://doi.org/10.1038/s41593-018-0118-0.

Speranza, L. *et al.* (2022) ‘Stabilization of Spine Synaptopodin by mGluR1 Is Required for mGluR-LTD’, *Journal of Neuroscience*, 42(9), pp. 1666–1678. Available at: https://doi.org/10.1523/JNEUROSCI.1466-21.2022.

Spruston, N. (2008) ‘Pyramidal neurons: Dendritic structure and synaptic integration’, *Nature Reviews Neuroscience*, 9(3), pp. 206–221. Available at: https://doi.org/10.1038/nrn2286.

Stefen, H. *et al.* (2016) ‘Regulation of the Postsynaptic Compartment of Excitatory Synapses by the Actin Cytoskeleton in Health and Its Disruption in Disease’, *Neural Plasticity*, 2016. Available at: https://doi.org/10.1155/2016/2371970.

Stevens, C.F. and Wang, Y. (1995) ‘Facilitation and depression at single central synapses’, *Neuron*, 14(4), pp. 795–802. Available at: https://doi.org/10.1016/0896-6273(95)90223-6.

Südhof (2012) ‘The Presynaptic Active Zone’, *Neuron*, 75(1), pp. 11–25. Available at: https://doi.org/10.1016/j.neuron.2012.06.012.The.

Südhof, T.C. (2013) ‘Neurotransmitter Release: The Last Millisecond in the Life of a Synaptic Vesicle’, *Neuron*, 23(1), pp. 1–7. Available at: https://doi.org/10.1016/j.neuron.2013.10.022.Neurotransmitter.

Sugita, S. *et al.* (2001) ‘Synaptotagmin VII as a Plasma Membrane Ca2+ Sensor in Exocytosis other protein’, 30, pp. 459–473.

Taub, A.H., Katz, Y. and Lampl, I. (2013) ‘Cortical balance of excitation and inhibition is regulated by the rate of synaptic activity’, *Journal of Neuroscience*, 33(36), pp. 14359–14368. Available at: https://doi.org/10.1523/JNEUROSCI.1748-13.2013.

Thome, C. *et al.* (2014) ‘Axon-carrying dendrites convey privileged synaptic input in hippocampal neurons’, *Neuron*, 83(6), pp. 1418–1430. Available at: https://doi.org/10.1016/j.neuron.2014.08.013.

Tønnesen, J. *et al.* (2014) ‘Spine neck plasticity regulates compartmentalization of synapses’, *Nature Neuroscience*, 17(5), pp. 678–685. Available at: https://doi.org/10.1038/nn.3682.

Trotter, J.H. *et al.* (2019) ‘Synaptic neurexin-1 assembles into dynamically regulated active zone nanoclusters’, *Journal of Cell Biology*, 218(8), pp. 2677–2698. Available at: https://doi.org/10.1083/JCB.201812076.

Venkatesh, H.S. *et al.* (2017) ‘Targeting neuronal activity-regulated neuroligin-3 dependency in high-grade glioma’, *Nature*, 549(7673), pp. 533–537. Available at: https://doi.org/10.1038/nature24014.Targeting.

Vevea, J.D. *et al.* (2021) 'Synaptotagmin 7 is targeted to the axonal plasma membrane through g-secretase processing to promote synaptic vesicle docking in mouse hippocampal neurons', *eLife*, 10, pp. 1–33. Available at: https://doi.org/10.7554/eLife.67261.

Vyleta, N. P. & Jonas, P. (2014) 'Loose Coupling Between Ca2+ Channels and Release Sensors at a Plastic Hippocampal Synapse', *Science*, 343(February), pp. 665–670.

Vyleta, N.P., Borges-Merjane, C. and Jonas, P. (2016) 'Plasticity-dependent, full detonation at hippocampal mossy fiber-CA3 pyramidal neuron synapses', *eLife*, 5(OCTOBER2016), pp. 1–12. Available at: https://doi.org/10.7554/eLife.17977.

Wan, X.Z. *et al.* (2012) 'Activation of NMDA receptors upregulates a disintegrin and metalloproteinase 10 via a Wnt/MAPK signaling pathway', *Journal of Neuroscience*, 32(11), pp. 3910–3916. Available at: https://doi.org/10.1523/JNEUROSCI.3916-11.2012.

Watanabe, M. *et al.* (1998) 'Selective scarcity of NMDA receptor channel subunits in the stratum lucidum (mossy fibre-recipient layer) of the mouse hippocampal CA3 subfield', *European Journal of Neuroscience*, 10(2), pp. 478–487. Available at: https://doi.org/10.1046/j.1460-9568.1998.00063.x.

Wichmann, C. and Kuner, T. (2022) 'Heterogeneity of glutamatergic synapses: Cellularmechanisms and network consequences', *Physiological Reviews*. American Physiological Society, pp. 269–318. Available at: https://doi.org/10.1152/PHYSREV.00039.2020.

Wiegert, J.S., Gee, C.E. and Oertner, T.G. (2017a) 'Single-cell electroporation of neurons', *Cold Spring Harbor Protocols*, 2017(2), pp. 135–138. Available at: https://doi.org/10.1101/pdb.prot094904.

Wiegert, J.S., Gee, C.E. and Oertner, T.G. (2017b) 'Viral vector-based transduction of slice cultures', *Cold Spring Harbor Protocols*, 2017(2), pp. 131–134. Available at: https://doi.org/10.1101/pdb.prot094896.

Wiesner, T. *et al.* (2020) 'Activity-Dependent Remodeling of Synaptic Protein Organization Revealed by High Throughput Analysis of STED Nanoscopy Images', *Frontiers in Neural Circuits*, 14(October), pp. 1–19. Available at: https://doi.org/10.3389/fncir.2020.00057.

Willems, J. *et al.* (2020) *Orange: A CRISPR/Cas9-based genome editing toolbox for epitope tagging of endogenous proteins in neurons*, *PLoS Biology*. Available at: https://doi.org/10.1371/journal.pbio.3000665.

Xu, C. *et al.* (2020) 'Structure and plasticity of silent synapses in developing hippocampal neurons visualized by super-resolution imaging', *Cell Discovery*, 6(1). Available at: https://doi.org/10.1038/s41421-019-0139-1.

Yizhar, O. *et al.* (2011) 'Neocortical excitation/inhibition balance in information processing and social dysfunction', *Nature*, 477(7363), pp. 171–178. Available at:

https://doi.org/10.1038/nature10360.

Yoshino, M. *et al.* (1996) ‘A metabotropic glutamate receptor agonist DCG-IV suppresses synaptic transmission at mossy fiber pathway of the guinea pig hippocampus’, *Neuroscience Letters*, 207(1), pp. 70–72. Available at: https://doi.org/10.1016/0304-3940(96)12486-1.

Yuan, Y. *et al.* (2015) ‘Differential regulation of apical–basolateral dendrite outgrowth by activity in hippocampal neurons’, *Frontiers in Cellular Neuroscience*, 9(AUGUST), pp. 1–8. Available at: https://doi.org/10.3389/fncel.2015.00314.

Yuste, R., Bonhoeffer, T. and Planck, M. (2004) ‘GENESIS OF DENDRITIC SPINES : INSIGHTS FROM ULTRASTRUCTURAL’, *Nature Reviews Neuroscience*, 5(January), pp. 24–34. Available at: https://doi.org/10.1038/nrn1300.

Zeng, H. and Sanes, J.R. (2017) ‘Neuronal cell-type classification: Challenges, opportunities and the path forward’, *Nature Reviews Neuroscience*, 18(9), pp. 530–546. Available at: https://doi.org/10.1038/nrn.2017.85.

Ziv and Smith (1996) ‘Evidence for a role of dendritic filopodia in synaptogenesis and spine formation’, *Neuron*, 17(5), pp. 91–102.

Zucker, R.S. and Regehr, W.G. (2002) ‘Short-term synaptic plasticity’, *Annual Review of Physiology*, 64, pp. 355–405. Available at: https://doi.org/10.1146/annurev.physiol.64.092501.114547.

Acknowledgments

During my doctoral studies, several amazing and inspiring people, from whom I shaped my route, joined me scientifically and privately. This work would never have been done without their support, assistance, and guidance.

Primarily, I want to express my gratitude to my supervisor, Prof. Dr. Marina Mikhaylova, for giving me the opportunity to be part of her research group and obtain my doctoral degree. Through her experience and broad knowledge, I further developed my own passion for science. I am very grateful for her assistance, guidance and the several opportunities she gave me to attend international conferences, meet excellent scientists also abroad in the country as well as to let me go at the Cajal school in Bordeaux, and use this experience as a starting point for the doctoral studies. It was my best pleasure to work in a highly interdisciplinary team, where people share their knowledge and expertise from multiple different areas. Specifically, I appreciate the deep support and guidance of Bas, especially at the beginning of the PhD, who have introduced me to several techniques used in the lab including immunolabeling and confocal microscopy as well as how to perform these techniques in different cell systems. Throughout my PhD, it has been an absolute pleasure to work closely and collaborate with Julia, an exceptionally talented scientist from whom I have gained precious knowledge in a wide range of laboratory techniques. Furthermore, I would like to express my deepest gratitude to Michi, an incredibly talented biophysicist, who provided a lot of support and assistance throughout my entire PhD journey. I consider myself incredibly fortunate to have had someone like him, not only as a colleague but also as a friend. His expertise and friendship have been valuable to me, and I am truly grateful for this. Also, I would like to extend my gratitude to Jasper Grendel and Anja Konietzny for their countless important discussions, feedback, and suggestions that positively influenced the progress of my project and supported me during my stay in Hamburg.

Besides, I want to say a special thanks to Arie Maeve Brückner, a really talented internship student who joined the lab during the second year of my PhD. Arie worked closely with me on establishing a slices culture sample system in order to investigate the morphological properties of neurons. Her contributions to my project were invaluable. It was truly a pleasure to have Arie as part of our team, and I wholeheartedly wish her the very best in her future career endeavors.

Over the PhD, our lab was lucky to welcome several people. I want to express my gratitude to Yannes, who initially joined as a master's student in our lab and later became one of the PhD students. Yannes played a crucial role in the starting development of my project, and his dedication and insights were significant. Furthermore, I would like to extend my

appreciation to Nathalie, Yuhao, Dani, and Chris, who also joined the lab during this time. Their presence and contributions enriched our team, and I consider myself incredibly lucky to have them as fellow lab members. In general, everyone brought unique perspectives, constantly providing input and ideas to optimize experiments, and helping with various organizational matters. I am grateful to everyone in the lab for their continuous support and the knowledge I gained from each. Their collective efforts and collaboration played an integral part in the success of my project.

Then, some of the lab members moved to Berlin as Marina was appointed as a full professor for optobiology at the Humboldt-University (HU) of Berlin, and therefore, the research group was split between two sites. From the Berlin team, I have to say thanks to Dominik who helped with many bureaucracy steps and organizational things to ensure smooth operations. I also wish all the best to the remaining people who I did not specifically mention here.

Special thanks also go to Iris Ohmert, Sabine Graf and Jan Schröder for excellent technical support and assistance throughout the years.

I would also like to thank Dr. Christine E. Gee and Prof. Dr. Thomas Oertner for letting me access to their equipment and rooms, for always sharing her knowledge and for very helpful discussions. I always learned and improved my knowledge a lot through their useful input.

Outside of the lab, but still part of the ZMNH community, I would like to express my gratitude to Mauro who has supported me constantly over the last four years as a colleague and as a friend. I would also like to give a special shout-out to Tim, for always keeping up the good and all the fun moments, and Franco for his suggestions and feedback on my progress of the project.

I want to say a deep thank to my parents who have given me the opportunity and freedom to choose what was best for my future. I am grateful for the trust you have shown me, as it has given me the courage to make certain choices in the past and in the present. I am truly thankful for the sacrifices you have made to allow me to study at university in Italy. Without your support, I would never have been able to achieve the PhD.

I also want to thank my brother Andrea who was always present and ready to give me braveness and transmitting positivity in a way that only a big brother can do. Then, I would like to express my deep appreciation to my incredible best friend, Claudio. Over the years, Claudio has been a resolute source of motivation and support, especially through his WhatsApp audios (from Sardinia).

Finally, I am overwhelmed with profound gratitude towards my dearest friend, my soulmate, and the love of my life, Chiara, as well as my sweetheart Rebecca.
Chiara, with her resolute belief in me and support has been the pillar of my success. Her love, understanding, and encouragement have been my guiding light, propelling me forward even when faced with adversity. I am forever grateful for her presence in my lifeline and for the immeasurable impact she has had on my journey.
Rebecca is a constant source of joy and inspiration. Her innocent laughter and boundless love have fueled my determination to achieve the end goal. Her presence in my life is a precious gift, and I am immensely thankful for the love and happiness she brings into our family. To both of them I am deeply thankful for being my steady support system. Nothing would have been done without them. I am forever grateful they are part of my life.

Eidesstattliche Versicherung

Declaration on oath

Hiermit erkläre ich an Eides statt, dass ich die vorliegende Dissertationsschrift selbst verfasst und keine anderen als die angegebenen Quellen und Hilfsmittel benutzt habe.

I hereby declare, on oath, that I have written the present dissertation by my own and have not used other than the acknowledged resources and aids.

Hamburg, den 09.06.2023 **Unterschrift** _____

Ich versichere, dass dieses gebundene Exemplar der Dissertation und das in elektronischer Form eingereichte Dissertationsexemplar (über den Docata-Upload) und das bei der Fakultät (zuständiges Studienbüro bzw. Promotionsbüro Physik) zur Archivierung eingereichte gedruckte gebundene Exemplar der Dissertationsschrift identisch sind.

Hamburg, 09.06.2023 **Tomas Fanutza,**

Ort, Datum Vorname und Nachname, Unterschrift

I, the undersigned, declare that this bound copy of the dissertation and the dissertation submitted in electronic form (via the Docata upload) and the printed bound copy of the dissertation submitted to the faculty (responsible Academic Office or the Doctoral Office Physics) for archiving are identical.

Hamburg, 09.06.2023 **Tomas Fanutza,**

Place, Date First name and surname, signature